

**DESIGN OF INNOVATIVE CLUTCHING  
MECHANISMS FOR HYBRID AUTOMOTIVE  
TRANSMISSIONS**

**Vikram Chopra**

Department of Mechanical Engineering  
McGill University, Montréal

March 2014

A Thesis submitted to the Faculty of Graduate Studies and Research  
in partial fulfilment of the requirements for the degree of  
Doctor of Philosophy

© VIKRAM CHOPRA, 2013



*Dedicated to my mother, Vandana Chopra (1951-2011), without whom I would not be the person I am.*



*Our first endeavors are purely instinctive prompting of an imagination vivid and undisciplined. As we grow older reason asserts itself and we become more and more systematic and designing. But those early impulses, though not immediately productive, are of the greatest moment and may shape our very destinies.*

Nikola Tesla<sup>1</sup>

---

<sup>1</sup>Nikola Tesla, 1919, "My Inventions," *Electrical Experimenter*, February-June and October.



# ABSTRACT

---

Innovative clutching mechanisms for hybrid automotive transmissions that yield low losses, while still satisfying the conflicting requirements of compactness, quick response, and high power density are explored in this thesis. Moreover, a systematic approach to automotive-transmission clutch design is proposed. The goal is to provide a complementary tool to aid the designer's judgment. The various design variants chosen serve two purposes, to demonstrate the foundation and to showcase approaches and solutions to specific problems that have a direct application in transmission design. The analysis of design variants goes into sufficient depth to be useful to both practicing automotive design engineers and academics.

The phenomenon of "spin loss" is well known in the automotive industry, for it affects all transmissions. One energy sink identified in this regard lies in traditional wet clutches and brakes, wherein an open clutch or, correspondingly, an open brake, creates drag on the transmission because of the oil churning around and between the rotating friction plates. A second source of spin loss, or energy sink, is of electromagnetic origin, as it occurs by virtue of spinning inactive motors that carry permanent magnets. Apart from spin losses, the hydraulic actuation of clutches and brakes suffers from head losses. Seals, pumps and valves incur leakages that cause energy loss.

## ABSTRACT

Using the techniques outlined in this thesis, two separate novel clutch variants are demonstrated to improve clutch and brake technology. One variant, the *electromechanical clutch* actuator, is based on a high-performance screw joint with a built-in locking mechanism. The screw joint was tested with two sub-variants, namely, a lead screw and a ball screw. One prototype of each of the two sub-variants was installed on a testbed, to mimic the installation of the actuator in place of the corresponding hydraulic components. To better reflect the elastostatic behaviour of the clutch disk assembly, a new model for its stiffness as a hardening spring was formulated. Proof-of-concept tests of both sub-variants, lead and ball screws, demonstrated their feasibility.

The second variant, the *electromagnetic dog clutch*, is directly aimed at minimizing spin and hydraulic actuation losses for clutched electric motors, wherein the motor is connected to a clutch. The system includes a unique contactless electromagnetic synchronizer and a synchronizing sleeve with dog teeth on the input and output components. The design study, focused on the electromagnetic part, strives to reduce clutch slip and control torque. The novel design features claw-like stator and salient rotor poles with good machinability within a restrictive design volume. A complete design analysis with physical proof-of-concept testing was conducted.

Reducing “spin-loss” in transmission assemblies will improve system efficiency and yield better fuel economy. The technological impact will benefit not only the user, who will obtain more mileage for her or his dollar, but also the environment.

# RÉSUMÉ

---

Dans cette thèse sont étudiés des mécanismes innovants d’embrayage pour transmissions automobiles hybrides qui n’engendrent que de faibles pertes, tout en satisfaisant les besoins parfois conflictives de compacité, de haute vitesse de réaction et de haute densité d’énergie. Une approche systématique de la conception de transmissions automobiles est proposée, dont l’objectif est d’offrir un outil complémentaire au jugement du concepteur. Les divers alternatives choisies servent à présenter les concepts fondamentaux, ainsi qu’à mettre en valeur les différentes approches et solutions à des problèmes spécifiques qui ont une application directe dans le domaine des conceptions de transmissions. L’analyse d’alternatives de conception va suffisamment en profondeur pour être utile à la fois aux ingénieurs de conception automobile et aux théoriciens.

Le phénomène de pertes d’énergie cinétique de rotation (PECR) est bien connu dans l’industrie automobile, car cela affecte toutes les transmissions. Un puits d’énergie mis en évidence à ce propos concerne les embrayages et freins traditionnels à fluides, pour lesquels un embrayage ouvert ou un frein ouvert, crée une traînée dans la transmission parce que l’huile tourbillonne autour et dans les plaques tournantes de friction. Un second puits d’énergie est d’origine électromagnétique, car générée par la rotation de moteurs inactifs contenant des aimants permanents. Hormis le PECR,

## RÉSUMÉ

l'actionnement hydraulique d'embrayages ou de freins entraîne des pertes de charges. Les joints, pompes et valves encourent des fuites qui engendrent de puits d'énergie.

En utilisant les techniques mises en avant dans cette thèse, deux nouvelles alternatives d'embrayages démontrent leurs capacités à améliorer les technologies des freins et des embrayages. L'une de ces alternatives, l'actionneur *électromécanique d'embrayage*, est basée sur une liaison à vis et dispose d'un mécanisme intégré de verrouillage. La liaison à vis a été testée au travers de deux sous-alternatives, à savoir une vis à filet trapézoïdal et une vis à billes. Un prototype de chacune des alternatives a été installé sur un banc d'essai, afin de reproduire l'installation de l'actionneur en lieu et place des composants hydrauliques correspondants. Pour mieux refléter le comportement élastostatique de l'assemblage des disques d'embrayage, un nouveau modèle de sa raideur, assimilée à un ressort durcissant, a été formulé. Des tests de preuve de concept des deux variantes, vis à filet trapézoïdal et vis à billes, ont montré leur faisabilité.

La seconde variante, l'embrayage électromagnétique à interférence, est directement utilisable pour minimiser les pertes en rotation et en actionnement hydraulique pour les moteurs électriques à embrayage, pour lesquels un moteur est connecté à un embrayage. Le système inclut un unique synchronisateur et des bagues de synchronisation avec des dents-de-chien sur les composants en entrée et en sortie. Le travail de conception a été concentré sur la partie électromagnétique, qui essaie de réduire le glissement de l'embrayage et le couple de commande. Le nouveau système conception est doté d'un stator en forme de griffes et des pôles de rotor saillants faciles à usiner et à installer dans un espace restreint dans la voiture. Une étude complète de conception avec des tests concrets de preuve de concept a été accomplie.

Réduire le PECCR dans les assemblages de transmissions améliorera l'efficacité du système et mènera à davantage d'économie de carburant. L'impact technologique

sera ainsi bénéfique non seulement pour l'utilisateur, qui profitera d'un kilométrage plus élevé pour son argent, mais aussi pour l'environnement.



# ACKNOWLEDGMENTS

---

Words escape me when trying to properly express my gratitude to my supervisor, Professor Jorge Angeles. As a second-year undergraduate student, I was fortunate enough to obtain a research assistant position in Professor Angeles' laboratory. Over the past seven years, he has motivated my interest in research and development. His discipline, ingenuity and hardwork have been a constant inspiration for my professional achievement. Without his guidance and persistent help this thesis would not have been possible. I am truly and deeply indebted to him for everything he has helped me accomplish. I would like to thank Professor David Lowther of McGill University for his guidance in the area of electromagnetic machines. Furthermore, I am grateful to Professors Peter Radziszewski, Damiano Pasini and Richard Chromik, for serving on my Ph.D. Committee and for their helpful comments.

I would like to express my sincerest gratitude to the members of General Motors R & D, as the research carried out in this thesis would not have been possible without their interest and technical support. I would like to thank and acknowledge Messrs. Anthony L. Smith and Alan G. Holmes for their knowledge, expertise, ideas and support. I have cherished my collaboration with Tony, who throughout the project has provided me with invaluable advice and suggestions. I especially would like to thank Dr. Madhu Raghavan for his vision, support and all the confidence he

## ACKNOWLEDGMENTS

had in me to carry out the research for this thesis. Support from Dr. Justin Gammage and Dr. Vijay Neelakantan are duly acknowledged.

I thank my colleagues and friends at the Centre for Intelligent Machines, which include Xiaoqing Ma, Toufic Azar, Jing-Jin Shen, Danial Alizadeh and Kamran Ghafari for their valuable support during my doctoral studies. Their enthusiasm made my experience in the lab more enjoyable. Juan Pedro Celis and Nicholas Tripp—undergraduate summer interns—aided me in producing manufacturing drawings. I also thank the staff of the Centre for Intelligent Machines and the Department of Mechanical Engineering, specially Mr. Jan Binder, Mrs. Cynthia E. Davidson, Mr. Gary Savard, Mr. John Boisvert, Mrs. Irène Cartier, Mrs. Joyce Nault and Ms. Nozomi Kanekatsu, for helping me with logistical and scholarship-securing support.

I extend my gratitude to my siblings, Divya Chopra and Anant Chopra. They have always been there for me without reservation. I appreciate the love and care of my aunt, Anju Bhargava, who has nurtured me since I was a child. I am grateful to Daniela Petrucci for all her patience and time she has given me. Her support throughout my difficult times has been extremely important.

I am immensely grateful to my parents, Dr. Ramesh Chopra and Mrs. Vandana Chopra. Their teachings, encouragement, optimism, love and ambitions have helped me throughout my life. I thank my father for always backing me up and for inducing the entrepreneurial spirit in me. I thank my mother for always encouraging me in my ambitions.

Finally, the funding of the FQRNT (Fonds de Recherche du Québec - Nature et Technologies), the NSERC (Canada's Natural Sciences and Engineering Research Council), General Motors Canada and McGill University's Faculty of Engineering are dutifully acknowledged.

# CLAIM OF ORIGINALITY

---

The author claims the originality of the main ideas and research results reported in this thesis. Specific claims include:

- The application of a ball screw with a ratchet and pawl mechanism in an automatic clutch actuator
- The design and application of an apply-plate with  $G^2$ -continuity curves to reduce stress concentrations
- A novel stiffness model of a clutch pack as a hardening spring
- The radial configuration of a 12 V reluctance brake synchronizer design using: a) equal number of rotor permanent magnets and stator electromagnets in one design; and b) half the number of rotor permanent magnets as stator electromagnets in an improved design
- The design and application of a 14 V contactless electromagnetic synchronizer with claw-shaped stator and rotor poles for use in clutched electric motors
- The application of a cam-roller translational mechanism in a dog clutch system for smooth actuation



# TABLE OF CONTENTS

---

ABSTRACT . . . . .	i
RÉSUMÉ . . . . .	iii
ACKNOWLEDGMENTS . . . . .	vii
CLAIM OF ORIGINALITY . . . . .	ix
LIST OF FIGURES . . . . .	xv
LIST OF TABLES . . . . .	xix
ABBREVIATIONS . . . . .	xxi
GLOSSARY . . . . .	xxiii
CHAPTER 1. Introduction . . . . .	1
1.1. Problem Statement . . . . .	3
1.1.1. Scope . . . . .	4
1.1.2. Objective . . . . .	5
1.2. Background and Literature Review . . . . .	7
1.2.1. Wet Clutch Tribology . . . . .	8
1.2.2. Hydraulic Actuation of Wet Clutches . . . . .	17
1.2.3. Research Landscape . . . . .	19
	xi

TABLE OF CONTENTS

1.3. Thesis Overview . . . . . 20

CHAPTER 2. Clutch Design Techniques . . . . . 23

2.1. Technical Specification . . . . . 24

2.2. Quality Function Deployment . . . . . 25

2.3. Functional Decomposition . . . . . 27

2.4. Conceptual Design . . . . . 29

2.4.1. Set of Design Variants . . . . . 30

2.4.2. Short List of Design Concepts . . . . . 34

2.4.3. Concept Evaluation . . . . . 36

2.4.4. Design Concept Selected . . . . . 38

2.5. Design Embodiment . . . . . 39

2.6. Summary of Techniques Applied to Clutch Design . . . . . 40

CHAPTER 3. Electromechanical Clutch Design . . . . . 43

3.1. Actuator System Embodiment . . . . . 43

3.1.1. Lead-screw Design Layout and Operation . . . . . 45

3.1.2. Ball Screw Design Layout . . . . . 46

3.2. Final Design . . . . . 48

3.2.1. Clutch Actuator Specifications . . . . . 48

3.2.2. Compact Packaging . . . . . 49

3.2.3. Review and Details of the EMC testbed . . . . . 50

3.2.4. Finite Element Analysis of the Apply-plate . . . . . 51

CHAPTER 4. Electromechanical Clutch Modelling and Experiments . . . . . 55

4.1. System Modelling . . . . . 57

4.1.1. Iconic Model of the Electromechanical Actuator System . . . . . 57

4.1.2. Modelling Assumptions . . . . . 59

4.1.3. Derivation of the Mathematical Model . . . . .	61
4.2. Simulation and Experimental Results . . . . .	64
4.2.1. First EMC Sub-variant: Lead Screw . . . . .	65
4.2.2. Second EMC Sub-variant: Ball Screw . . . . .	66
CHAPTER 5. Electromagnetic Dog Clutch Design . . . . .	71
5.1. Concept Development . . . . .	71
5.2. Computer-Aided Design and Modelling . . . . .	73
5.3. Simulation and Results . . . . .	76
5.4. Reduction in Cogging Torque . . . . .	79
5.5. Prototyping Considerations . . . . .	82
5.6. Design and Discussion of a Potential Dog Clutch System . . . . .	85
CHAPTER 6. Design and Analysis of the Electromagnetic Synchronizer . . . . .	89
6.1. Brake-clutch Synchronizer Design . . . . .	89
6.1.1. Design Principle and Operation . . . . .	89
6.1.2. Design Specifications and Layout . . . . .	90
6.2. Electromagnetic Modelling . . . . .	92
6.3. Finite Element Analysis . . . . .	94
6.4. Experimental Testing . . . . .	100
CHAPTER 7. Conclusions and Recommendations for Future Research . . . . .	109
7.1. Conclusions . . . . .	109
7.2. Recommendations for Future Research . . . . .	111
BIBLIOGRAPHY . . . . .	115
APPENDIX A. Spatial Clutch Linkage Analysis . . . . .	129
APPENDIX B. Eddy-current Clutch Analysis . . . . .	135



# LIST OF FIGURES

---

1.1	The design process overview by Dieter (2000). . . . .	2
1.2	A flowchart of steps involving conceptual design (Pahl et al., 2007). . . . .	2
1.3	Parasitic loss distribution in automatic transmissions (Kluger and Long, 1999) . . . . .	6
1.4	Sectional view of a typical multi-plate disk clutch assembly. . . . .	9
1.5	Clutch disks . . . . .	10
2.1	Range clutch pack with the transaxle . . . . .	25
2.2	Brake-clutch assembly within the transmission . . . . .	26
2.3	House of Quality diagram for clutch designs (Hauser and Clausing, 1988) . . . . .	28
2.4	A schematic of a pneumatic-spring clutch . . . . .	32
3.1	Schematic diagram of the clutch actuator concept . . . . .	44
3.2	Cross-sectional view of the lead screw clutch-actuator embodiment . . . . .	46
3.3	Cross-sectional view of the ball screw clutch actuator embodiment . . . . .	47
3.4	Packaging of: (a) the lead screw variant; (b) the ball screw variant . . . . .	50
3.5	Front perspective view of the CAD model of the actuator testbed . . . . .	51
3.6	Cross-section of the clutch actuator testbed. . . . .	52

LIST OF FIGURES

3.7 CAD model of the apply-plate . . . . . 53

3.8 Apply-plate FEA results: (a) von Mises stress distribution; (b) Elastic deformation displacement plot . . . . . 53

3.9 Front, back and side view of the machined apply-plate . . . . . 54

4.1 The electromechanical actuator testbed . . . . . 56

4.2 Iconic model of the electromechanical actuator . . . . . 57

4.3 Coulomb friction torque  $\tau_f$  and force  $f_f$  . . . . . 60

4.4 Plot of  $\kappa$  versus  $\eta$  plot . . . . . 61

4.5 Motor input current command for the EMC lead screw sub-variant . . 67

4.6 Comparison of the experimental and simulation results of the motor shaft velocity for the EMC lead screw sub-variant . . . . . 67

4.7 Comparison of the experimental and simulation results of the clutch clamping force for the EMC lead screw sub-variant . . . . . 68

4.8 Comparison of the experimental and simulation results of the motor shaft velocity for the EMC ball screw sub-variant . . . . . 69

4.9 Comparison of the experimental and simulation results of the clutch clamping force for the EMC ball screw sub-variant. . . . . 69

5.1 Preliminary brake clutch concept: (a) assembly in lock mode; (b) exploded view . . . . . 73

5.2 Proposed PM DC brake layout . . . . . 76

5.3 (a) Switch circuit for the PM brake; (b) Voltage across the two switches . . . . . 78

5.4 Current in the circuit. . . . . 79

5.5 Rotor speed plot of the proposed design . . . . . 79

5.6	Braking torque plot of the proposed design . . . . .	80
5.7	Magnetic flux density plot at 250 ms. . . . .	80
5.8	A 16 EM-pole stator with eight PM and eight salient steel poles on the rotor . . . . .	82
5.9	A zoom-in on a section of the rotor surface . . . . .	83
5.10	Rotor speed plot of the eight PM pole rotor . . . . .	83
5.11	Rotor torque plot of the eight-PM pole rotor . . . . .	83
5.12	Magnetic flux density plot of the eight-PM pole rotor at 250 ms . . . .	84
5.13	Drag torque of the open PM-based brake operation of the two designs	84
5.14	Dog clutch synchronizer: (a) disengaged; (b) engaged . . . . .	85
5.15	Compact translational mechanism . . . . .	86
5.16	Interpolating 4-5-6-7 polynomial . . . . .	87
5.17	Sliding grooved ring: (a) top view; (b) 3D view. . . . .	88
6.1	Schematic of the EM synchronizer . . . . .	92
6.2	MagNet model of one stator claw and one rotor pole . . . . .	96
6.3	Current in the coil winding . . . . .	97
6.4	Rotor speed . . . . .	98
6.5	Rotor torque. . . . .	98
6.6	Flux density plot of one-sixteenth of the geometry . . . . .	99
6.7	A MagNet extrapolation of the initial B-H curves of 1010 steel and FY-4500 . . . . .	100
6.8	Rotor speed using FY-4500 . . . . .	101
6.9	Rotor load using FY-4500 . . . . .	101
6.10	The testbed for the EM synchronizer. . . . .	102

## LIST OF FIGURES

6.11	Cross-sectional view of the testbed . . . . .	102
6.12	Static loading conditions for rotor FEA . . . . .	103
6.13	von Mises stress distribution in the rotor . . . . .	103
6.14	Elastic deformation displacement plot of the rotor FEA . . . . .	104
6.15	Machined rotor . . . . .	104
6.16	Machined stator . . . . .	105
6.17	Renshape coil bobbin. . . . .	106
6.18	Rotor speed recorded. . . . .	106
6.19	Rotor load torque. . . . .	107
A.1	RSSR linkage representation (Liu and Angeles, 1992) . . . . .	130
A.2	RURUR clutch linkage . . . . .	133
A.3	The input-output curve of the clutch linkage . . . . .	133
B.1	A 72° pie section of a four-electromagnetic-pole configuration . . . . .	136
B.2	Magnetic-flux contour and arrow plot . . . . .	137
B.3	Rotor speed response. . . . .	138

# LIST OF TABLES

---

2.1	Clutch concept evaluation using Pugh's method . . . . .	37
3.1	EMC specifications . . . . .	48
4.1	Lead screw model parameters . . . . .	66
4.2	Ball screw model parameters . . . . .	68
5.1	Design specifications for the PM DC brake synchronizer . . . . .	74
6.1	Summary of maximum torque of each claw-pole set . . . . .	96
6.2	Final prototype performance . . . . .	108

## LIST OF TABLES

# ABBREVIATIONS

---

ATF: Automatic transmission fluid

DC: Direct current

ED: Engineering design

EDC: Electromagnetic dog clutch

EM: Electromagnetic

EMC: Electro-mechanical clutch

EV: Electric vehicle

FEA: Finite element analysis

FEM: Finite element magnetic

HEV: Hybrid electric vehicle

MRF: Magneto-rheological fluid

PM: Permanent magnet

SRM: Switched reluctance motor

## ABBREVIATIONS

# GLOSSARY

---

In this glossary, some of the frequent terms used in this thesis are described below:

- *Brake-clutch*: A type of clutch that holds or prevents the motion of its connecting component by coupling it to a fixed end.
- *Closed or Engaged or Locked-up Clutch State*: A state in which the clutching mechanism is active and transmits power.
- *Clutch Slip*: The relative angular velocity between the two rotating components of a clutch assembly.
- *Design Specification*: A set of quantitative conditions or requirements to be satisfied by the object under design.
- *Design Technique*: The procedure by means of which a product, tangible or intangible, intended to satisfy a human need, is taken from concept to product.
- *Design Variables or Design Parameters*: The defining characteristics of the designed object that the designer must specify as a result of the design process.
- *Dog Clutch*: A type of clutch that couples two rotating shafts or other rotating components by interference. The two parts of the clutch are designed such that one pushes the other, causing both to rotate at the same speed.

## GLOSSARY

- *Electric Vehicle*: A type of vehicle that uses one or more traction motors for propulsion. Electric power is made available through batteries.
- *Hybrid Electric Vehicle*: A type of vehicle that combines an internal combustion engine system with an electric motor to produce propulsion.
- *Open or Disengaged or Unlocked Clutch State*: A state in which the clutching mechanism is inactive.
- *Spin Loss*: The energy lost due to the rotation of a component or object about its axis in the presence of a drag torque because of dissipative effects.
- *Synchronizer*: A mechanism that causes its components to operate at the same rate.

# CHAPTER 1

---

## Introduction

The field of engineering design (ED) is large and applicable to almost all aspects of engineering practice. Engineers use engineering design as an important tool to develop, research, troubleshoot, investigate, analyze and maintain products and services that meet the user-prescribed objectives. ED commonly involves an iterative process where the designer's decision-making skills and disciplinary knowledge are coherently applied. Moreover, by properly following the engineering design process, one can synthesize, build, test and evaluate products to achieve results.

The design process consists of several steps leading to the finalization of the design, followed by fabrication, as illustrated in Fig. 1.1. Dym and Little (2000) gave an adequate overview of the design process with elements from Dieter (2000), which entailed problem definition, concept generation, concept evaluation, detailed design and design communication. The phases of conceptual design were given due attention by Pahl et al. (2007) within their formulation known as *systematic design*; this proved to be an efficient methodology for concept generation and evaluation. The different stages involved in conceptual design are shown in Fig. 1.2, as a flowchart that helps one arrive at a suitable concept.

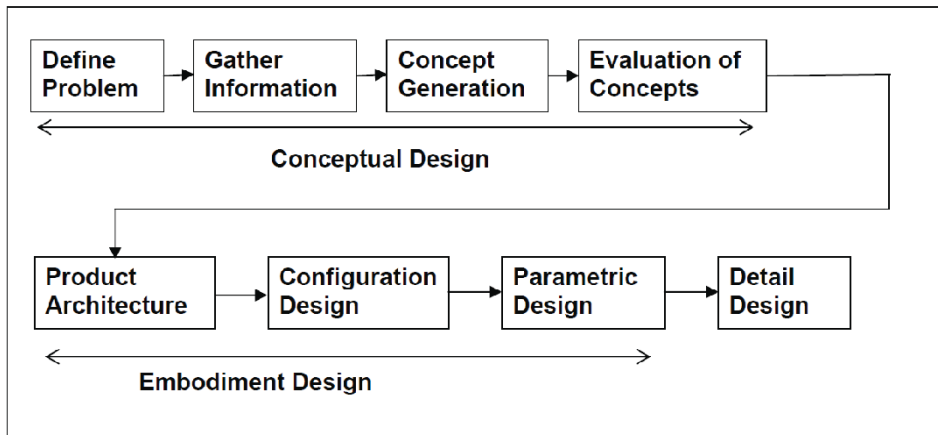


FIGURE 1.1. The design process overview by Dieter (2000)

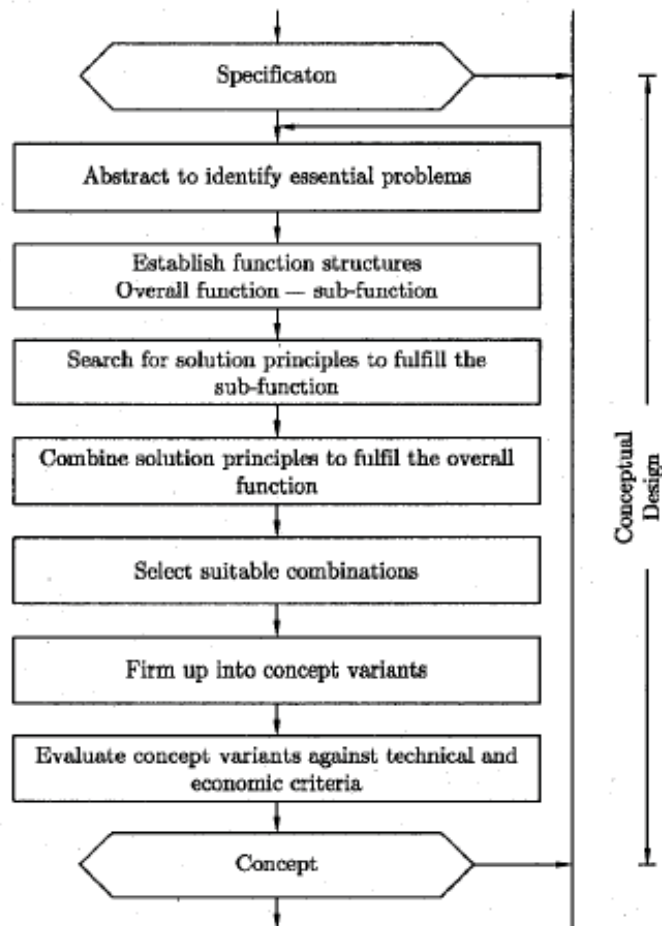


FIGURE 1.2. A flowchart of steps involving conceptual design (Pahl et al., 2007)

In engineering design, individuals have divergent opinions on: how to design, what distinguishes a good design from a bad design, whether design is more art than science, and so forth. So much has been written about engineering design that no attempt is made here to cover such a wide range of opinions on the subject. It seems the harder the design problem, the less likely that two individuals will agree on its solution. This probably is an asset, as it leads to a diversity of solutions, more thorough deliberation, and usually better designs. Although a designer's pride may get in the way, peer-review is an important element to a successful design. Self-review of the design should occur all along the process. All aspects of a design should have a reason for being while one should be able to defend the logic or agree when it is arbitrary. Artificial constraints in the creative thinking process tend to obscure the simple and elegant design solutions that most strive to achieve. Peer- and self-reviews tend to uncover the constraints that complicate the design or lead to unnecessary aspects.

How does one go about solving a new design problem? It all depends on the problem, one's knowledge, available resources, besides the physical, legal and financial constraints. Sometimes the design solution is found as a result of an analysis task, for instance, optimizing the profile of a cam or synthesizing the geometry of an aircraft wing. Experience and practice lead to a variety of problems and solutions, as one becomes adept at solving new design problems. Creativity is an exceptional ability of the human mind, which is intriguing and poorly understood, yet fascinating as a philosophical subject.

## 1.1 Problem Statement

In solving any design problem, one needs a complete problem definition in order to properly understand the underlying challenges. The need that motivates the design

job can be specified by the client’s statement of work. Task-clarification can be carried out by

- Identifying the design objectives and goals
- Becoming knowledgeable in the field by gathering technical information from the literature on the state of the art
- Establishing functional requirements. Connect apparent problems to more fundamental sources.
- Thoroughly defining the design specifications at hand.
- Understanding the constraints and challenges in achieving the solution.

**1.1.1 Scope.** The motivation behind this thesis is the need of clutching devices for next-generation propulsion systems that yield low losses while matching the performance of current clutching technology. Consequently, a structured framework is provided in order to design clutches for automotive transmissions. The scope of the work done on clutch design, described in this thesis, is relevant to automatic, hybrid-electric-vehicle (HEV) and electric-vehicle (EV) transmissions within the automotive industry. Using a clean-sheet approach, a thorough investigation on the physical principles governing the operation of a clutch is undertaken. These principles then lead to the generation of creative designs. The basic function of a clutch is defined as:

*Allow for the coupling and decoupling of two shafts so that: (i) when the shafts turn at different speeds, coupling ensues; and (ii) when the shafts are coupled, and hence, turning at the same speed, decoupling takes place. In both cases, a swift, smooth, and efficient transition should be secured by means of a compact device.*

Here “swift” means a transition with minimum possible delay, typically on the order of milliseconds; “smooth” is a gradual, soft, “jerk-free” transition, by allowing controlled

slippage; and “efficient” means an operation which minimizes power loss. This is a preliminary statement of the design task; it is further clarified under Section 2.1.

**1.1.2 Objective.** The objective of this thesis is to provide a systematic approach to design within the realm of automotive design engineering. The goal is to provide a complementary tool to aid the designer’s judgment. In order to improve the efficiency of *wet multi-plate clutch packs*, power losses are to be minimized. Several energy sinks exist in the powertrain; however, the work focusses on those associated with wet clutches in automatic hybrid transmissions, namely, their hydraulic actuation and spin losses.

Hydraulic actuation provides the high clutch forces that are needed in clutches with high torque-transfer capacity. However, hydraulic actuation systems are relatively complex and feature elements such as pumps, pressure-regulating valves, control valves, oil filters, oil lines and oil bores. These take up space and increase the weight of the transmission housing them. Current clutch hydraulic actuation methods suffer from head losses because of fluid flow within channel lines. Seals, pumps and valves suffer leakages, which lead to power loss. When a clutch is engaged, hydraulic pressure must be maintained in order to transmit torque. To maintain this pressure, energy must be consumed, the level of which can be substantial during long clutch engagements.

The phenomenon of “spin loss” is well known in the automotive industry because it affects all transmissions operating with fluids and lubricants. Shown in Fig. 1.3 is a distribution of the losses present within typical automatic transmission gearboxes. Although these transmissions differ from hybrid transmissions, they have many similar components. Fluid-based drag torque is a major contributor to spin loss in wet clutches. According to Kluger and Long (1999), clutch pack drag is a constant parasitic loss during vehicle operation. The pie chart also includes losses due to windage

(drag caused by fluid movement around gears), poor seals, bearings/brushing and gear geometry. Clutch-pack drag has been identified as predominant in an open clutch; however, minimal drag torque may exist in a closed clutch as well, similar to windage. In an open clutch, where the friction and separator plates are rotating at different speeds, the shearing force of the fluid between them causes a drag torque, as explained by Kitabayashi and Hiraki (2003). Therefore, reduction of this drag is vital, especially in HEV transmissions.

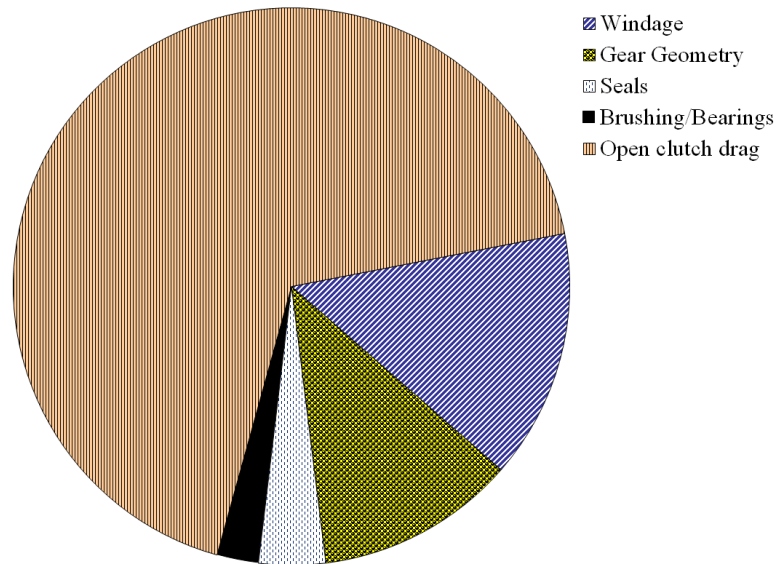


FIGURE 1.3. Parasitic loss distribution in automatic transmissions (Kluger and Long, 1999)

These losses typically increase with the size and torque transfer capacity of wet multi-plate clutch packs. Wet clutch packs are used as input, range and brake clutches, as explained further in Section 1.2, where range and brake clutches suffer the most from the aforementioned losses.

In summary, a favourable clutching system must:

- match the power density of current clutches;
- achieve quick engage/disengage action;
- achieve “jerk-free” transition during engagement/disengagement;

- fit within a volumetric budget.

Moreover, in order for the system to warrant a change to new technology, it should

- minimize drag torque, a major source of spin loss;
- improve clutch actuation technology;
- decrease energy expenditure to maintain clutch lock-up, especially for clutches that are engaged over long periods.

## 1.2 Background and Literature Review

Clutches are mechanical subsystems of the power-train. For intermittent periods only, the transmission of rotary motion from one shaft to another is achieved by a clutch. A clutch function is to produce a smooth, i.e. “jerk free”, and gradual increase in the angular velocity of the driven shaft, until full coupling between the two shafts is achieved. Then, this coupling must be maintained for transmitting the entire mechanical power from the driving shaft to the driven shaft without subsequent slip (Bezzazi et al., 2006).

In vehicles equipped with automatic or hybrid transmissions, several types of clutches exist that allow transmission of torque, switching of gears and prevention of rotation of certain elements, as needed (Ingram et al., 2010). Moreover, these transmissions remove the need for the user to operate a manual clutch. The *torque converter*, featured in some automatic transmissions (GM Powertrain, 2007), is a special fluid coupling that includes a stator component. The converter usually forms the primary component for the transmittal of power from the engine flywheel to the transmission input shaft. The torque converter allows the engine to run when the vehicle is stationary. In some HEV transmissions such as the GM two-mode powertrain (Hendrickson, Holmes and Freiman, 2009), a torque converter is not required, since there is an operating mode where the engine can be rotating while the vehicle is at a

standstill. In that case, the torque converter is typically not used in order to remove the losses associated with torque converter slip and the design compensates for the loss of the torque converter's torque multiplication factor. However, this varies for different manufacturers.

Mechanical multi-plate disk clutches can be *input*, *range*, or *brake clutches*, all being of the “wet” type, i.e. their friction surfaces are wetted by the working fluid. These clutches are located at several places within the gear transmission assembly. The input clutch assembly is located inside the input shaft and housing assembly. When fully applied, the input clutch provides the power to the gear sets. Correspondingly, range clutches allow selective components of the respective gear range in operation to rotate. Brake clutches, on the other hand, mechanically hold their transmission element at rest with respect to the transmission case.

A typical multi-plate disk *clutch pack* consists of a number of alternating friction and separator plates as displayed in Fig. 1.4, a clutch hub, pistons, return springs, snap rings, a retainer-ball assembly, bearings, a backing plate and a clutch drum. With the engine running, the line pressure from the oil pump assembly is fed through drilled holes in the valve body, through the case cover assembly to the clutch housing. Automatic transmission fluid flows in between these plates and soaks the friction material. Therefore, the fluid wets the surfaces of the plates and forms an oil film between them. This fluid typically enters through the clutch hub, flows radially between the plates by centrifugal force, and is discharged through the oil orifices of the clutch drum (Yang and Lam, 1998).

**1.2.1 Wet Clutch Tribology.** Clutch performance is highly dependent on the high friction interface between the disks. The friction disk consists of a steel ring coated by a friction material (usually a paper-based material) on both sides; the separator disk consists of a steel counter-surface, which leads to a combination of high

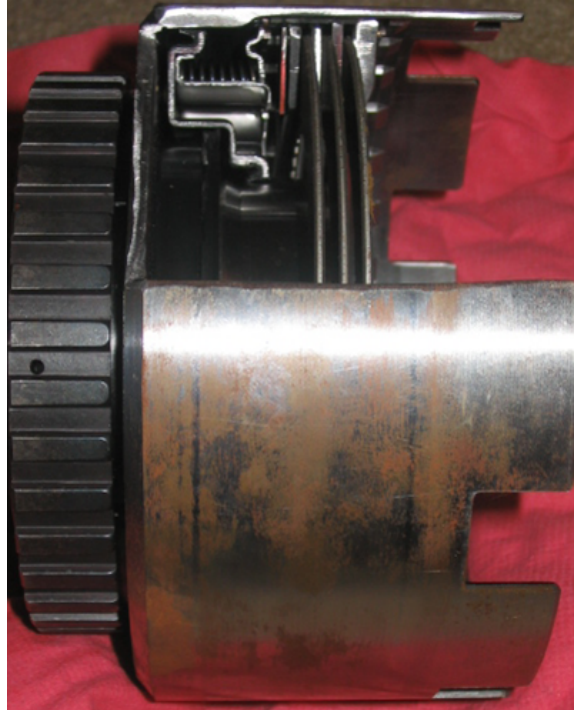


FIGURE 1.4. Sectional view of a typical multi-plate disk clutch assembly

friction coefficient with low wear. Shown in Fig. 1.5 is the combination of friction and separator disks in a clutch pack. This friction material must be capable of operating at very high temperatures, and must provide a high coefficient of friction throughout the life of a transmission (Ingram et al., 2010). An extensive literature is available on the tribology of wet clutches, explaining the different phenomena involved. Important tribological observations are outlined below.

1.2.1.1 *Lubrication in All Regimes.* A wet clutch pack is immersed in a lubricant oil commonly called automatic transmission fluid (ATF). The main functions of the ATF are to perform lubrication, to maintain a suitable temperature within the transmission, and to aid in transporting chemical additives to the disk surfaces (Ingram et al., 2010). The working of a wet clutch demands lubrication in all regimes (Larsson, 2009), such as:



FIGURE 1.5. Clutch disks

- *Hydrodynamic lubrication*, or full film lubrication, which exists when the clutch is disengaged (Yuan et al., 2007; Rivire and Myhra, 2009). A thick ATF film—typical thickness of  $100\ \mu\text{m}$  (Yuan et al., 2007)—is maintained between the contacting disk surfaces. The lubrication here is mostly affected by the viscosity of the ATF and the relative speed between the disks (Rivire and Myhra, 2009). Viscous shearing of the ATF between the plates in this regime causes a drag torque (Yuan et al., 2007; Kitabayashi, Li and Hiraki, 2003).
- *Elastohydrodynamic lubrication*, which occurs at the very beginning of clutch engagement. As the contacting disks approach each other, a squeezing effect by the hydrodynamic film pressure reduces the film thickness (Ting, 1975; Gao and Barber, 2002). ATF begins to escape through tiny pores and grooves on the friction disc (Ingram et al., 2010). A low film thickness (typically from  $0.01\ \mu\text{m}$  to  $10\ \mu\text{m}$ ) and increase in contact pressures result

in local elastic deformation on the surfaces without any asperity contact (Rivire and Myhra, 2009).

- *Mixed lubrication* begins as the fluid film undergoes a squashing effect and the surface asperities begin to come into contact. With the engagement of the clutch close to completion, deformations begin on the contacting surfaces and torque is transmitted by both asperity contact and viscous friction (Ting, 1975). A mixture of elastohydrodynamic lubrication and boundary lubrication (i.e. the next lubrication regime) is noticed with an ATF film thickness between  $0.01 \mu\text{m}$  and  $1 \mu\text{m}$ . Moreover, the fluid behaves more like a solid than a liquid (Rivire and Myhra, 2009).
- *Boundary lubrication* exists when the clutch is completely engaged (Ingram et al., 2010; Gao and Barber, 2002). This complex phenomenon occurs when the two disks and the thin oil film rotate as a rigid body. Film thickness typically ranges between  $1 \text{ nm}$  and  $100 \text{ nm}$ , with the ATF usually being adsorbed in the solid surface via its pores and asperities. The ATF reduces wear and lowers the coefficient of friction because of the lower shear stress of the fluid, as compared to that of the solid disk (Larsson, 2009; Rivire and Myhra, 2009). The real surface contact area mainly consists of deformed asperities and, hence, is only a fraction of the nominal surface area (Ingram et al., 2010; Eguchi and Yamamoto, 2005). Friction-produced heat occurs in this regime; it is a major cause of material and ATF degradation (Gao, Barber and Chu, 2002; Yang and Lam, 1998).

1.2.1.2 *Friction Material.* Several types of friction material combinations are used in automatic transmissions. These include paper-based friction-steel disks, sintered bronze-steel disks, steel-steel disks, carbon fibre-steel disks and Kevlar disks (Ingram et al., 2010; Lam, Chavdar and Newcomb, 2006; Marklund and Larsson,

2007). The most commonly used paper-based friction material is manufactured in the same fashion as regular paper. A stock is prepared by mixing fibrous material, fillers and chemical additives together, then soaking the mixture in water. This is dried on a moving wire line, and then pressed into rolls of paper. After saturating and curing this paper with resin, it is bonded adhesively onto a steel core plate, thereby forming the friction disc. The separator counter-face disk is made of steel (Ingram et al., 2010). Fibres include materials such as asbestos, cellulose, cotton linter, aramid, Kevlar, carbon fibre, lapinus and basalt, while fillers can be diatomaceous earth, clay, silicone particles, cashew dust, barites and calcium carbonate (Lam, Chavdar and Newcomb, 2006). Chemical additives usually include alumina, chromium oxide and silicone. Several resins can be used such as phenolic resin, modified phenolic resin and cresylic phenolic resin (Ingram et al., 2010). The frictional properties of the material can be altered by varying the components used, or by changing the steps involved in the manufacturing process (Lam, Chavdar and Newcomb, 2006).

The porosity is one important property that can be modified during the friction material design process. The permeability of the friction material is a measure of the ATF ability to flow, or penetrate the friction material via its pores (Marklund and Larsson, 2007). The permeability varies with mechanical wear and thermal degradation of the friction material, and consequently changes over the life of the clutch (Yang and Lam, 1998). A new wet friction material possesses good permeability; however, a glazed friction material shows poor permeability (Gao and Barber, 2002; Marklund and Larsson, 2007). This effect, influencing the frictional behaviour and engagement time of the clutch, will be briefly discussed.

**1.2.1.3 Friction Characteristics.** Two main types of friction exist in wet clutches, Coulomb friction and Eyring viscosity friction (Eguchi and Yamamoto, 2005). The coefficient of friction,  $\mu$ , in wet clutches is dependent on several parameters such as

material, type of ATF used and contact surface nature. Its value is strongly influenced by the sliding velocity,  $v$ , of the clutch disks, the operating temperature, and the applied normal loads (Gao and Barber, 2002; Gao, Barber and Chu, 2002; Lam, Chavdar and Newcomb, 2006). Friction characteristics are well described by  $\mu$ - $v$  ratios for a given set of temperature, pressure, geometry and ATF. These  $\mu$ - $v$  curves have a strong dependence on the unstable *shudder effect*. Stick-slip-induced friction causes undesirable vibrations that are responsible for the shudder effect, and are also a major cause of discomfort to the users during clutch engagement (Gao and Barber, 2002). Their detrimental effects can hamper the performance of the clutch, and cause fatigue failure, surface damage, noise and severe wear. Positive slopes of  $\mu$ - $v$  curves generally show no shudder effects, these curves commonly appearing among new friction material and new oils. Negatively sloped curves are common in worn-out friction material and degraded oils. Shudder is mostly noticed in the negatively sloped  $\mu$ - $v$  curves (Gao, Barber and Chu, 2002; Lam, Chavdar and Newcomb, 2006).

1.2.1.4 *Contact Properties of the Friction Material.* The real area of contact is only a small percentage of the nominal surface area (Ingram et al., 2010; Gao and Barber, 2002). This contact area can be calculated by capturing grey-scale images, and then converting them into binary images, where the perimeters of the contact area can be traced. This real contact area increases with the contact pressure, as more fibres deform and wear. It is also observed that the shear strength of the boundary film has a strong dependency on the contact area (Ingram et al., 2010; Eguchi and Yamamoto, 2005).

1.2.1.5 *Automatic Transmission Fluid.* The automatic transmission fluid (ATF) is an important part of the clutch system. It must provide the desired friction characteristics, and maintain its performance throughout the working life of the transmission. Moreover, it must lubricate all elements within the automatic transmission

housing. Current ATFs manufactured have been standardized (Arakawa, Yauchibara and Murakami, 2003), such as DEXRON-VI, to meet stringent requirements.

The formulation of ATF involves several base oils and additives, with surface-active additives enhancing the frictional performance. Base oils are usually mineral oils and synthetic fluids like paraffinic oil (Kugimiya et al., 1997). The additives usually include properties such as anti-oxidant, dispersant, detergent, anti-wear, viscosity-index improver, anti-rust, corrosion inhibitor, anti-forming and friction modifier, among others (Shirahama, 1994).

1.2.1.6 *Clutch Engagement: Torque Transmission.* The ATF film thickness between clutch disks varies with time during engagement. As the clutch plates approach each other this film thickness rapidly decreases. Numerical simulations were carried out by Gao and Barber (2002) using the Runge-Kutta method. These simulations were conducted for a wet clutch functioning as a brake, i.e., with the relative angular velocity between the friction and separator plates decreasing to zero and one side of the clutch at zero angular velocity. The instant this velocity reaches zero is denoted as the end-of-engagement. Film thickness is also observed to decrease rapidly until it nearly plateaus when the clutch plates are completely engaged (Gao and Barber, 2002).

The torque transferred on engagement consists of *hydrodynamic* and *boundary* torque. Boundary torque,  $\hat{T}_c$ , is noticed when the asperities come into contact, while hydrodynamic torque  $\hat{T}_v$ , occurs as the fluid film between the plates shears. The total torque rises rapidly at the beginning of engagement, and continues to increase smoothly until a jump occurs at the end of engagement. This discontinuity is the cause for stick-slip-induced shudder. This results in rapid engagement of the clutch because of the increased friction coefficient as the slip decreases to zero. The total

torque  $\hat{T}$  can also be related to relative angular acceleration,  $\dot{\hat{\omega}}_{rel}$ , of the disk by:

$$\hat{T} = \hat{T}_v + \hat{T}_c = \hat{I}\dot{\hat{\omega}}_{rel} \quad (1.1)$$

where  $\hat{I}$  represents the disk moment of inertia. The expressions for  $\hat{T}_c$  and  $\hat{T}_v$  were derived by Gao and Barber (2002). The effects of parameters such as surface roughness, ATF viscosity, coefficient of friction, permeability, moment of inertia, groove area and Young's modulus on clutch engagement are briefly summarized below, as per the findings reported by Gao and Barber (2002).

- Using a Gaussian asperity height distribution to model the real contact area ratio and considering the root-mean square surface roughness, it was found that a coarser surface shows a lower  $\hat{T}$  at the beginning of engagement, and takes longer to engage.
- It was seen that an ATF with half the viscosity appears to produce twice the torque. A higher viscosity provides better lubrication in reducing friction and increases the net moment of inertia. This results in higher angular acceleration and quicker engagement time. ATF viscosity is observed to be very important in the performance of wet clutch packs.
- Reduced permeability of the friction material leads to a longer engagement time, as ATF infiltration into the material is comparatively lower, and hence, more fluid in-between the contacting surfaces. This also affects the torque response to have a more gradual rise at the beginning of engagement.
- The moment of inertia of the disk and all its corresponding rotating components connected to the driven shaft plays an important role in the engagement time of wet clutches. A disk with lower moment of inertia produces a quicker engagement time, which shows that the relative angular velocity of the disk decreases faster without a major effect on the total torque.

- Friction disks usually have a groove pattern on their surfaces to allow ATF to flow in and also cool the interface (Yang and Lam, 1998). By altering the nominal contact area, i.e., by introducing more grooves, one observes no major effect in the torque and time response.
- It was found that a friction material with a lower Young's modulus causes a lower total torque with a longer engagement time than a material with a higher Young's modulus.

1.2.1.7 *Hot Spot Generation during Short-Term Engagement.* A common problem observed in clutches is the formation of hot-spots caused by thermo-elastic instabilities. Local areas of surface failure caused by substantially high temperatures and high pressures are macroscopically seen on the steel separator surface. Hot spots cause high thermal stresses, which lead to plastic deformation, and transformation of the ferrous material into martensite. This results in cracks and, ultimately, in clutch failure. Severe hot spotting occurs during high initial sliding speeds, small geometric imperfections being capable of triggering large hot spot formations. Lowering the Young's modulus of the friction material can effectively lower the hot spots growth area (Zagrodzki and Truncone, 2003).

1.2.1.8 *Clutch Disengagement: Drag Torque.* The generation of undesirable hydrodynamic torque is inherent to a disengaged clutch pack. It is deemed an energy sink that lowers the efficiency of all transmissions that employ them. The viscous effect of the ATF causes a drag on the rotating member of the disengaged clutch. A number of factors can influence drag torque, most notably, the distance between the clutch disks, ATF flow rate, groove patterns, disk facing area and the waviness of the disk plates (Kitabayashi, Li and Hiraki, 2003). A hydrodynamic model was developed for the drag torque and shear stress on the rotating plate (Yuan et al., 2007). This model, which incorporated the surface-tension effects of the oil film, showed better

agreement with test data for a non-grooved clutch pack. According to this model, for an open clutch pack operating at steady state in an incompressible ATF film, rotating in a turbulent regime, the shear stress and parasitic drag torque vary with the radius where full oil film breaks due to centrifugal effects, the inner radius of the rotating disc, the ATF viscosity, the angular velocity of the rotating disc, the clearance between disk and the Reynolds number based on the clutch clearance (Yuan et al., 2007).

Fish (1991) evaluated drag losses in wet clutches using the SAE #2 machine and concluded that drag torque can be minimized by

- increasing the gap between clutch plates, i.e. pack clearance;
- lowering the ATF level and flow;
- reducing the viscosity of the ATF;
- lowering the clutch speed;
- altering the grooves on the friction plates;
- altering the geometry of the clutch plates, e.g. introducing waves.

**1.2.2 Hydraulic Actuation of Wet Clutches.** Transmission pumps deliver fluid from a low pressure reservoir to a high pressure line in order to actuate several elements, such as clutch packs, regulating valves, torque convertor clutch, and band clutches. They also aid in circulating the fluid to regulate the transmission temperature and in fluid filtration. However, they have several losses which correspond to parasitic losses in the transmission.

Typical range clutches of automatic transmission are actuated hydraulically by feeding in ATF through the driven sprocket support and into the input shaft-housing assembly. A feed hole in the input shaft allows fluid to enter between the piston and the input shaft-housing assembly. Fluid pressure seats a ball check valve assembly, that allows the movement of the piston to compress a spring-retainer assembly.

The piston continues to move until it contacts the apply plate, where it compresses the neighbouring plate to cushion the apply plate, and holds the alternating plates against the backing plate and snap ring. When fully closed, the range clutch provides the power to the corresponding transmission component through the friction and separator plates. To release the range clutch assembly, fluid pressure exhausts through the apply passage in the input shaft-housing assembly and driven sprocket support. In the absence of fluid pressure, the input spring-retainer assembly moves the piston assembly and releases the apply plate, the cushion plate, and other stacked plates from the backing plate and snap ring. During the release of the fluid, the ball check valve assembly, located in the clutch housing, unseats. Centrifugal force, resulting from the rotation of the input shaft-housing assembly, drives residual clutch fluid to the outer perimeter of the piston housing, and through the unseated retainer-ball assembly. If the fluid does not completely exhaust, there can be partial engagement (GM Powertrain, 2007).

According to Kluger et al. (1996), hydraulic pumping systems commonly used can account for up to 20% of the total parasitic losses in a typical automotive automatic transmission during the Environmental Protection Agency (EPA) city cycle. Moreover, Kluger et al. (1996) reported that the pumping pressure, fluid temperature and component clearances had the largest influences on pump leakage. In their paper, Kluger et al. evaluated several pumping systems on the basis of their mechanical efficiency, volumetric efficiency, pumping torque, discharge flow and overall efficiency. Hysteresis pressure losses have been commonly found in brake actuation systems and have been identified as another energy sink in hydraulic systems (Tretsiak et al., 1975). Besides these losses, unavoidable head losses inherent in fluid flow in line channels are a consistent drawback of hydraulic actuation.

**1.2.3 Research Landscape.** Several automotive researchers have focused on the development of electromechanical systems in powertrains. Electric power is readily available in most powertrains, especially in hybrid transmissions. “Drive-by-wire” technology has gained tremendous importance as the demand for high efficiency in automotive transmissions continues to rise. Electromechanical systems boast several benefits such as compactness, simple controls, fast response and reliability. Numerous electromechanical actuators for clutches and brakes have been designed. Generally, the actuator force is provided by an electric motor and a torque-to-thrust converter. Intricate mechanisms for torque-to-thrust systems have involved a worm-gear-crank (Moon et al., 2004), a ratchet ring (Treder and Woernle, 2004), a mechanical wedge (Yao et al., 2010), and a unique self-energizing mechanism (Kim and Choi, 2011). In order to provide high clamping forces from low-torque motors, designers have used a gearing system in conjunction with the electric motor (Line, Manzie and Good, 2004; Hoseinnezhad, Bab-Hadiashar and Rocco, 2008; Jo, Hwang and Kim, 2010). Furthermore, some researchers have also explored electromechanical systems using piezoelectric actuators in providing very high clamping forces (Xu and King, 1998; Thornley, Preston and King, 1991; Neelakantan, Washington and Bucknor, 2008).

Electromagnetic systems based on eddy-currents have found widespread automotive applications. These systems have been used, for example, as reliable industrial variable-speed drives (Bloxham and Wright, 1972). Lee and Park (1999) reported on the robust control of eddy-current brakes in vehicles, which allows for a more powerful and reliable braking system. An eddy-current brake system with constant torque control, used in high-speed railway trains, was analyzed by Ryoo et al. (2000). Magnetic brakes based on eddy-currents are used in almost all state-of-the-art roller coasters (Pendrell et al., 2012).

Electric motors have a very wide operating range, but that does not imply that they are equally efficient at every speed and torque level. The torque curve of a typical traction motor is well suited to vehicle propulsion, having maximum torque up to the base speed and a wide constant power region above the base speed. However, there is a sweet spot, typically at medium speed and medium-to-high loads, where the delivery of power is most efficient. A choice of gear ratios allows the motor to be kept in this operating region for the majority of the drive cycle, thus resulting in better performance and higher battery life (Wu, Zhang and Dong, 2013). All transmissions, hybrid or otherwise, employ range and brake clutch packs (Eberleh and Hartkopf, 2006; Lhomme et al., 2008; Estima and Marques-Cardoso, 2012). Brake clutches are actuated hydraulically (Chen et al., 2003), while braking torque is produced by coupling the rotating member to a fixed end (Zagrodzki, 1990). In HEVs, electric motor spin losses occur by virtue of spinning inactive motors that carry permanent magnets (Syed et al., 2006). There are several techniques for minimizing these losses, such as gap-flux weakening (Daun, Zhou and Wang, 2013), among others. However, the simplest approach is to limit the speed of the motors using gearing and to completely disengage the motors via clutches when motor torque is not needed (Bertoluzzo and Buja, 2011; Mapelli, Tarsitano and Mauri, 2010).

### 1.3 Thesis Overview

Designing an automotive clutch that warrants a change in technology requires one to start with a clean slate. In Chapter 2, an attempt is made at providing techniques for designing automotive clutches. The techniques are built within the framework of systematic design which are applied to clutch designs. Design concepts are generated, synthesized and then short-listed. Four design concepts are subjected to evaluation,

following which, the top two concepts are embodied and developed for two different clutch applications.

In Chapter 3, the embodiment of the *electromechanical clutch* (EMC), based on a high-performance screw joint and a built-in locking mechanism for clutch actuation is described. This clutch can be applied to a range clutch requiring a translational actuation. The chapter gives the background on its comparable existing technology. The concept is divided into two sub-variants, the lead screw and the ball screw, which are designed in detail for prototyping. Finite-element analysis is conducted to ensure that the system is readied for proof-of-concept tests.

In Chapter 4, both EMC sub-variant systems are analyzed. The actuation system is mathematically modelled. A novel feature in the modelling of the clutch-pack stiffness with variable stiffness is shown. A simulation of the EMC testbed model is carried out. Experimental tests of the two sub-variants are conducted, the results then compared to simulation data. Additionally, parameter estimates are also obtained for Coulomb friction.

In Chapter 5, a design based on an electromagnetic system is introduced for brake-clutch applications. Specifically, the clutch is designed to be applied in clutched electric motors in HEVs or EVs for next-generation propulsion systems. The design, dubbed *electromagnetic dog clutch* (EDC), includes an electromagnetic synchronizer and a synchronizing sleeve. Here, too, the EDC concept is developed with two sub-variants; one utilizing permanent magnets on the rotor, the other using a steel rotor. Novel design modifications to the former sub-variant are proposed to yield a better product.

In Chapter 6, the second sub-variant of the EDC system is developed. An electro-magneto-mechanical model of the electromagnetic synchronizer design is formulated. Using finite element magnetic software, simulation of the electromagnetic field is

## CHAPTER 1. INTRODUCTION

carried out to evaluate the design. Materials for mass-production are also evaluated. The design is machined and mounted on a testbed which provided the proof-of-concept tests.

At the end of the thesis, conclusions and recommendations for future research are given in Chapter 7.

## CHAPTER 2

---

# Clutch Design Techniques

In simplest terms, design is about thinking. Creative ideas may come from anywhere, but pulling all the ideas together into something that works requires thought more than anything else. This chapter presents techniques that help stimulate and/or give structure to one's thinking. The underlying framework is based on the *systematic design* process. The words of the chapter title were chosen carefully to emphasize design as a creative process, whereas words like methodology and procedure imply strict adherence.

Handbooks on machine-element design or gearbox design help engineers select different pre-existing clutching systems (Stokes, 1992). However, producing designs from the ground up leads to a higher probability of invention and innovation. The work done here showcases the creative thinking process capable of venturing into novel design concepts. At the end of the chapter, a summary of the techniques observed in the clutch design process is outlined. This section is a brief exposition on the conceptual design of clutches, which is based primarily on the author's knowledge, thoughts and experience. It has been difficult to provide much substance beyond what may seem obvious to some.

## 2.1 Technical Specification

With a background study and clear understanding of wet clutches, information is gathered to aid in solving the design task. Technical specification set forth here apply to the specific clutches considered in this thesis, namely, a range clutch applicable to conventional automatic, HEV or EV transmissions, and a brake-clutch applicable only to HEV or EV transmissions. One important difference between clutches in HEV or EV transmissions and those in conventional automatic transmission is that the initial slip speed prior to engagement of HEV transmission clutches is altered by electric motors (Zhang et al., 2001). Slip speeds of clutches in conventional automatic transmissions depend on several factors such as the transmission lever diagram (Benford and Leising, 1981), desired gear shift and initial vehicle speed, to list a few.

The specifications are a set of quantitative conditions that designers use to judge the capability of the proposed device. Essential *design specifications* to be considered in the design of clutches are:

- Volume: A volume budget must be established. A front wheel drive (FWD) transmission (Lewis and Bollwahn, 2007) has to fit, along with the engine, transversely in between the frame rails of the vehicle. As such, the length restriction on a FWD transmission design is much more constraining. For a FWD hybrid transmission, packaging two motors, range clutches and a final drive in the allowable length becomes much more difficult (Hata et al., 2005). Hence, a hollow cylindrical section of an existing range clutch pack, as shown in Fig. 2.1, and a brake-clutch, as shown in Fig. 2.2, is used as the volume available.
- Inertia: The moment of inertia on both the input and output components can be  $0.05 \text{ kg}\cdot\text{m}^2$ . This, however, does not include the moment of inertia of the clutch components itself.

- Actuation power: Most vehicle batteries typically supply 12 to 14.4 V, while HEVs and EVs are capable of 42 V and higher (Karden et al., 2007). The hydraulic pump is capable of providing pressurized ATF for use.
- Operating Environment: Selection of high-strength, durable, minimal wear, and light-weight material is to be considered. The clutch will be contained within a transmission housing; an environment with ATF. Therefore, its comparability with ATF is important. Transmission temperature is maintained at around 100°C.



FIGURE 2.1. Range clutch pack with the transaxle

## 2.2 Quality Function Deployment

Quality function deployment (QFD) is predominately a graphical method that systematically examines components of the problem definition. QFD streamlines the client's requirements, and expresses them as measurable engineering design targets. QFD was first developed in Japan in the 1970s, and since has been popular as an important tool at the early design stage (ReVelle et al., 1998). The layout of the QFD

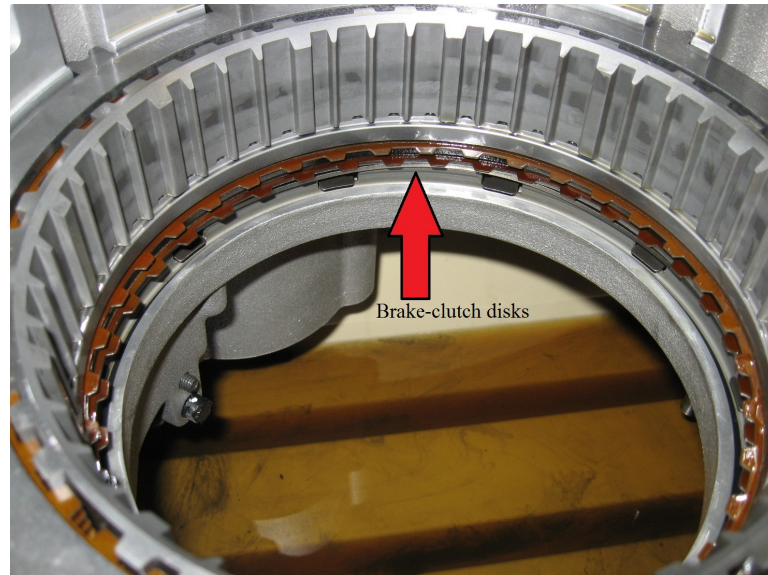


FIGURE 2.2. Brake-clutch assembly within the transmission

is often called the *House of Quality* and can be segmented into different categories (Hauser and Clausing, 1988).

A configured QFD diagram pertaining to the criteria set forth in the design task is shown in Fig. 2.3. The QFD outlines the client's requirements, engineering characteristics, client's priorities, technical difficulty, absolute importance and relative importance. The client's requirements, "*the whats*", are gathered through the client's statements and problem definitions. The engineering characteristics, "*the hows*", are measurable attributes with units that can satisfy the client's requirements. Using 9 to represent a strong, 3 a moderate one and 1 a weak relationship, the requirements are related to the engineering characteristics in a relationship matrix array. The *roof of the house*, dubbed correlation matrix, shows the interdependence of engineering characteristics. The client's priorities are rated on a scale of 1 to 5, where 5 means the highest importance. Absolute importance of each engineering characteristic is calculated by multiplying the numerical values of each cell of the relationship matrix

by the client's importance, and then summing all of its column entries. The relative importance is then calculated by normalizing the absolute importance to show which engineering characteristics have the greatest effect upon the client's satisfaction. Technical difficulty is an indication on the attainability of each engineering characteristic, and is measured on a scale of 1 to 5, where 1 indicates the lowest probability of success (Dieter, 2000).

The QFD generated for clutch design summarizes a large amount of information in one single robust diagram, providing the designer with the big picture of the identification, and translation of the client's requirements into engineering design specifications.

## 2.3 Functional Decomposition

To design any complex engineering device, its functions must be identified. Decomposing the system into subsystems that are easier to manage makes it convenient in design problem-solving. The advantage of functional decomposition is that it facilitates the investigation of options which are often overlooked when designer hastily selects specific physical principles.

Wet clutch packs provide the clutching functions conveniently and hence, they have been widely used. *Functions* are set forth *at the highest possible level of abstraction* with the intention of preventing the introduction of artificial constraints that would bias the creative-thinking process of the designer. The overall function of the clutching mechanism that needs to be accomplished is power transmission from its input to its output. The subfunctions involved in the overall function of a clutch are listed below:

CHAPTER 2. CLUTCH DESIGN TECHNIQUES

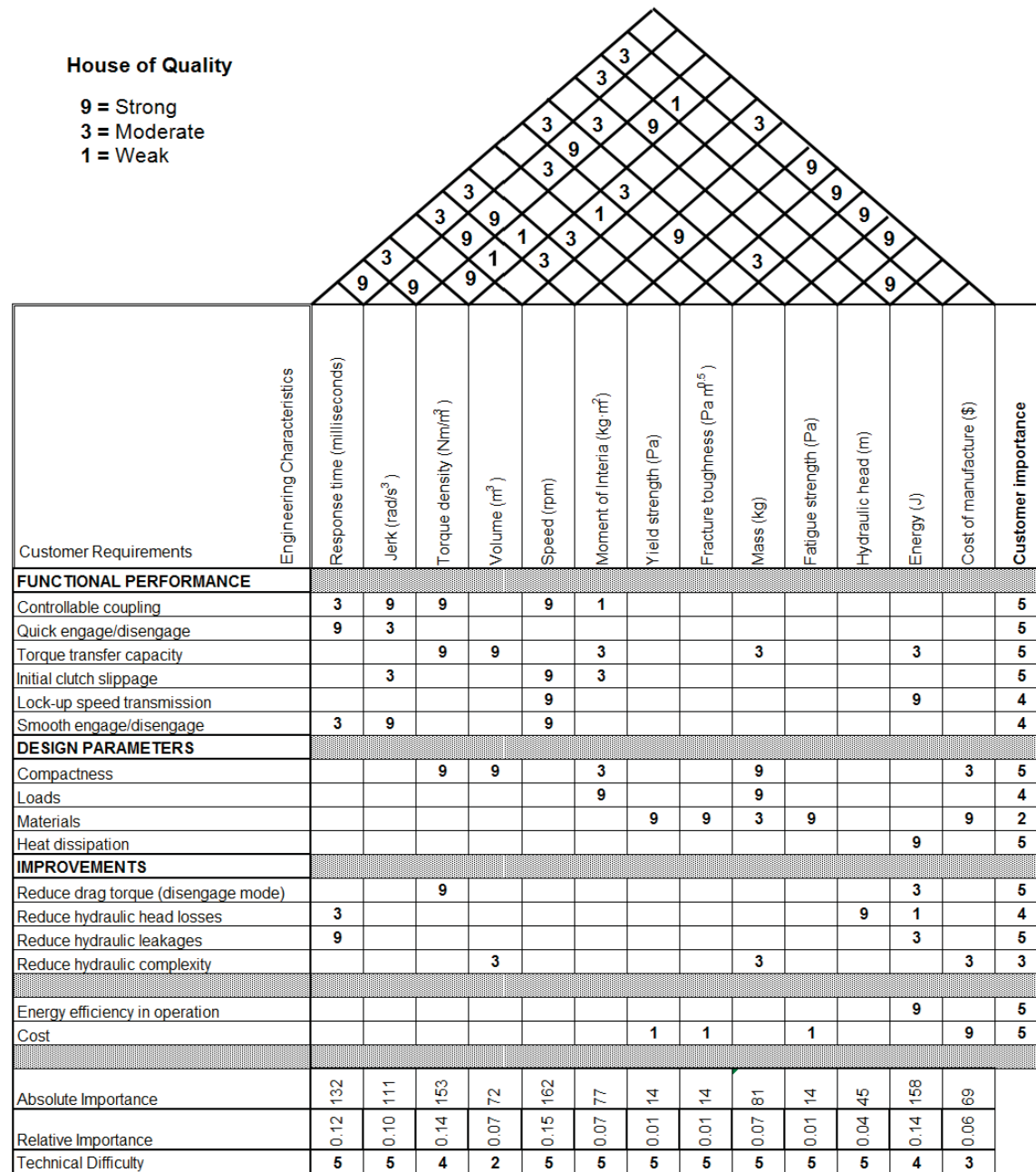


FIGURE 2.3. House of Quality diagram for clutch designs (Hauser and Clausing, 1988)

- Coupling: The clutch can function either as a brake or as a torque- and speed-transmitter. It must provide controllable coupling for variable *duty cycles*.

- Response: The time response of coupling or de-coupling must be agile. The response is usually measured from the instant the actuation system is triggered until the termination of the full engagement/disengagement.
- Torque density: The clutch must be capable of high torque transmission. The magnitude of torque must be capable of bearing vehicle loads. Depending on the type of clutch, torque capacity is to be specified at the outset. Moreover, the torque density must be maximized within a prescribed volume.
- Speed transmission: Initial relative speeds between the input and output members of the clutch is called *clutch slippage*. The clutch must engage with an initial slip to a state of zero slip, i.e. *lock-up*. Subsequently, the clutch must maintain lock-up and be capable of transmitting high rotational speeds or, when used as a brake-clutch, to prevent any rotation of the input component.
- Transition: Clutch slippage must be controlled in order to couple/decouple smoothly. The high inertial loads of the vehicle, if subjected to a sudden speed discontinuity, are bound to produce undesirable vibration and jerk.

## 2.4 Conceptual Design

A designer must proceed to produce concepts that will aim to solve the issues within the technical specifications at hand. Here *form follows function*, where, with a proper understanding of the functions of the design problem, the solution follows readily. By balancing creativity and experienced problem-solving approaches, the designer is capable of synthesizing ideas and meaningful concepts. The most common method of idea generation was publicized by Osborn (1953). He proposed the technique of *brainstorming*, capable of generating a large number of solutions to a

problem. Osborn believed, and the author of this thesis strongly agrees, that group brainstorming sessions can double the number of creative solutions generated by a group. Applying these group-dynamics techniques, the author collaborated with other researchers to establish a set of design alternatives for clutches.

**2.4.1 Set of Design Variants.** For the sake of completeness, all ideas, whether viable, suitable, “wild” or “out of the box”, that display the creative thinking of the brainstorming sessions, are briefly documented. Unless otherwise specified, the actuation of the clutch alternatives below is left open to electromechanical, electric, pneumatic, or even improved hydraulic methods; this will be further decided on during the selection of the design variant.

Idea # 1: Dry clutch: uses a resilient friction material. Since spin losses are caused by the viscous forces present in the ATF that floods the clutch assembly, one could consider removing the fluid altogether.

Idea # 2: Wet on-demand clutch: controls the volume of ATF within the clutch pack. At the outset, it is noted that ATFs play a vital role in cooling, corrosion-preventing, vibration-damping and wear-reduction on the friction plates. When the clutch is disengaged, empty the chamber of the ATF and flood it right on engagement.

Idea # 3: Single-cone clutch: replaces the multi-disks pack with a single cone disk. A conical surface provides a large contact surface area, for a given axial length, than its cylindrical counterpart. High torque transmission is thus possible with a reduction in drag torque (Froslic, Milek and Smith, 1973). Actuation is left open to electric or even piezoelectric means.

Idea # 4: Air torque convertor: works as a pneumatic coupling. Similar to conventional torque converters, a compressible fluid, namely, air, or any other gas for that matter, can be used instead of the typical incompressible viscous

ATF. Pressurizing the gas is necessary to transmit the torque for engagement, while lowering the gas pressure would result in disengagement.

Idea # 5: Magneto-rheological fluid (MRF) clutch: allows the fluid viscosity to be changed upon application of a magnetic field. Magnetic particles suspended within the fluid are mutually attracted on the application of a magnetic field, which allows power transmission. Consequently, the clutch could be actuated electrically (Rabinow, 1948). MR fluids have been found to be applicable in low-torque, fan-drive systems for automotive use (Smith and Kennedy, 2007).

Idea # 6: RURUR<sup>1</sup> clutch linkage: uses a four-bar linkage to transmit motion. A special linkage can produce a clutch effect when the linkage is designed as a constant-branch linkage (Liu and Angeles, 1992). The clutch effect is deemed “disengaged” in the constant-branch mode, wherein the output link remains stationary while the input link turns as a crank. With a small change in its geometry, e.g., by changing the length of a link, the linkage can switch out of constant to the nonconstant-branch mode, thereby producing clutch engagement and allowing motion to be transmitted via the double-crank linkage. A spatial RURUR linkage is proposed to function as a clutch linkage as discussed in Appendix A.

Idea # 7: Pneumatic-spring clutch: uses air to provide a cushioning effect that dampens impact occurring on the engagement. This clutch would work as a dry clutch with an air medium, where the air behaves as a pneumatic spring. Pneumatic valve springs are widely used as they offer an operation smoother than springs made of solids (Palej et al., 1993). Shown in Fig. 2.4, is a sketch of a potential pneumatic spring clutch that would work as follows: in order to produce a gear change, the clutch actuating force is subdued, allowing

---

<sup>1</sup>R denotes a revolute pair and U denotes a universal joint.

the return springs to pull the driven clutch plates and backing plates away from the driving plates. During this event, an external air compressor will

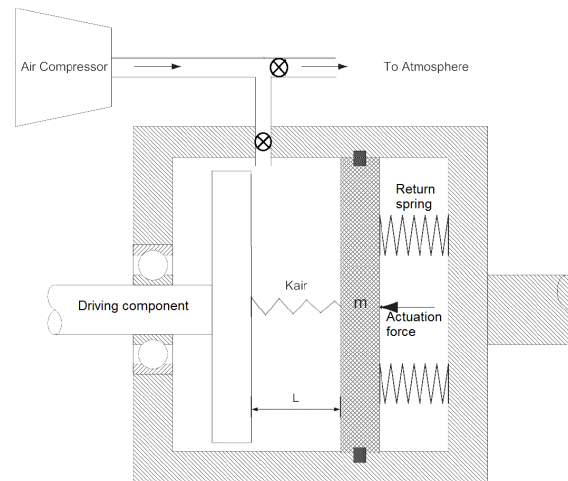


FIGURE 2.4. A schematic of a pneumatic-spring clutch

pressurize the chamber with air. When the clutch chamber has reached the desired pressure, a chamber valve is closed, sealing the system from the outside environment. Next, the actuating force will be applied to bring the clutch plates together. The chamber valve will regulate the air pressure between the clutch plates in order to allow the air to dampen axial impact.

Idea # 8: Eddy-current clutch: uses controllable magnetic induction to provide coupling. It can function as an eddy current clutch or brake. The system would consist of a set of electromagnets on one member and a non-ferreous conductor on the other member, separated by an air gap (Bloxham and Wright, 1972). A varying magnetic field generated by the electromagnets would induce eddy currents on the conductor. The generation of eddy currents would result in the production of torque which is either transmitted or used as a brake.

Idea # 9: Magnetic coupling: requires permanent magnets (PMs) that align over an air gap where, on turning one member, the other member would follow. The

strength of the coupling lies on the magnetic flux density and the air gap distance. By effectively increasing or decreasing the air gap size, coupling and de-coupling can be achieved, respectively. Strong PM material would be essential, with a likely choice being: Neodymium Iron Boron (Nd-Fe-B).

Idea # 10: Synchronous electromagnetic clutch: consists of PMs on one member and electromagnets on the other, separated by a small air gap. Here, actuating the clutch would be achieved by carefully activating the electromagnets, which would align its poles with the permanent magnetic poles, thereby transmitting motion synchronously.

Idea # 11: Dog clutches: couples the input and output components by interference. Using a shift fork, the splined synchronizer sleeve is slid partly over from the synchronizer hub to engage with the drive dogs of the gear, thus forming a rigid coupling. Mechanical dog clutches are widely used in manual transmissions (Lovas et al., 2006). Dog clutches do not require an external force to maintain the lock-up and to transmit torque. Automating the actuation of the shift fork with electric, pneumatic or even hydraulics could render them applicable in HEV transmissions.

Idea # 12: Iris clutch: uses a mechanism that can change its diameter. Common examples are observed in camera lens apertures and a rugged iris mechanism as used by NASA (2001). The mechanism consists of overlapping blade-like sheets connected at the bottom by a roller-slider assembly. These overlapping sheets would slide and rotate in order to close or open its diameter (NASA Tech Briefs, 2001). This could be applied as a clutch where the varying diameter could grip or release a shaft.

Idea # 13: Spiral jaw clutches: uses sloping surfaces that allow for engagement at a slip speed. The system consists of spiral teeth, with a ramp mechanism that

would lock into mating recesses in the facing member. It would provide a positive lock, and could operate only in one direction.

Idea # 14: Translational screw clutches: uses a power screw to clamp clutch disks.

Similar to screw jacks and screw clamps, an *electromechanical clutch* can be designed with a power screw actuated by a compact electric motor. By constraining the rotational degree-of-freedom of the nut, rotations of a power screw would be converted into axial translation of the nut.

**2.4.2 Short List of Design Concepts.** A short list of the design concepts from Subsection 2.4.1 is needed to effectively evaluate them, for which a designer is forced to eliminate some conceptual candidates at this preliminary stage, with limited knowledge on the ideas. To this end, an initial screen to filter out unfeasible ideas is put forth. Initially, ideas: 1–5, 7, 9, 12 and 13 were eliminated.

Ideas 1–3 were found impractical for automated use, as they fail to provide a smooth, jerk-free operation. Excessive heating results in decomposition of resin-based friction material and leads to a rapid decline of dry-friction coefficients, as reported by Haung et al. (2010). High abrasive and adhesive wear in dry clutches are extremely hard to reduce. Furthermore, using a conical interface increases the contact area, consequently increasing adhesive friction, which makes swift disengagements difficult in cone clutches (Orthwein, 1991).

An air coupling (idea 4) would require compressing air to pressures as high as 70 MPa, which can be shown to be highly inefficient. Although drag torque would be greatly reduced; however, other losses commonly seen in torque convertors would arise. MRF clutches (idea 5) require large clutch sizes for the high torque capacities. It has been found that iron particles, being dense, tend to settle. They require re-dispersing within the fluid medium. Moreover, for high torque and high stress

applications, field-induced changes in rheological properties require high current levels (Klingenberg, 2001).

Pneumatic spring clutches (idea 7) failed to qualify, as the pressurized air in the clutch chamber did nothing to dampen torsional vibration in the power train, also known as the clutch *shudder*, sometimes as *judder*. Judder, a well-known phenomenon in dry clutches, is a friction-induced vibration between two masses with sliding contact. These effects introduce undesirable dynamic loads, increase slip and wear effects, besides reducing driver comfort. Moreover, the dampening of impact seemed redundant, as cushion spring plates in current dry clutch packs are capable of better performance.

The controllable magnetic coupling (idea 9) would require large forces to pull apart the PMs on the input and output components designed for high-torque applications. Moreover, in order to reduce magnetic spin losses, the air gap separation would have to be large, thus resulting in large volume requirements. Air gap control in PM devices is relatively complex, rendering it unsuitable to pursue further.

Interestingly, ideas 8 and 10 were both competent concepts but needed a lock-up mechanism. Dog clutches (idea 11) have conical contact surfaces that allow for the mechanical synchronization of input and output components. Under high torque and inertial loads, disengagement of such an interface would be extremely difficult. Moreover, the synchronizing sleeve that engages with the drive dog teeth will not be able to conveniently mesh. The concept on its own cannot be applied to automated clutch shifting, as the relative slip between the input and output clutch component need to be synchronized. Therefore, ideas 8 and 10 can be combined with idea 11 to yield two novel concepts that would operate under two sequential modes: 1) an electromagnetic synchronizer; and 2) a dog-clutch lock-up. The electromagnetic

synchronizer can be designed to be an eddy-current drive (idea 8) or a synchronous electromagnetic clutch (idea 10).

Spiral jaw clutches (idea 13) can engage with a certain slip speed; however, their disengagement/engagement under high torque transmission would be unfeasible. Idea 12 is an iris mechanism consisting of blade-like flaps; it would be incapable of initiating and maintaining lock-up because it would not be able to provide sufficient clutching force and there would be not enough contact area to support the torque required. Moreover, the blades would provide a fragile arrangement and thus would not be durable.

Following an initial analysis, the set of design variants chosen to consider for the evaluation stage were

- (i) RURUR clutch linkage
- (ii) Eddy-current dog clutch
- (iii) Synchronous electromagnetic dog clutch
- (iv) Electromechanical clutch

**2.4.3 Concept Evaluation.** The success of the design project rests mainly on answering most, if not all, of the client requirements, as summarized in the House of Quality matrix in Section 2.2. The next process in the conceptual design phase involves the evaluation of the concepts. The winning design concept is the one that fulfills all the client's needs, carries all functions and meets the engineering specifications at best. In order to identify the top concepts, the design concepts are subject to a criteria-based evaluation process. Here, after a more in-depth assessment, the unfeasible alternatives are eliminated, while retaining the top two feasible ones.

**2.4.3.1 Pugh Concept Selection Process.** A particularly reliable, well-known method of decision-making is the *Pugh concept selection process* (Dieter, 2000). This is a relative comparison technique where all concepts are compared to an existing

datum concept. The datum at hand is the wet multi-plate clutch pack used in current transmissions. Comparing each of the four concepts against the function criteria already established in the House of Quality and to the datum will allow the formulation of Pugh's decision matrix. The comparative evaluation is carried out by means of a + sign for each concept better, a - sign for each concept worse and a S for each concept about the same as the reference datum concept.

Table 2.1 shows the RURUR clutch linkage (CL), the eddy-current dog clutch (ECDC), the synchronous electromagnetic dog clutch (SEDC) and the electromechanical clutch (EMC) in a Pugh's decision matrix. The matrix shows that concepts 3 (SEDC) and 4 (EMC) contain the maximum number of + scores and the minimum number of - scores. However, these ratings are only a qualitative measure and cannot be solely used to select the best concept. Though this helps with comparing each concept, these were further investigated as described in Appendices A and B.

<b>Criterion</b>	<b>CL</b>	<b>ECDC</b>	<b>SEDC</b>	<b>EMC</b>	<b>Datum</b>
Response	+	+	+	+	S
Torque transfer capacity	-	-	+	+	S
Smooth engage/disengage	-	+	+	S	S
High speed transmission	-	-	S	S	S
Compactness	-	+	-	+	S
Inertial loads	-	+	+	+	S
Heat dissipation	+	-	+	S	S
Wear	+	+	+	S	S
Lower spin loss	+	+	+	S	S
Actuation improvement	+	+	+	+	S
Energy to maintain lock-up	+	+	+	+	S
Clutch mass	-	-	-	+	S
Manufacturing feasibility	-	+	+	+	S
Manufacturing cost	-	-	-	+	S
$\Sigma+$	6	9	10	9	N.A.
$\Sigma-$	8	5	3	0	N.A.
$\Sigma S$	0	0	1	5	N.A.

TABLE 2.1. Clutch concept evaluation using Pugh's method

An alternative evaluation process is the concept of *complexity* in the realm of design (Khan, 2007). Simply put, this evaluation process leads to the choice of the simplest alternative, where the complexity of a design candidate is quantified in terms of its *information content* (Shannon, 1948). A novel scheme, it still lacks an implementing methodology, for which reason it was not pursued. Here, Pugh's methodology provided an advantageous start.

**2.4.4 Design Concept Selected.** From Subsection 2.4.3.1, it is observed that concepts 3 and 4 were favoured. However, the elimination of other two is discussed here.

The analysis of the RURUR clutch linkage is given in Appendix A. On simulating a spatial clutch linkage, it was observed that with a minute perturbation in dimension, this linkage would snap out of the constant-branch mode, thus falling in the nonconstant-branch. This would produce catastrophic results if implemented in an automobile, where vibration is present. Moreover, the dimensions needed to be accurate to several nanometers. This would require the manufacturing of the linkage to be extremely accurate, making the linkage too expensive to fabricate and to maintain. Hence, this concept is unfeasible for automotive application.

The eddy-current dog clutch concept is short of the demands of a clutch application because the generation of eddy current in the rotor is velocity-dependent. At low speeds (<150 rpm), the magnitude of the eddy currents produced is small, which results in the production of a very low clutching torque and almost negligible holding torque (Liu et al., 2011). With a stationary rotor, the eddy-current generation is absent, thus creating no braking torque. This is seen in the simulation results reported in Appendix B, where the rotor slips continuously. Hence, the concept cannot be used at very low slip speed and in high-torque applications. Eddy-current designs with alternating current (AC) sources are employed to combat this but this tends to

generate high levels of thermal energy, thereby requiring additional cooling. Higher voltage, in excess of 13.8 V, is needed to produce a substantial magnetic field for the induction system.

The synchronous electromagnetic dog-clutch and electromechanical-clutch concepts remained as the top two candidates to be carried on to the embodiment stage.

## 2.5 Design Embodiment

The next stage after conceptual design, is *preliminary design*. Pahl et al. (2007) refer to this stage as *embodiment design*, an important step in the design process, where the design engineer realizes a reduced number out of the richer set of design variants generated at the conceptual stage. These are those that survived an elimination procedure in light of various conditions: feasibility; compliance with specifications; budgetary constraints; and so on. In the embodiment stage, most of the time is devoted to determining the physical architecture, configuring the various parts of the design and arriving at a final design with near-final dimensions (Dixon and Poli, 1995). It is a phase where the selected design variants from the conceptual design stage are laid out in physical form for further development. Simply put, one can summarize this stage as “adding flesh to the bones.”

The next four chapters detail the embodiment and detail design of each of the two selected design concepts. The designs were equally competitive; in discussions with the client team, a decision was made to develop the two design concepts in different clutching applications. The details of each clutching system include component selection, packaging, with overall design specifications laid out. Each design variant is tested in proof-of-concept tests to showcase their performance and feasibility. Both concepts feature novel technology that strives to produce efficient mechanisms, a quintessential requirement in the development of next-generation propulsion systems.

## 2.6 Summary of Techniques Applied to Clutch Design

Several factors are to be considered when designing clutches or brakes. A summary of the design techniques used in this thesis is given below:

- Determine the clutching-mechanism performance goals. This provides the motivation for the design task.
- Fully understand the existing clutch technology, in light of its performance capabilities.
- Establish a set of design specifications: torque capacity, slip speed, speed transmission, response time, and inertia loads.
- Automotive applications demand a compact solution. Therefore, a design volume must be identified. Subscribing the design to a restrictive volume budget is important, even in the early development stage.
- Assess applicable input power availabilities. Most automotive component designs favour the standard 14 V power capabilities. HEVs and EVs have higher voltage capacities; however, the use of higher voltage levels requires additional high-voltage DC bus architectures and wire mechanization (Anwar, Gleason and Grewe, 2010).
- Investigate several clutching interfaces, e.g., frictional, fluid—liquid or pneumatic, contactless—magnetism, linkage, etc.
- Clutch configuration can be radial, axial or a combination thereof. Explore all possibilities.
- Examine the actuation method. Some designs lead to obvious actuation means, such as electromagnetic; others are more open.
- With a set of design ideas, establish kinematic relations of each concept to understand the clutch operation.

## 2.6 SUMMARY OF TECHNIQUES APPLIED TO CLUTCH DESIGN

- Assess plausible feasibility of design concepts within all constraints, technical or financial, and then evaluate concepts.
- Produce design embodiments, mathematical models and virtual prototypes. Choose as many off-the-shelf components as possible while minimizing machining work. The latter yields lower cost and reduces production time. Detail design all machining components.



## CHAPTER 3

---

# Electromechanical Clutch Design

Several types of mechanical clutches are currently available: square jaw; sliding key; shoe-drum; plate (or multi-plate); cone; pawl and ratchet; wrapped spring; sprag-roller; cam-roller; and centrifugal clutches are all considered mechanical, i.e., their clutching interface is primarily a rough surface (Parmley, 2000). Power screws have been around for centuries and have widespread applications. Their ability to convert torque into thrust and self-locking capacity can be harnessed to develop a compact translational clutch actuator. The architecture of power screws lends to a “bolt-on, plug and play” scheme that is simple and reliable. In this chapter, the design embodiment of the actuators based on the power screw is described. It strives to minimize energy consumption in order to maintain clutch lock-up without additional power. The reduction in actuation energy is a highly desired feature in transmissions, especially when operating in higher gears for prolonged periods (Kim, Oh and Choi, 2012).

### 3.1 Actuator System Embodiment

The concept of the electromechanical clutch (EMC) actuator is realized from mechanisms that convert rotary motion into uni-axial translational motion. Shown

in Fig. 3.1 is a schematic diagram of the clutch actuator concept. The actuator system would require three subsystems, namely, an electrical-to-mechanical-energy converter, a torque-to-thrust converter, and a locking mechanism, to allow the actuator to remain in operation when the power supply is cut-off.

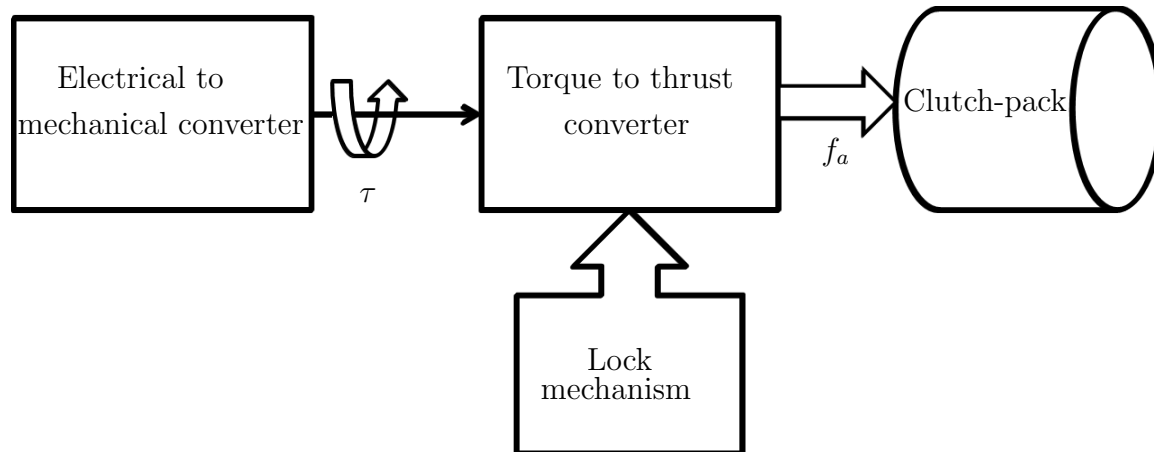


FIGURE 3.1. Schematic diagram of the clutch actuator concept

An electrical motor is used to convert electrical to mechanical energy for the first subsystem. Nearly all transmissions have an on-board DC power supply, which facilitates the use of DC motors. A power screw to convert rotary motion into axial stroke can be used as the primary actuating means for translating the clutching components. Parameters such as pitch, thread type, screw lead and lead angle, coefficient of friction on thread surface, pitch diameter, and load to move are essential in power screw design (Juvinal and Marshek, 2000). The third subsystem, i.e., a locking mechanism, creates two actuation embodiments, which are proposed here: 1) employing a *self-locking* lead screw assembly; and 2) using a ball-screw assembly in combination with a ratchet-and-pawl mechanism. Between the third subsystem and the clutch pack, an axial thrust bearing is required to allow the clutch disks to rotate independently from the actuation system. This lowers the effective moment of inertia

of the clutch pack, but does so at the expense of bearing drag at the thrust bearing. However, the two proposed clutch actuators would offer advantages such as a simpler design, lower power consumption, easy control, weight reduction, and lower power losses, when compared to existing hydraulic mechanisms.

**3.1.1 Lead-screw Design Layout and Operation.** One embodiment containing a self-locking lead power screw is laid out here. By virtue of its self-locking property, the coupling of the system is irreversible. This implies that a lead screw assembly can be designed such that the lead screw can drive its corresponding nut but the assembly would lock when the nut attempts to drive the lead screw (Mott, 2004).

Shown in Fig. 3.2 is an embodiment of a lead screw clutch actuator. This consists of a DC motor coupled to the lead screw shaft. The external threads on the latter mesh with the internal threads of the bronze nut, which slides within the transmission casing. The nut presses on to an *apply-plate*, which compresses the six pairs of clutch disks. A set of thrust and radial bearings supports the load-carrying components within the actuator assembly.

Note that a backing-plate is rigidly connected to the lead screw shaft as it accommodates a thrust bearing. This bearing takes up the axial reaction thrust load upon compressing the clutch-pack. A flange connected to the bronze nut accommodates the design to fit with another thrust bearing. Axial thrust is transmitted from the nut to the apply-plate through the thrust bearing. The apply-plate is designed such that it turns at the same speed as the clutch-pack, and can axially translate to compress/release the clutch disks. Moreover, a set of compression springs aids in the release of the apply-plate and provides a pre-load to the thrust bearings. By turning the motor-screw shaft assembly in the opposite direction, the nut-apply-plate assembly retracts, thereby disengaging the clutch-pack.

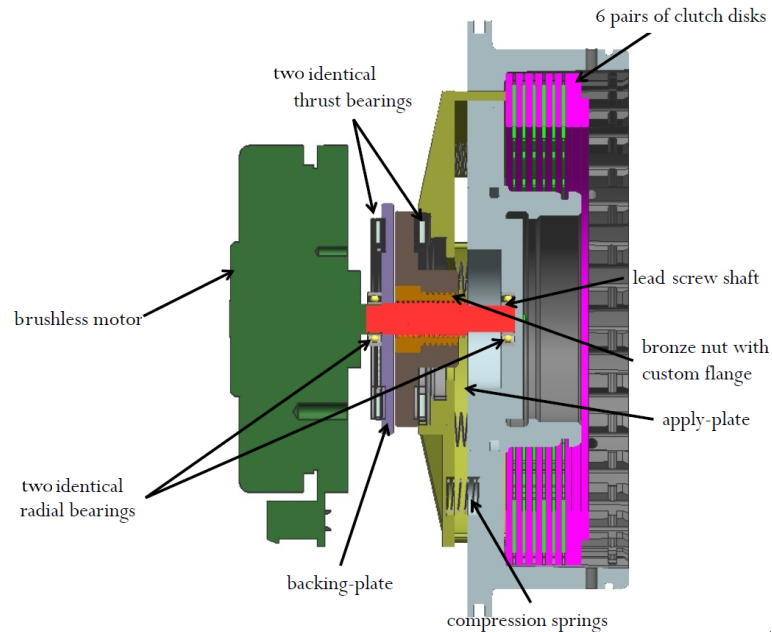


FIGURE 3.2. Cross-sectional view of the lead screw clutch-actuator embodiment

**3.1.2 Ball Screw Design Layout.** The second sub-variant of the clutch-actuator assembly has a similar layout and function as that of the lead-screw embodiment, but the configuration is different. The nut contains a plurality of small spherical balls that make rolling contact with the threads of the screw. This yields a low friction and a high efficiency system that provides fast dynamics. The actuator assembly consists of a DC motor coupled with a ball-screw shaft, as shown in Fig. 3.3. This shaft carries a ball nut over a set of spherical balls. The nut is constrained by the transmission casing to prevent rotation, but is free to slide axially. The ball screw-nut assembly converts motor torque into axial thrust. The latter compresses the six pairs of clutch friction-disks. A set of thrust and radial bearings supports the load-carrying components of the system, as shown in Fig. 3.3.

A ratchet and pawl mechanism is used to provide a lock on the rotating components. This allows elements to relatively rotate in one direction only, while preventing relative rotation in the other, by means of an opposing torque. This is implemented

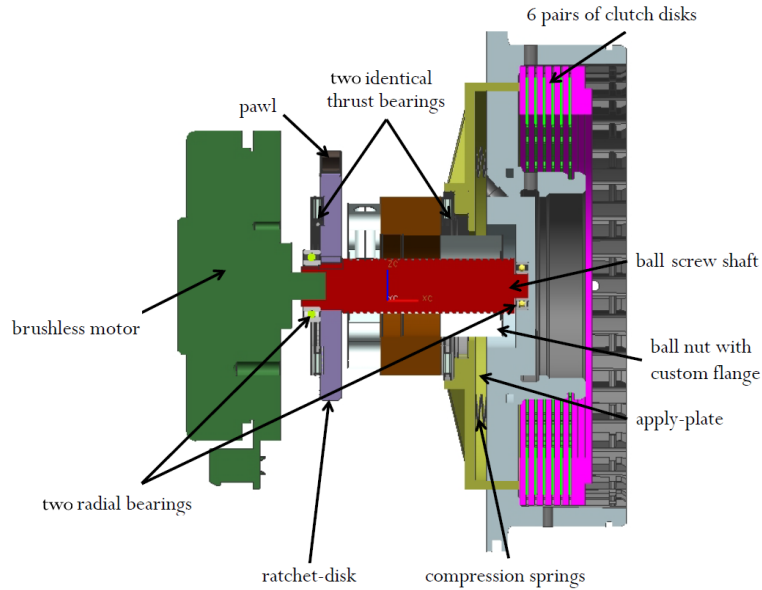


FIGURE 3.3. Cross-sectional view of the ball screw clutch actuator embodiment

by engaging a pivoting element, called a pawl, that latches onto the ratchet-disk teeth. The engaging end of the pawl is shaped to fit the ratchet tooth flank. The pawl is to be pivoted about a pin located on the casing. The pawl is independently actuated via a compact servo motor. The ratchet disk is rigidly coupled to the ball screw shaft and connected to one side of a thrust bearing.

Contrary to lead screws, ball screws are back-driveable, by virtue of the low friction in their screw interface. The ratchet-and-pawl system compensates for this feature. Once the primary DC motor produces enough torque and clamping force, the pawl engages the ratchet to maintain the torque/clamping force. Both actuators can then be powered off without losing clutch engagement. To disengage the clutch-pack, the primary DC motor would have to momentarily re-apply its required stall torque in order to remove the forces acting on the ratchet-pawl subsystem. The pawl can then be pivoted by its secondary stepper motor, to release the ratchet-disk, thus allowing the primary DC motor to spin the ball screw shaft in reverse to retract the ball-nut-apply-plate assembly.

## 3.2 Final Design

In designing the actuator, a volume is prescribed to house its mechanical components, not including the motor, as a 560 W brushless motor with its amplifier and controller was available at the *Robotic Mechanical Systems Laboratory* (RMSLab), McGill University. Hence, the design job focused on the torque-to-thrust system. Technical specifications, of Section 2.1, are fine-tuned to define the design volume, the clutch torque capacity for a typical range clutch, and the clutch clamping force requirements.

**3.2.1 Clutch Actuator Specifications.** Listed in Table 3.1 are the design specifications used for both the lead and the ball screw variants. The dimensions used in terms of volume of the actuator system were taken from a typical range clutch-pack assembly of an automatic transmission (GM Powertrain, 2007), as shown in Fig. 2.1.

Peak torque capacity $\tau$	500 Nm
Axial stroke $a$	2.4 mm
Number of clutch disk $n$	12
Coefficient of friction of clutch disk $\mu$	0.12
Clutch disk outer diameter $d_o$	121 mm
Clutch disk inner diameter $d_i$	100 mm
Clutch pack axial length $b$	37 mm
Actuator outer diameter	120 mm
Actuator axial length	60 mm
Lead screw lead	1.27 mm
Lead screw pitch diameter	8.89 mm
Ball screw lead	2.00 mm
Ball screw pitch diameter	15.00 mm

TABLE 3.1. EMC specifications

The axial clutch clamping force is directly proportional to the torque transmitted by the clutch, as a result of the torque generated by Coulomb friction forces distributed over the contact surfaces. For a disk clutch of inner and outer diameters

$d_i$  and  $d_o$ , respectively, under the assumption of an axial force  $f_a$  uniformly distributed over the contact surfaces, the torque transmitted is known to be given as (Mott, 2004)

$$\tau = \frac{\mu f_a (d_o^3 - d_i^3)}{3(d_o^2 - d_i^2)} \quad (3.1)$$

If  $n$  friction disks are in contact, the total torque capacity of the clutch increases by a factor of  $n$ . Taking this into account and rearranging eq.(3.1) yields the required axial clamping force for the clutch-pack in terms of the torque requirement as

$$f_a = \frac{3\tau(d_o^2 - d_i^2)}{n\mu(d_o^3 - d_i^3)} \quad (3.2)$$

Using the values from Table 3.1, the axial clamping force is computed as  $f_a = 6.28$  kN. Typical clutching operations need to take place within 500 ms. Parameters such as pitch, thread type, screw lead and lead angle, coefficient of friction on thread surface, pitch diameter, and load to move are essential in power-screw design (Juvinal and Marshek, 2000). Choosing appropriate lead-screw parameters, the mechanical advantage of the power screw would convert a low motor torque into a high clutch-pack axial thrust, without the use of an intermediate gear train.

**3.2.2 Compact Packaging.** Staying within the packaging volume budget is a major design challenge in the automotive industry. Although designing a clutch-pack to properly fit within a hybrid transmission is beyond the scope of this thesis, the proposed design is laid out as close to a commercial prototype as possible. Figure 3.4 showcases a compact design layout of the actuator of the two sub-variants without the motor. Both are constructed mostly with off-the-shelf components to minimize cost and prototyping time. Standard machine components come with rated load capacities and manufacturer warranties, which are favourable features.

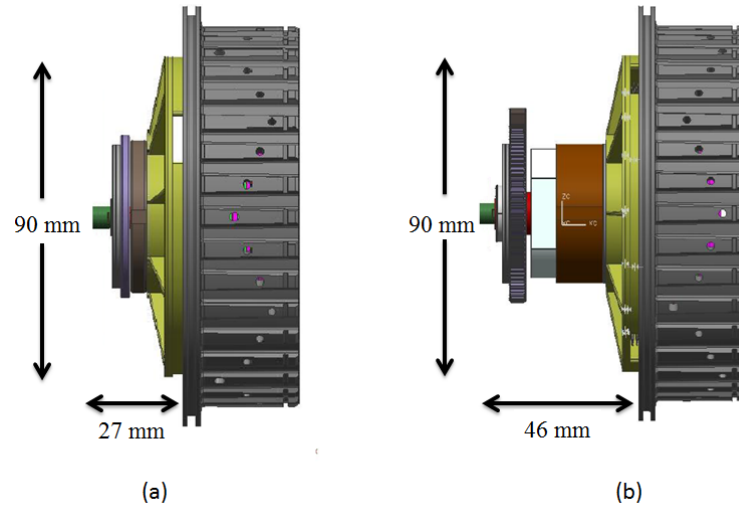


FIGURE 3.4. Packaging of: (a) the lead screw variant; (b) the ball screw variant

**3.2.3 Review and Details of the EMC testbed.** A testbed was set up to assess the performance of both screw variants. In order to keep costs to a minimum, most of the components for the testbed were designed such that only replacement of the lead-screw and ball-screw components were needed. Shown in Fig. 3.5 is an overview of the final CAD model of the entire testbed, while displayed in Fig. 3.6 is a cross-sectional view of the same model. The 560 W brushless motor was coupled via a flexible coupling to the screw shaft. A load cell mounted on the fixed end of the clutch-pack measured the thrust forces within the clutch disks. The flexible coupling, lead screw shaft and nut assembly, a radial and two thrust bearings, clutch-pack, clutch casing, and load cell were selected off-the-shelf.

All supports and adapters were machined out of Aluminum 6061-T6 alloy blocks. Static finite-element analysis (FEA) was conducted on each machined component to ensure that all components were capable of withstanding the high compressive loads. A safety factor of 2.0 was maintained. Detail drawings and FEA results are available in a technical report (Chopra et al., 2012). It is noteworthy that the testbed

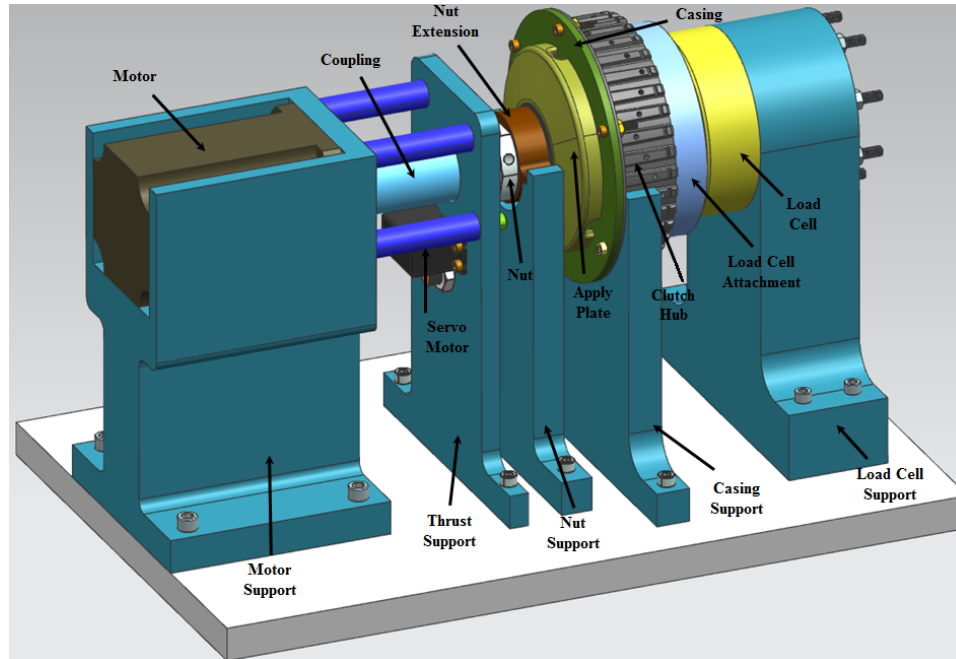


FIGURE 3.5. Front perspective view of the CAD model of the actuator testbed was designed for compressive clamping tests only, and hence dynamic, fatigue and durability analysis had not be carried out.

**3.2.4 Finite Element Analysis of the Apply-plate.** The apply-plate is a critical component of the design job as it transmits force from a small-diameter lead nut to a large-diameter clutch disk. A FEA of the plate is conducted with Unigraphics NX 7.5 Nastran<sup>1</sup>. The material selected was Aluminum 6061-T6 alloy, as it offered a relatively high yield stress, light weight (density 2700 kg/m<sup>3</sup>), and high machinability. The apply-plate is designed to be lightweight and bear high compressive loads. The apply-plate underwent several design iterations in order to ensure as uniform a stress distribution as possible. First, all sharp edges were rounded using circular fillets. The apply-plate geometry was analyzed statically using a compressive load of about 9 kN ( $> f_a$ ). The stresses within the apply-plate were observed to yield a safety factor of 1.88. A higher safety factor was desired while keeping the apply-plate as light as

<sup>1</sup><http://www.plm.automation.siemens.com/>

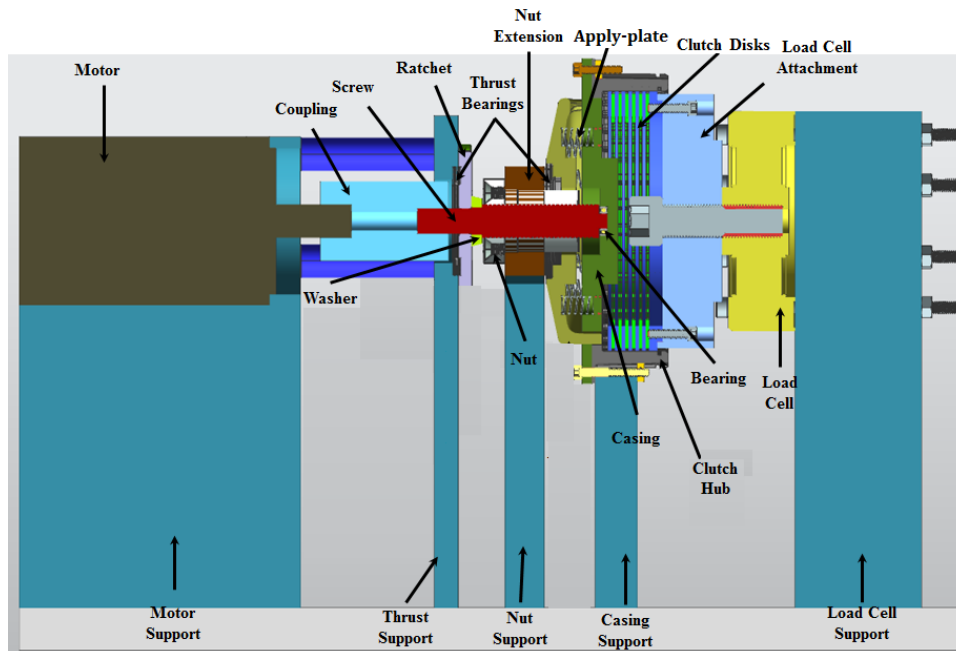


FIGURE 3.6. Cross-section of the clutch actuator testbed

possible. To this end, smooth blendings produced with Lamé curves (Gardiner, 1965) were used, as shown in Fig. 3.7. A  $G^2$ -continuous<sup>2</sup> geometry was achieved with 4th- and 8th-order Lamé curves. A combination of the two Lamé curves yielded an improved geometry, as shown in the FEA results of Fig. 3.8. The maximum stress developed provides a safety factor of 2.12, thereby showing the effectiveness of Lamé curves in reducing stress concentrations in regions where a line (or a plane) is blended with a curve (or a curved surface). A photograph of the machined apply-plate is shown in Fig. 3.9.

<sup>2</sup>Geometric continuity at blending points of tangent and curvature.

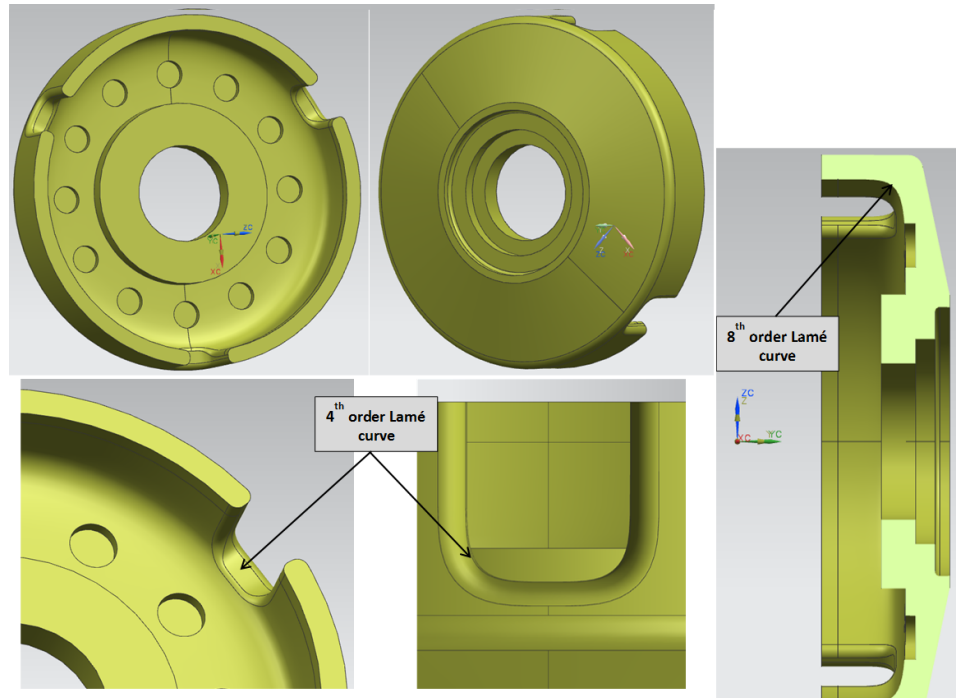


FIGURE 3.7. CAD model of the apply-plate

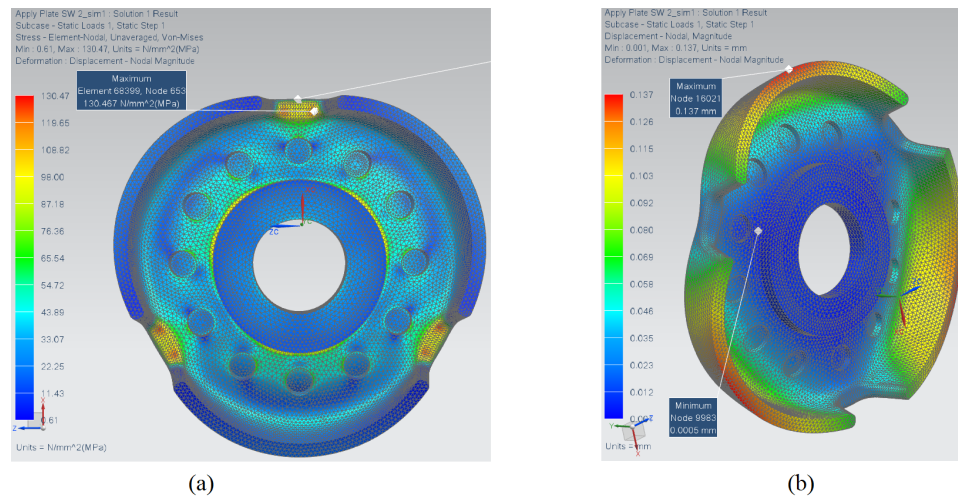


FIGURE 3.8. Apply-plate FEA results: (a) von Mises stress distribution; (b) Elastic deformation displacement plot

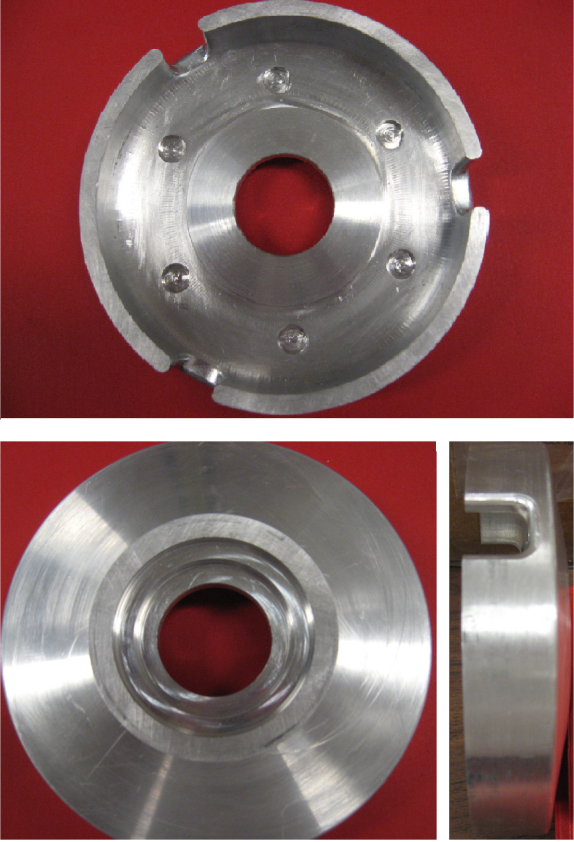


FIGURE 3.9. Front, back and side view of the machined apply-plate

## CHAPTER 4

---

# Electromechanical Clutch Modelling and Experiments

The design of the EMC actuator consists of its component selection, finite element analysis, and design for manufacturing. The latter targeted conditions for one single testbed, not for mass production. Here, the mathematical model of the actuator testbed is formulated based on its iconic model. A novelty feature lies in the modelling of the clutch-pack stiffness with variable stiffness to better reflect the behaviour of the clutch-pack: through independent testing, the clutch-pack stiffness was observed to increase exponentially in compression, similar to a hardening spring. Friction within the screw has a considerable impact on the performance of the actuator. To account for this, a Coulomb friction model whose coefficient of friction is a function of the relative velocity is introduced in the model.

It is noteworthy that the models for both lead and ball screws are essentially similar. The pitch diameter, lead travel, moment of inertia of the screw shafts, mass of the screw nuts, and frictional parameters are assigned according to the model and used correspondingly. Simulation of the model in each case, implemented in Matlab/Simulink, provided results that were compared to experimental data, to aid in

fine-tuning the model parameters. The experiments provide proof-of-concept results to demonstrate the capabilities of each design sub-variant.

Figure 4.1 shows the fabricated EMC actuator testbed and the individual mounting of the various components. The motor of the testbed was calibrated and tuned using the motor supplier's in-house software. The data-acquisition system was set up to command voltage signals to the motor amplifier in order to control motor current. The load-cell was originally calibrated by the supplier; however, independent tests were conducted to verify its parameters.

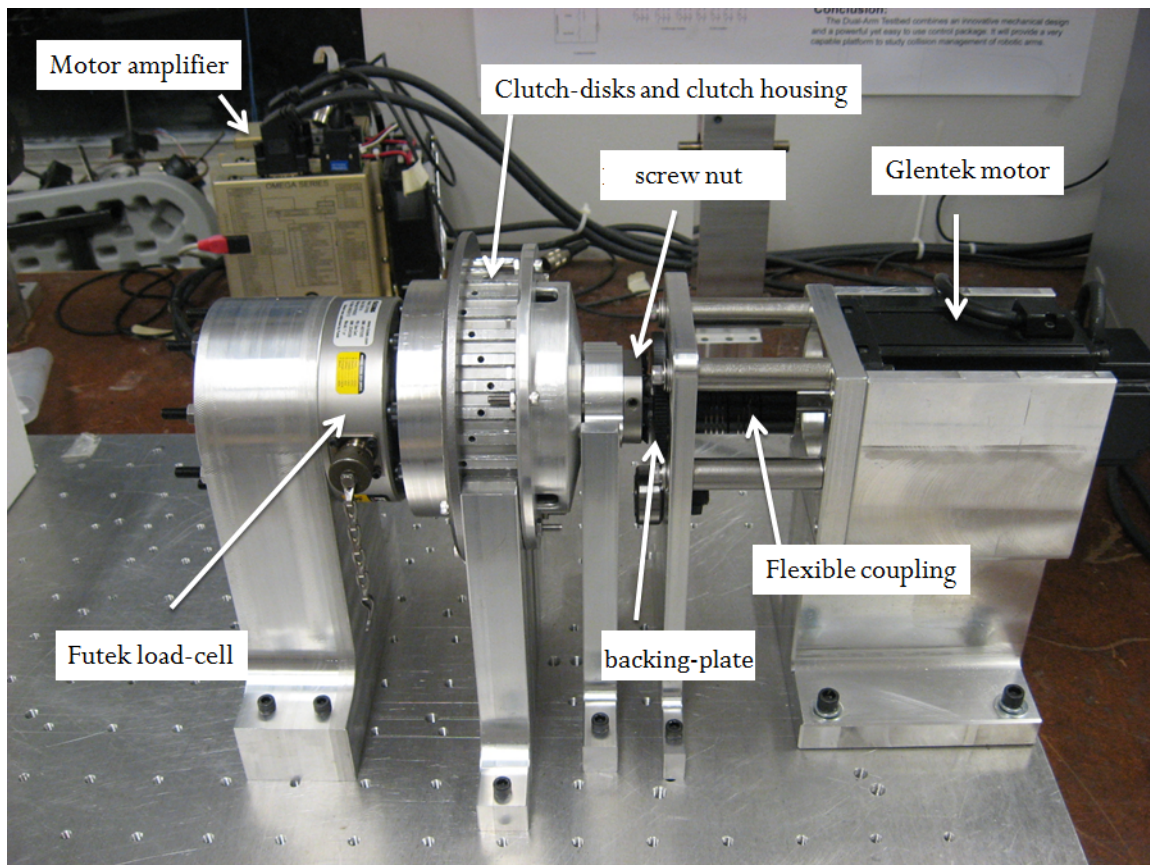


FIGURE 4.1. The electromechanical actuator testbed

## 4.1 System Modelling

First, an *iconic model* of the system is produced. Based on this, a mathematical model is formulated that captures the main features of the system.

**4.1.1 Iconic Model of the Electromechanical Actuator System.** The iconic model, shown in Fig. 4.2, integrates the various components of the design: clutch-pack, motor, coupling, bearing elements, and screw assembly. The stiffness and viscous damping of the thrust bearing between the nut and the apply-plate is ignored for modelling purposes. The nut, the apply-plate and the clutch-pack slide over various lubricated surfaces but still maintain solid-to-solid contact, which brings about Coulomb friction. A description of the parameters and variables of the model

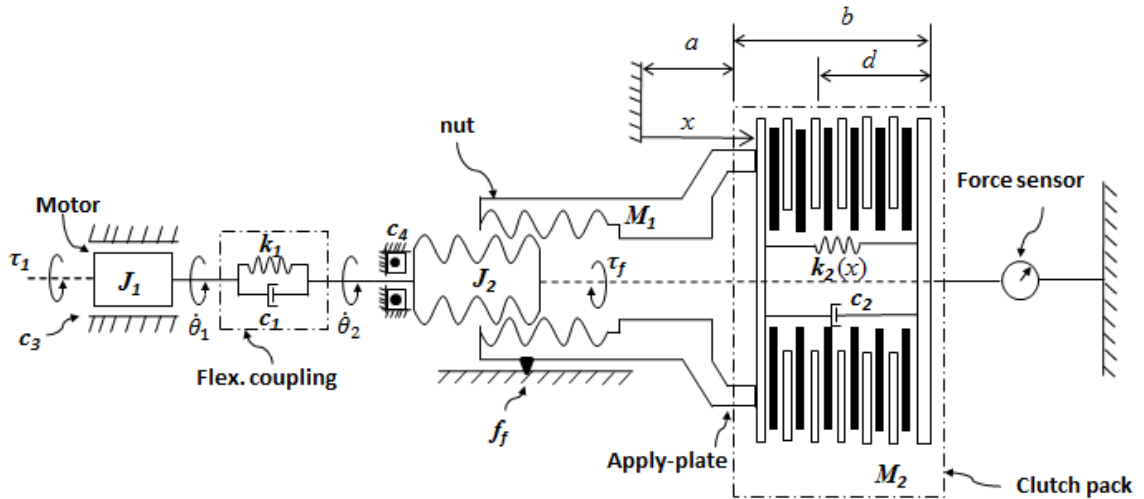


FIGURE 4.2. Iconic model of the electromechanical actuator

follows:

$a$ : value of  $x$  at which the apply-plate comes into contact with the clutch pack

$b$ : thickness of clutch-pack when unloaded

$c_1$ : coefficient of torsional viscous damping of the flexible coupling

$c_2$ : coefficient of viscous damping of the clutch-pack

- $c_3$ : coefficient of viscous damping of the motor
- $c_4$ : coefficient of viscous damping of the thrust and radial bearings that support the screw shaft
- $c_5$ : coefficient of viscous damping caused by the lubricant present within the screw threads
- $d$ : thickness of the clutch pack when fully compressed
- $f_f$ : Coulomb friction force due to the sliding of the nut, the apply-plate and the clutch-pack over their support surfaces
- $J_1$ : moment of inertia of the motor rotor
- $J_2$ : moment of inertia of the screw shaft
- $k_1$ : torsional stiffness of the flexible coupling
- $k_2(x)$ : variable stiffness of the clutch-pack
- $M_1$ : combined mass of the nut, flange, and apply-plate
- $M_2$ : equivalent mass of the clutch-pack
- $x$ : displacement of the apply-plate
- $\dot{\theta}_1$ : angular velocity of the motor shaft
- $\dot{\theta}_2$ : angular velocity of the screw shaft
- $\tau_1$ : motor torque ( $= K_\tau i_m$ ), with  $K_\tau$  = motor torque constant and  $i_m$  = motor current
- $\tau_f$ : Coulomb friction due to the sliding of the nut over the screw threads
- $\mu_s$ : coefficient of static friction
- $\mu_k$ : coefficient of kinetic friction

The relationship between screw rotation and nut displacement is given by

$$x = \frac{l}{2\pi}\theta_2 \quad (4.1)$$

where  $l$  is the lead of the screw thread.

**4.1.2 Modelling Assumptions.** Some assumptions are made in order to simplify the derivation of the mathematical model. All shafts, keys, plates and fasteners are assumed to be rigid bodies, and all bodies of the electromechanical actuator system are lumped into three rigid bodies: motor rotor shaft; screw shaft and the assembly of internally threaded nut with the apply-plate. The clutch-pack assembly is modelled as a deformable, viscoelastic body of equivalent mass  $M_2$ , internal viscous damping coefficient  $c_2$  and variable stiffness  $k_2(x)$ . The flexible coupling is assumed to be linearly viscoelastic.

**4.1.2.1 Friction Model.** The generalized forces arising from friction, torque  $\tau_f$  and force  $f_f$ , are defined by Coulomb friction with the *Stribeck effect* (Armstrong-Helouvry, 1991). Coulomb friction occurs where there is relative motion between solid bodies in direct contact. The stiction frictional torque  $\tau_s$  and force  $f_s$  hold out the applied torque  $\tau_a$  and force  $f_a$ , right up to and including  $\tau_s$  and  $f_s$ . Thus,

$$\tau_f = \begin{cases} \tau_v & \text{if } \dot{\theta}_2 \neq 0 \\ \tau_a & \text{if } \dot{\theta}_2 = 0 \text{ and } \tau_a < \tau_s \\ \tau_s \operatorname{sgn}(\tau_a) & \text{otherwise} \end{cases} \quad (4.2a)$$

$$f_f = \begin{cases} f_v & \text{if } \dot{x} \neq 0 \\ f_a & \text{if } \dot{x} = 0 \text{ and } f_a < f_s \\ f_s \operatorname{sgn}(f_a) & \text{otherwise} \end{cases} \quad (4.2b)$$

where  $\tau_v$  and  $f_v$  are the velocity-dependant friction torque and force, correspondingly. Moreover,  $\tau_v$  and  $f_v$  are given by

$$\tau_v = [\tau_k + (\tau_s - \tau_k)e^{-|\dot{\theta}_2|/\dot{\theta}_s}] \operatorname{sgn}(\dot{\theta}_2) + c_5 \dot{\theta}_2$$

$$f_v = [f_k + (f_s - f_k)e^{-|\dot{x}|/\dot{x}_s}] \operatorname{sgn}(\dot{x}) + c_2 \dot{x}$$

with  $\tau_k$  and  $f_k$  defined as the kinetic friction torque and force;  $\dot{\theta}_s$  and  $\dot{x}_s$  are the *Stribeck angular velocity* and *Stribeck translational velocity*, respectively. Note that  $\tau_s(f_s)$  and  $\tau_k(f_k)$  are dependent on parameters  $\mu_s$  and  $\mu_k$ . A plot of the Coulomb friction torque (force) model is displayed in Fig. 4.3.

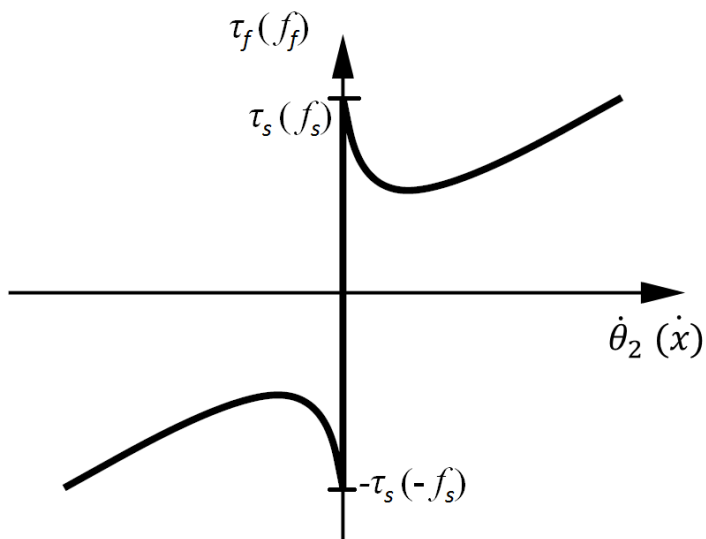


FIGURE 4.3. Coulomb friction torque  $\tau_f$  and force  $f_f$

4.1.2.2 *Clutch-pack Stiffness.* The clutch disks are made up of alternating steel and friction disks. The soft paper-based material used in the friction disk is deformable. The clutch disks are usually not completely flat, i.e., they carry a certain degree of waviness (Fatima, Marklund and Larsson, 2013). Numerical and experimental tests have shown that the clutch-pack stiffness increases exponentially with an increase in compressive force (Sfarni et al., 2011). By fixing one end of the clutch pack, the clutch disks are compressed; force and displacement data are readily obtained. The variable clutch-pack stiffness is observed to behave as a hardening spring. Therefore, the model for a hardening spring with the clutch-pack stiffness is given by

$$k_2(x) = A_1 \kappa(x) \quad (4.3a)$$

where  $A_1$  is an empirical parameter with units of N/m, while  $\kappa(x)$  is defined by

$$\kappa(x) = \tan\left(\frac{\pi}{2} \frac{x-a}{b-d}\right) u(x-a) \quad (4.3b)$$

with  $u(x-a)$  denoting the unit step (Heaviside) function applied at  $x=a$ . Shown in Fig. 4.4 is a plot of  $\kappa$  versus  $\eta \equiv x/a$ , with  $\eta_{\max} = (a+b-d)/a$ .

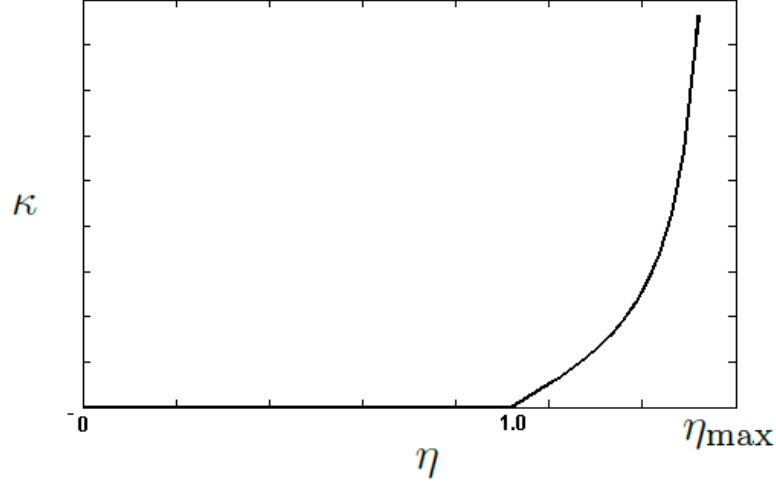


FIGURE 4.4. Plot of  $\kappa$  versus  $\eta$  plot

**4.1.3 Derivation of the Mathematical Model.** In formulating the system model, it is pertinent to note that the current commanded to the brushless DC motor is controlled by an amplifier. Motor-amplifier tuning was conducted prior to the beginning of the experiments. Hence, the electromechanical dynamics of the motor is not included in the model.

In order to formulate the governing equations of the mechanical system at hand,  $\mathbf{q}$  is defined as the vector of *independent* generalized coordinates. The Lagrange equation of the system can then be written in the form (Meirovitch, 1967):

$$\frac{d}{dt} \left( \frac{\partial L}{\partial \dot{\mathbf{q}}} \right) - \frac{\partial L}{\partial \mathbf{q}} = \boldsymbol{\phi}_f - \boldsymbol{\phi}_d \quad (4.4)$$

with the notation below:

$L$ : the Lagrangian of the system, given by  $L = T - V$

$T$ : the total kinetic energy of the system

$V$ : the total potential energy of the system

$\phi_f$ : the two-dimensional vector of generalized input torque contributed by the current-controlled motor,

$\phi_d$ : the two-dimensional vector of generalized dissipative torque, associated with all the viscous and Coulomb-friction forces and torques in the system

$q$ : the two-dimensional vector  $[\theta_1, \theta_2]^T$  of independent generalized coordinates

In deriving the kinetic energy of the clutch plates in series, one must notice that not all plates translate the same distance. That is, for a clutch-pack consisting of  $n$  pairs of disks, the disk-pair closest to the actuator end moves by a distance  $x$ , while the disk-pair closest to the fixed end is assumed to move by a distance of about  $x/n$ . Following this notion, the translation of each disk-pair in series is represented as  $i(x/n)$ , where  $i = 1, 2, \dots, n$  (Chopra, Smith and Angeles, 2013). The clutch-pack used on the testbed is composed of six steel and six friction disks. Therefore, the clutch-pack kinetic energy,  $T_c$ , is represented by

$$T_c = \frac{1}{2} \left[ \frac{M_2}{6} \sum_1^6 \left( i \frac{\dot{x}}{6} \right)^2 \right] = \frac{1}{2} 0.421 M_2 \dot{x}^2$$

The total kinetic energy is determined as the sum of all the individual kinetic energies of the different components in the system, namely,

$$T = \frac{1}{2} J_1 \dot{\theta}_1^2 + \frac{1}{2} (J_2 + J_3) \dot{\theta}_2^2 \quad (4.5)$$

where  $\dot{x}$  was expressed in terms of  $\dot{\theta}_2$  from eq.(4.1), and hence,

$$J_3 = \frac{l^2 (M_1 + 0.421 M_2)}{4\pi^2 \cos(\phi)}$$

with  $\phi = 14.5^\circ$  for the ACME lead screw thread angle. The potential energy  $V_c$  of the clutch-pack is primarily composed of the spring-effect of its components, which is proportional to the work produced by the nonlinear spring of stiffness  $k_2(x)$  upon compressing the spring from  $\xi = a$  to  $\xi = x \leq a + b - d$ , namely<sup>1</sup>

$$\begin{aligned} V_c &= \int_a^x A_2 k_2(\xi) d\xi \\ &= \frac{A_2(b-d)}{\pi} \ln \left[ 1 + \tan \left( \frac{\pi}{2} \frac{x-a}{b-d} \right)^2 \right] u(x-a) \end{aligned} \quad (4.6)$$

where  $A_2$  is an empirical parameter with units of displacement. Using eq.(4.1),  $V_c$  can be readily obtained in terms of  $\theta_2$ . The total potential energy includes  $V_c$  and that of the flexible coupling, while gravity does not intervene. Therefore,

$$V = \frac{1}{2} k_1 (\theta_1 - \theta_2)^2 + \frac{A_2(b-d)}{\pi} A_0 u \left( \frac{l}{2\pi} \theta_2 - a \right) \quad (4.7a)$$

where

$$A_0 = \ln \left[ 1 + \tan \left( \frac{\pi}{2} \frac{\frac{l}{2\pi} \theta_2 - a}{b-d} \right)^2 \right] \quad (4.7b)$$

The power dissipated by the Coulomb friction forces is computed as

$$\Delta_c = \int_0^{\dot{x}} f_f d\dot{\xi}_1 + \int_0^{\dot{\theta}_2} \tau_f d\dot{\xi}_2$$

The dissipation  $\Delta$  associated with the system stems from the viscous damping present in the flexible coupling, bearings and clutch-pack fluid, and the Coulomb friction.

Hence,

$$\Delta = \frac{1}{2} c_1 (\dot{\theta}_1 - \dot{\theta}_2)^2 + \frac{1}{2} c_3 \dot{\theta}_1^2 + \frac{1}{2} c_4 \dot{\theta}_2^2 + \Delta_c$$

<sup>1</sup>The integral of eq.(4.6) was obtained by computer algebra from the expression for  $k_2(\cdot)$  given in eq.(4.3a).

its partial derivative w.r.t.  $\dot{\mathbf{q}}$  yielding  $\phi_d$ , i.e.,

$$\phi_d = \frac{\partial \Delta}{\partial \dot{\mathbf{q}}} \quad (4.8)$$

The electromechanical actuator system has two independent generalized coordinates, and hence, two degrees of freedom. Under these conditions, eqs.(4.5)–(4.8) are substituted into eq. (4.4), the Lagrange equation then leading to the mathematical model

$$\mathbf{M}\ddot{\mathbf{q}} = \phi_p + \phi_f + \phi_d \quad (4.9)$$

with the two-dimensional vectors of generalized forces given as

$$\phi_f = \begin{bmatrix} \tau_1 \\ 0 \end{bmatrix}, \quad \phi_p = \begin{bmatrix} -k_1\theta_1 + k_1\theta_2 \\ k_1\theta_1 - k_1\theta_2 - A_2 \frac{l}{2\pi} k_2 \left( \frac{l}{2\pi} \theta_2 \right) \end{bmatrix},$$

$$\phi_d = \begin{bmatrix} -(c_1 + c_3)\dot{\theta}_1 + c_1\dot{\theta}_2 \\ c_1\dot{\theta}_1 - (c_1 + c_4)\dot{\theta}_2 - \tau_f - f_f \frac{l}{2\pi} \end{bmatrix}$$

where the stiffness function  $k_2(\cdot)$  is defined in eq.(4.3a). Furthermore, the  $2 \times 2$  mass matrix  $\mathbf{M}$  of the system is given by

$$\mathbf{M} = \begin{bmatrix} J_1 & 0 \\ 0 & J_2 + J_3 \end{bmatrix}$$

## 4.2 Simulation and Experimental Results

Simulation and experimental testing of each sub-variant, lead- and ball-screws, were done independently. The inertial parameters were obtained directly from the CAD model of each screw sub-variant of the EMC testbed. The flexible coupling parameters were identified earlier (Chopra, Zargarbashi and Angeles, 2013). Other parameters such as viscous damping, *Stribeck velocities* and friction coefficients, are derived on comparison. Simulation of the mathematical model of eq.(4.9) was carried

out in Matlab/Simulink. Data acquisition and processing of the experiments relied on Matlab/Simulink with Quanser's QuaRC embedded software package. In this environment, command voltage signals are sent, while measured data are collected via Simulink's block functions using a real-time hardware-in-the-loop platform. Numerical data are recorded from the load cell and motor amplifier at a sampling frequency of 1 kHz and for a duration of 0.5 s. The motor amplifier is equipped with a digital signal processor which is capable of capturing the motor angular velocity from the position encoder of the motor. The motor angular-velocity signal had been previously validated (Chopra, Zargarbashi and Angeles, 2013). Moreover, the motor amplifier was tuned to control the motor current input. The experiments were conducted primarily to evaluate the feasibility of each sub-variant in delivering the required clamping force of  $f_a = 6.28$  kN.

**4.2.1 First EMC Sub-variant: Lead Screw.** The parameters used in the lead screw model simulation are listed in Table 4.1. A current input in the form of a ramp signal is commanded to the motor as shown in Fig. 4.5. Plotted in Figs. 4.6 and 4.7 are the experimental and simulation results. An error of 6.0% is observed between the experimental and simulated clamping forces. The motor-velocity plot, drawn from the experiment, is raw data as displayed in Fig. 4.6. The plot shows a noisy signal as the motor velocity approaches zero, past the 0.32 s mark. The average of this noisy signal is observed to be zero.

The results show that the design is capable of providing 6.3 kN of clutch clamping force. Frictional losses, inherent in lead-screw devices, are apparent in the results. High motor torque is required to operate the actuator, despite greasing the screw threads. The motor torque overcomes the static friction to allow the motor velocity to reach a steady-state of 540 rpm. As the lead screw shaft turns, it translates the lead nut and apply-plate towards the clutch disks. The clutch-pack stiffness takes

Model Parameter	Value
$A_1$	29000 N/mm
$A_2$	0.344828 mm
$a$	2.4 mm
$b$	37 mm
$c_1$	0.0003769 Nms/rad
$c_2$	0.0003 Nms/m
$c_3$	0.015 Nms/rad
$c_4$	0.0099 Nms/rad
$c_5$	0.01 Nms/rad
$d$	36.1 mm
$J_1$	$1.51027 \times 10^{-4}$ kg m <sup>2</sup>
$J_2$	$1.5335 \times 10^{-5}$ kg m <sup>2</sup>
$J_3$	$3.37 \times 10^{-8}$ kg m <sup>2</sup>
$k_1$	3.32 Nm/rad
$K_\tau$	0.7
$\dot{x}_s$	0.02 m/s
$\dot{\theta}_s$	98.94 rad/s
$\mu_s$	0.23
$\mu_k$	0.08

TABLE 4.1. Lead screw model parameters

effect as soon as the apply-plate compresses the clutch-pack. This happens at about 0.25 s into the experiment, that is, at the point where the motor velocity begins decreasing, as illustrated in Fig. 4.6. The hardening effect of the clutch-pack stiffness displays a rapid increase in clamping force to reach a maximum at 0.33 s in Fig. 4.7. The lead screw self-locks to maintain a compressive force of 6.3 kN.

**4.2.2 Second EMC Sub-variant: Ball Screw.** The EMC ball screw sub-variant requires an additional motor to actuate the pawl lock, which locks the ratchet. This servo motor is controlled by an Arduino board. A piece of code was written to command a pulse-width modulation (PWM) signal of  $\pm 5$ -V. The code was then synchronized with Matlab in order to activate the pawl to demonstrate its locking capability. The experimental tests for the ball-screw variant were conducted while recording the load cell and motor angular velocity measurements. The parameters

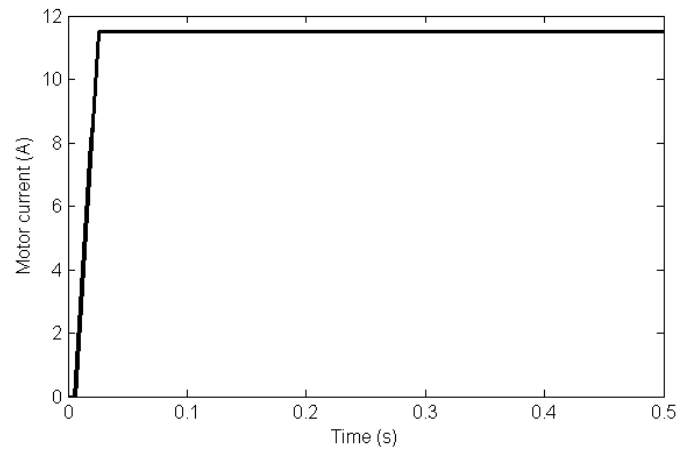


FIGURE 4.5. Motor input current command for the EMC lead screw sub-variant

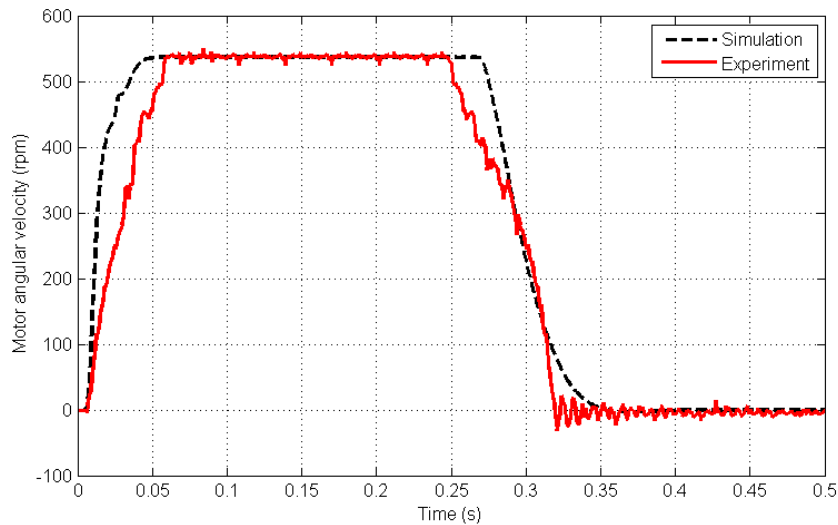


FIGURE 4.6. Comparison of the experimental and simulation results of the motor shaft velocity for the EMC lead screw sub-variant

replaced in the ball-screw simulation are listed in Table 4.2, while all other parameters were kept the same as in Table 4.1.

A similar motor current ramp input command, as in Fig. 4.5, with the peak current input of 7 A was used. Plotted in Fig. 4.8 is the motor output velocity for both experiments and simulation. The pawl was rotated in place at the 0.25 s mark, where the motor angular velocity reached zero. The ratchet and pawl assembly was

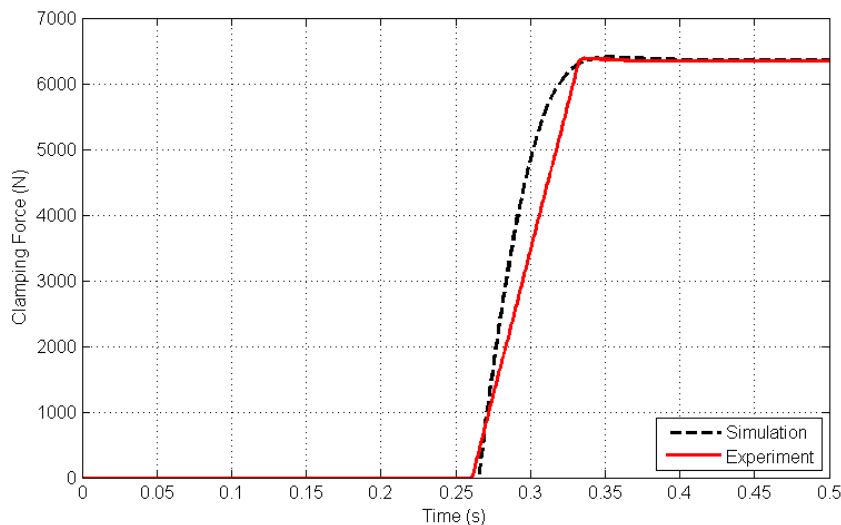


FIGURE 4.7. Comparison of the experimental and simulation results of the clutch clamping force for the EMC lead screw sub-variant

Model Parameter	Value
$c_4$	0.02 Nms/rad
$c_5$	0.007 Nms/rad
$J_2$	$1.0895 \times 10^{-4}$ kg m <sup>2</sup>
$J_3$	$1.1079 \times 10^{-7}$ kg m <sup>2</sup>
$\dot{x}_s$	0.01 m/s
$\dot{\theta}_s$	49.47 rad/s
$\mu_s$	0.0625
$\mu_k$	0.011

TABLE 4.2. Ball screw model parameters

able to maintain clamping force for the 12-disk clutch pack. Shown in Fig. 4.9 are the clamping force results recorded of the simulation and experiments. An error of 1% is observed between the experimental and simulated clamping forces.

The results show that the ball-screw variant is capable of providing a clamping force of 6.35 kN for a clutch torque capacity higher than 500 Nm. In order to produce this clamping force, the ball-screw system required an input motor torque of 4.9 Nm, as opposed to the lead screw variant's requirement of 8.05 Nm. The response of the ball screw set-up was faster as well; it completed the engagement phase within 0.26 s.

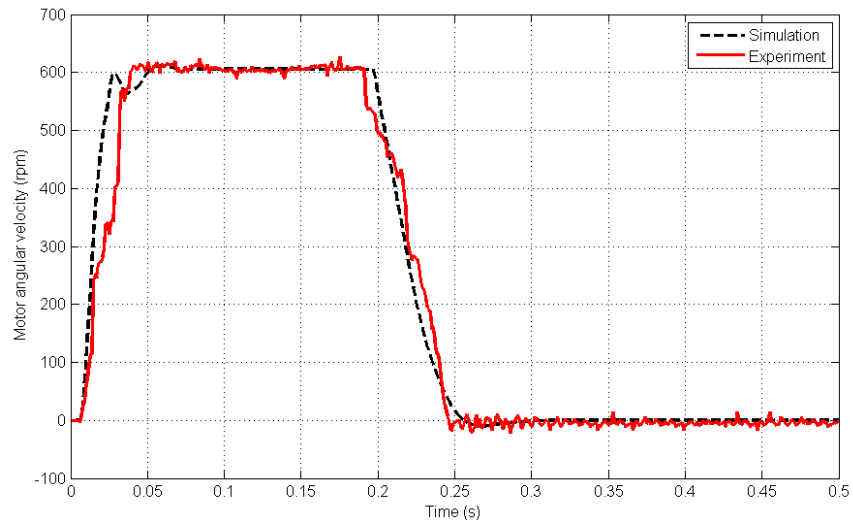


FIGURE 4.8. Comparison of the experimental and simulation results of the motor shaft velocity for the EMC ball screw sub-variant

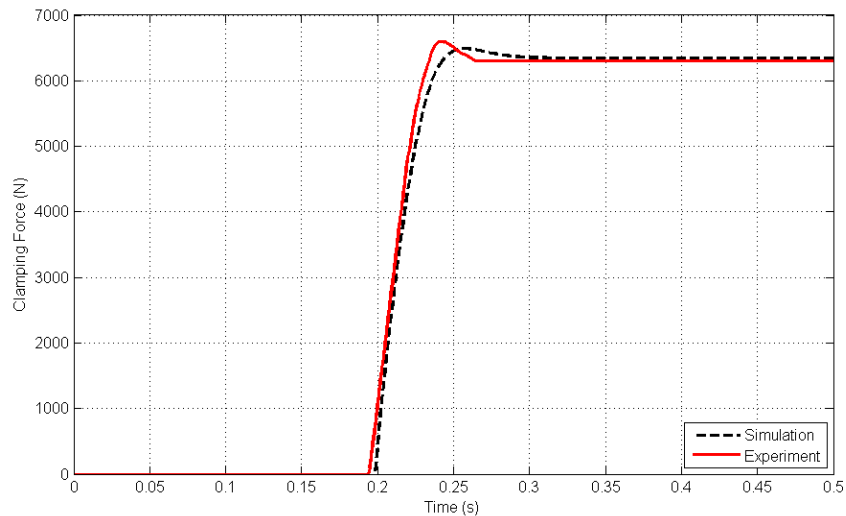


FIGURE 4.9. Comparison of the experimental and simulation results of the clutch clamping force for the EMC ball screw sub-variant

Both sub-variants entail their advantages and drawbacks. The ball screw system exhibits lower friction and faster response. However, it is heavier, larger and requires an additional motor for its locking mechanism. The lead-screw system is compact, lightweight and features its self-locking capability but at the expense of higher friction.



## CHAPTER 5

---

# Electromagnetic Dog Clutch Design

In this chapter, the design of the PM DC brake synchronizer, and its performance when subjected to simulation tests using Infolytica’s MagNet<sup>1</sup>—a commercial finite element software package—is reported. The use of finite element magnetic (FEM) packages offers tremendous benefits in the development of electromagnetic devices, allowing for high-throughput numerical experiments and performance analyses. In several cases, full 3D dynamic simulations are capable of providing substantial information without requiring the fabrication of a prototype (Vidal et al., 2006). With the aid of MagNet, the design geometry is analyzed right at the outset and a unique modification is proposed that ultimately lowers cogging torque and potential manufacturing costs. Furthermore, the design allows for the use of a low voltage power supply, readily available in most automobiles.

### 5.1 Concept Development

The concept stemmed from the application of *mechanical synchronizers* of dog clutches to automatic transmissions. Manual gearbox transmissions contain synchronizers; *synchronizing* means eliminating angular-velocity slip between the input hub

---

<sup>1</sup><[www.infolytica.com](http://www.infolytica.com)>

and output gear, upon bringing two coaxial shafts to turn at the same speed. Upon sliding a synchronizing sleeve into position, the input and output shafts become rigidly coupled. Clutch lock-up is maintained without any external energy source. The synchronizer is actuated by a linkage system, whose pivoting is done by the vehicle operator's hand, the gear lever thereby being manually shifted in order to select the corresponding gear (Kim et al., 2003). Angular velocities are generally synchronized by conical friction clutches, while power transmission is usually implemented through dog tooth spline couplings of the sleeve and output (Lovas et al., 2006). It is noteworthy that the synchronizers are activated when no engine torque is applied to the transmission. This allows for low stresses and ease in the positioning of the sleeve.

Dog clutches are currently being used in some EVs and HEVs (Wishart, Yuliang and Dong, 2007; Chen et al., 2003). Clutch shifting in HEV transmissions is typically carried out at synchronous speed, where the input and output speeds are matched to reduce the slip power of the shift event (Lee et al., 2000). Therefore, the clutch packs are made smaller since the thermal capacity required is reduced with a reduction in slip. Dog clutches are used in this case, where torque and slip speeds are synchronized. The motor control system strives to reduce the rotor slip to zero, but with feedback error and exogenous disturbances may result in a slip error of up to 100 rpm. Moreover, when trying to lock the clutch via the synchronizing sleeve of the dog clutch system, the traction motors apply an active resistive torque. The latter is substantial which leads to additional difficulty in synchronizing, while, compromising the durability of the dog-clutch system. Hence, a need for designing a contactless synchronizer arose to eliminate the clutch slip.

Shown in Fig. 5.1 is a preliminary layout of the design concept. The clutch would provide on-demand coupling, when the contactless synchronizer is actuated using magnetic energy. The field generated would be capable of coupling the input and

output elements of the clutch assembly, thereby causing a reduction in slip velocity between them. Then, using an external actuator, a locking sleeve can be slid from the output member to the input member, thereby forming a rigid coupling. Once in operation, all power to the system would be cut-off in order to reduce energy consumption (Holdstock et al., 2012).

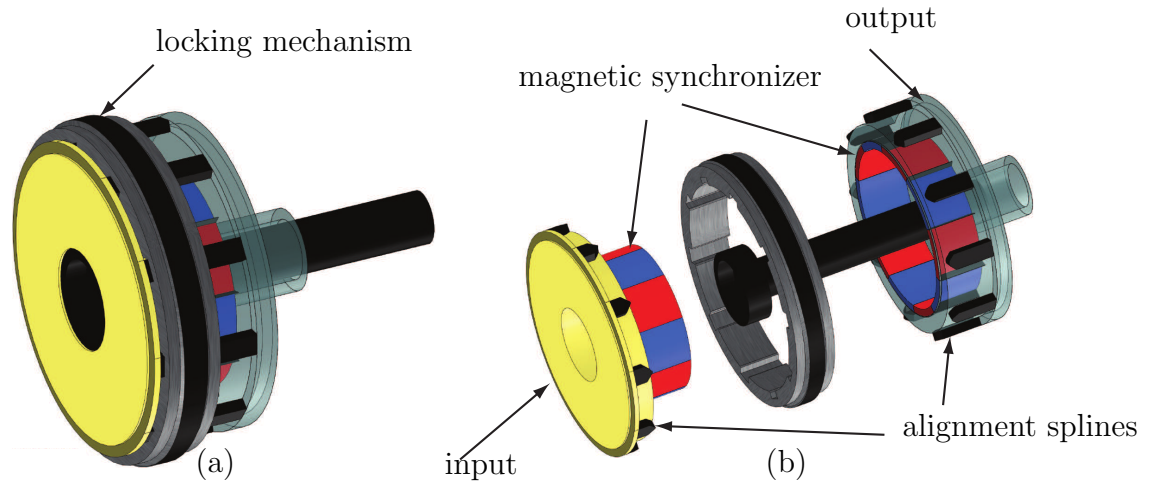


FIGURE 5.1. Preliminary brake clutch concept: (a) assembly in lock mode; (b) exploded view

## 5.2 Computer-Aided Design and Modelling

Prior to designing the electromagnetic system at hand some ground rules were established. Most importantly, we chose a restrictive design volume. Typical brake-clutches used in automatic transmissions consist of a number of alternating friction and steel disks, hydraulic pistons, return springs, snap rings, a ball check valve assembly, bearings, a backing plate and a clutch drum. The volume occupied by typical brake-clutches is selected to ensure that our design is compact. Furthermore, other design specifications such as power supply, initial rotor speed and torque capacity were set as shown in Table 5.1. Maximum duration for engagement and subsequent disengagement need to be within 500 ms, which is readily achieved by electromagnetic brakes (Anwar and Stevenson, 2011). For the simulation tests to be realistic, an

Outer diameter	250 mm
Inner diameter	160 mm
Axial depth	55 mm
DC Power supply	12 V
Maximum current	10 A
Zero-slip load torque $\tau_{\max}$	42 Nm
Additional rotor inertia	0.05 kg m <sup>2</sup>
Stator-rotor air-gap	0.8 mm
Rotor initial slip $\omega_0$	100 rpm
Coil packing factor	65%

TABLE 5.1. Design specifications for the PM DC brake synchronizer

additional inertia was added to the rotor inertia to replicate the attachment of a gear element. A load torque is applied to the rotor that varies with the rotor speed; we start at 100 rpm with zero load torque and linearly increase the load torque to 42 Nm at zero rpm. This load-rpm relation, which extends linearly past the aforementioned speed range, is given by

$$\tau_L = \tau_{\max} \left( 1 - \frac{\omega}{\omega_0} \right) \quad (5.1)$$

where  $\tau_L$  is the load torque applied on the rotor,  $\omega$  is the rotor angular velocity,  $\tau_{\max}$  is the maximum load torque applied, and  $\omega_0$  is the initial rotor slip. The values for  $\tau_{\max}$  and  $\omega_0$  are given in Table 5.1.

The best available high-energy PMs are made of Neodymium Iron Boron (NdFeB), a rare-earth magnetic material (Hanitsch, 1991). However, NdFeB magnets are extremely expensive and offer a low service-temperature range, between 100°C and 150°C (Thompson, 2009). Samarium Cobalt magnets (SmCo), though less powerful than NdFeB, exhibit a better temperature tolerance, but are substantially expensive as well. Alnico magnets are known to operate at temperatures of up to 550°C; they have proven to be an alternative to the costly rare-earth magnets for some applications (Rao, 1993). However, a major drawback of Alnico magnets is their failure to retain a magnetic remanence on exposure to air or any other non-magnetic medium.

This renders them very unstable. A lower class of permanent magnets is available in the form of ferrites. These are the least expensive and correspondingly exhibit lower magnetic energy. However, ceramic-based ferrites are known to be stable and reliable under a wide range of operating temperatures, making them a suitable choice for use in this application.

The proposed design of a PM DC brake synchronizer consists of a set of alternating, polarizing electromagnet (EM) poles on the stator and a corresponding set of alternating radially-polarized PMs on the rotor, separated by a radial air gap. The PM material chosen is Strontium Iron Oxide—Ceramic 11 (residual induction at 20°C: 0.42 T)—with anisotropic magnetization in the radial direction. The rotor consists of surface PMs placed circumferentially around a solid ring of 1010 *cold-rolled* (CR) steel. The stator houses its EMs in a corresponding fashion, with a solid ring of 1010 CR steel serving as the iron yoke to close the magnetic flux path. Each EM pole consists of a core made of solid 1010 CR steel with a single-phase compound wound coil. Notice the use of solid 1010 CR steel (Gutierrez-Castaneda and Salinas-Rodriguez, 2011), and not laminated steel, as solid steel will lead to the generation of eddy currents to facilitate energy dissipation and greatly reduce fabrication costs (Hauser et al., 2008). Moreover, a higher number of phases for the coil windings, commonly found in PM-based motors, was unnecessary here. The coil wire was selected as No. 13 AWG, with 76 turns around each EM core. A 2D FEM analysis was conducted to help choose a pole number. In 2D simulation, the EM coil end-turns are not taken into account, which is vital for designs with axial depth smaller than the radial length. Nevertheless, to discern a trend in the pole number, the tests suffice. As a 16-pole array was observed to be optimum, it was selected and modelled in 3D. Additionally, full 3D simulation tests were conducted for a 14-pole and an 18-pole

design to confirm this. The 16-pole radial configuration of the device is shown in Fig. 5.2.

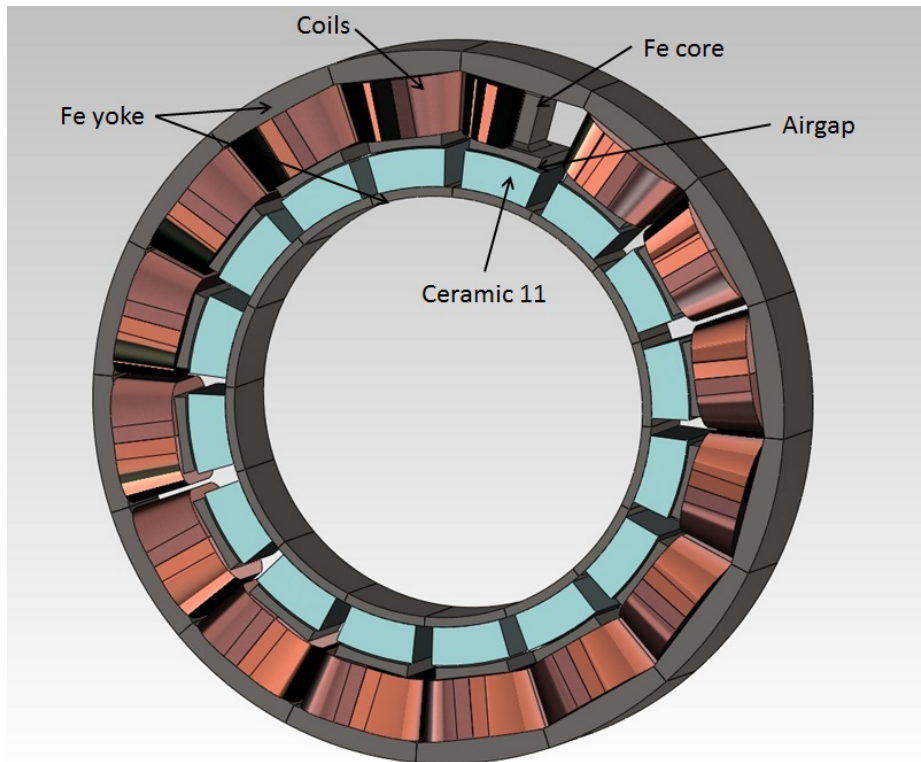


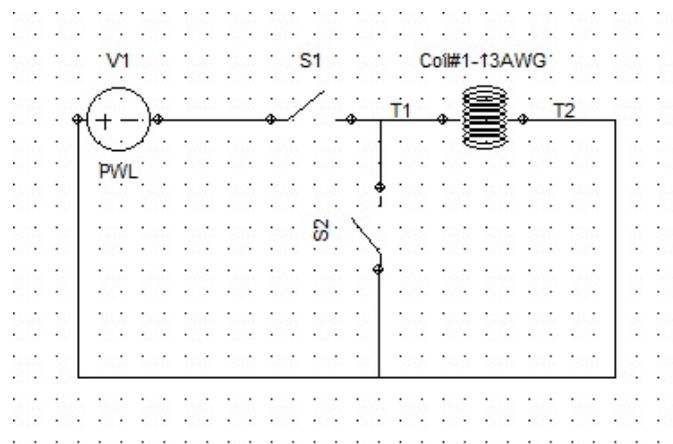
FIGURE 5.2. Proposed PM DC brake layout

### 5.3 Simulation and Results

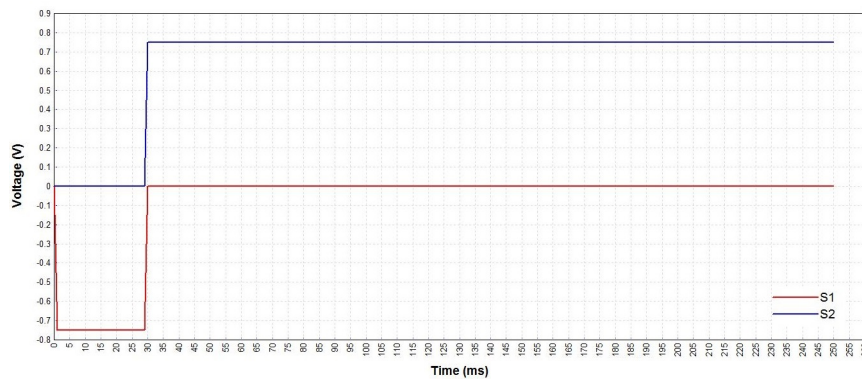
The periodic reluctance torque, dependent on the rotor position, is calculated using the Maxwell stress method and time-stepping approach in MagNet, where the transient-with-motion solver is utilized to dynamically simulate the geometry in both 2D and 3D. The nonlinear problem is solved in MagNet using the Newton–Raphson method (with a 1% convergence tolerance), the linearized system of equations is solved using the conjugate gradient (CG) iterative method (with a CG tolerance: 0.01%), and the torque calculation is carried out using the Maxwell stress tensor (Lowther and Silvester, 1986). A simulation time-step of 1 ms is assigned, which is sufficient

for this low-frequency application. For 2D and 3D simulation tests of a device with a periodic architecture such as this, the modelling of one single pole set is required, which reduces the computation time to  $1/64$ . All parameters associated with the periodicity of the device were adjusted accordingly. As mentioned in Section 5.2, 2D simulation tests were only conducted for a trend analysis. A sensitivity analysis was carried out to ensure that the FEM results were stable and the torque calculations as accurate as possible. The sensitivity analysis involved refining the mesh and solver settings. The meshing in the air gap and components of steel material were refined. The second-order polynomial interpolation for these elements showed results with good accuracy and reasonable computation time.

Preliminary simulation tests were completed by connecting a 12 V DC supply across the coil terminals. However, it was observed that by doing so, the current in the coil circuit was very low, a consequence of the rotating magnetic field produced by the rotor magnets, which induces a back electromotive force (emf) across the EM coil. Furthermore, this emf lowers with a reduction in the rotor speed. Hence, a more efficient layout of the electrical circuit connection was sought. To this end, we designed a switching circuit which would close the EM coil circuit independently, thereby allowing the emf-induced current within the EM coils to produce a magnetic field. This helps in producing the low initial braking torque. Then, as the rotor speed decreases and the resistive load torque increases, the 12 V DC supply (0.75 V for  $1/16$  of the geometry) is switched on, which results in a higher effective current. Simple electric circuit elements are used to perform this switching action, a layout of the circuit being shown in Fig. 5.3(a). Switch S2 was closed at the start of the simulation. Then, by sensing the voltage drop across the coil terminals, S2 is opened, thus triggering the switch S1 to a step-input voltage, as displayed in Fig. 5.3(b), the effective current within the circuit thereby being maintained. Shown in Fig. 5.4 is the



(a)



(b)

FIGURE 5.3. (a) Switch circuit for the PM brake; (b) Voltage across the two switches

current in the circuit during the simulation test. This allows for quick and efficient braking, utilizing some of the energy of the system itself.

The 3D dynamics simulation results of the design are illustrated in Figs. 5.4–5.7, where all parameters are adjusted to simulate only 1/16 of the geometry. The rotor slip starting at 600 deg/s (100 rpm) was reduced to zero with a synchronization time of 180 ms. The braking torque is capable of balancing the resistive load torque, as seen in Fig. 5.4. The magnetic flux density plot is shown in Fig. 5.7.

Open-clutch, or disengaged clutch conditions, were also simulated. The PM DC brake was prone to producing cogging torque, an inherent drawback of PM-based

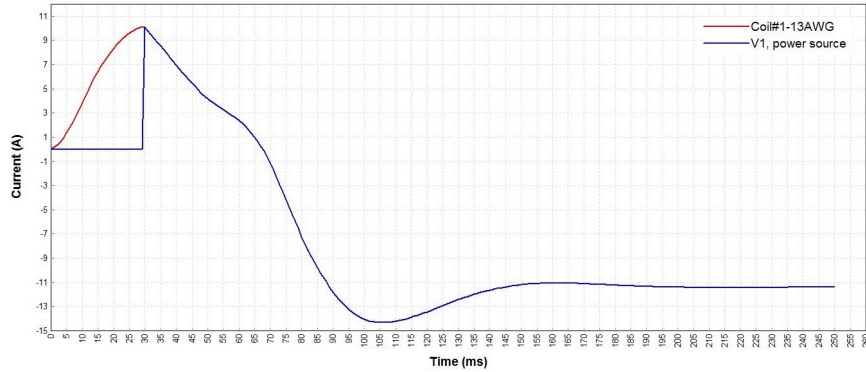


FIGURE 5.4. Current in the circuit

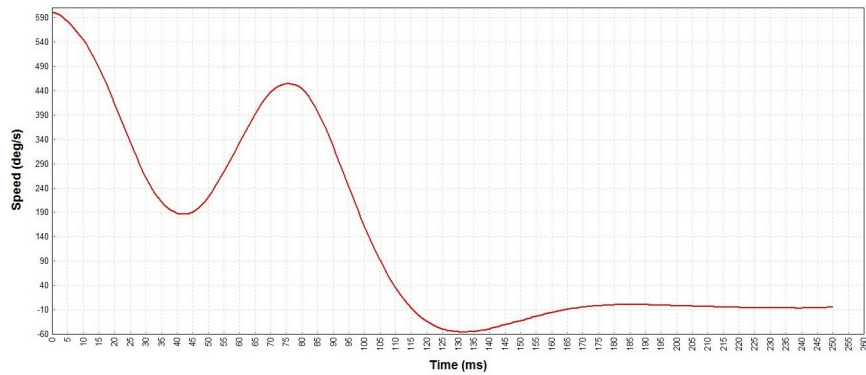


FIGURE 5.5. Rotor speed plot of the proposed design

machines. Simulated results of open-clutch operation are discussed in Section 5.4. Cogging torque on the rotor will produce drag and potential vibration disturbances proportional to the torque amplitude. It is noteworthy that this amplitude is independent of the rotor speed, which only affects the frequency of the cogging torque. At high rotor speeds, the effects of cogging torque are extremely undesirable, resulting in high open-clutch drag losses and disturbance.

## 5.4 Reduction in Cogging Torque

The need for reducing cogging torque in PM-based machines is an area of active research (Bianchi and Bolognani, 2002; Hwang, Wu and Cheng, 2006; Fan and Wu,

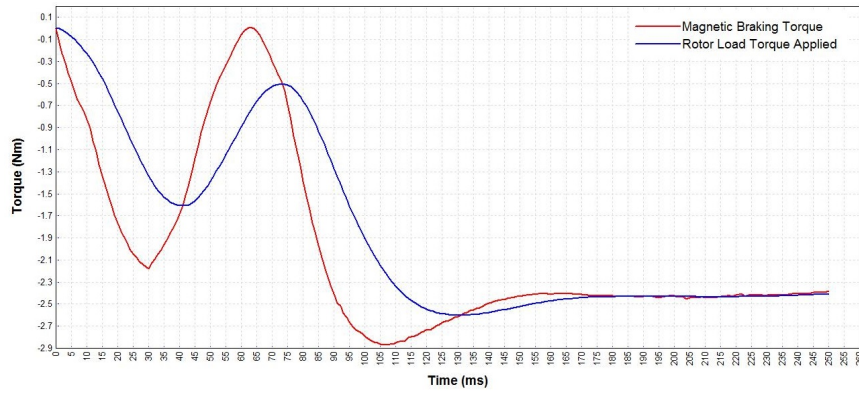


FIGURE 5.6. Braking torque plot of the proposed design

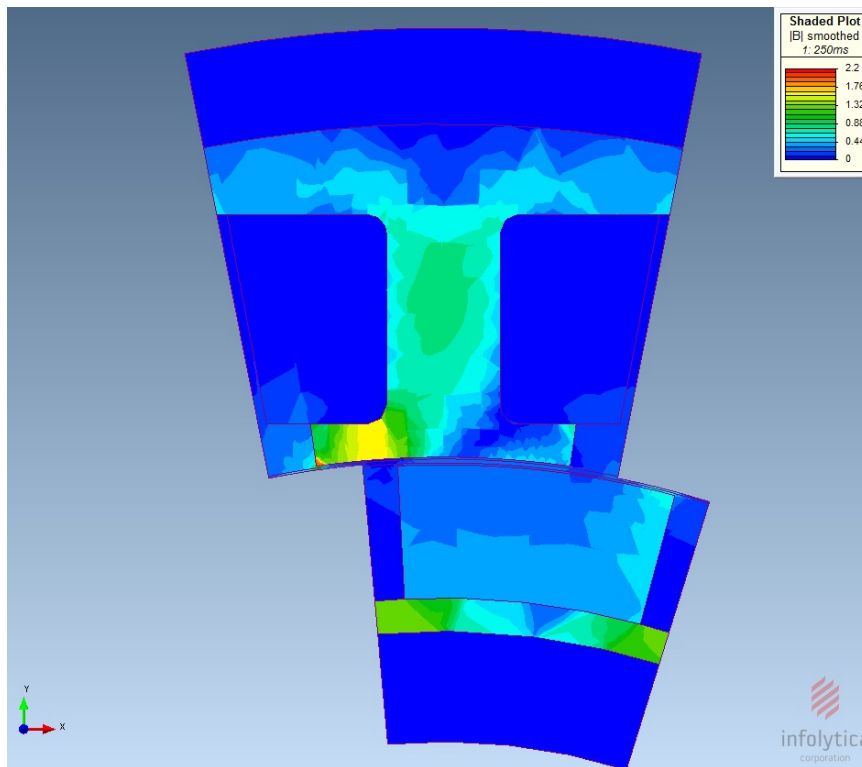


FIGURE 5.7. Magnetic flux density plot at 250 ms

2013). Skewing the stator EMs or the rotor PMs by an angle over a pole generally reduces cogging torque significantly. However, doing so results in higher manufacturing costs and lower reluctance torque, corresponding to lower braking torque.

Therefore, an innovative design modification is proposed that reduces the number of PMs on the rotor to eight poles by replacing them with salient steel poles. Shown in Fig. 5.8 is an eight-surface PM with an eight T-shaped steel pole rotor against a 16-pole single-phase wound stator, separated by an air gap of 0.8 mm. A close-up of the rotor pole, shown in Fig. 5.9, displays the solid 1010 steel pole to be machined and fixed to the steel yoke of the rotor. Under the same test conditions of Table 5.1, one-eighth of the periodic geometry was simulated in MagNet. No switching circuit strategy has been applied here as the back emf induced is greatly reduced with a lower number of PMs. The 12 V DC (1.5-V for 1/8 of the geometry) was applied as a step input at the start of the simulation.

The simulation test shows that the rotor speed diminishes to zero using the magnetic reluctance torque of the system. As the EM coils are energized, the simulation yields the rotor speed plot shown in Fig. 5.10; the rotor reaches a standstill in under 250 ms. Shown in Fig. 5.11 is the rotor braking torque (for 1/8 of the geometry), thereby, meeting the performance specification of the design task at hand. A magnetic flux density plot of the modified design is shown in Fig. 5.12.

Furthermore, simulating the open-clutch mode for this configuration shows a great reduction in the cogging torque. The two designs, one with 16-PM, the other with eight PM pole rotor, were subjected to a constant rotor velocity simulation test. The rotor speed was maintained at 600 rpm and the rotor torque in each case was recorded. The cogging torque result is shown in Fig. 5.13, for both designs. At steady state, the design with the 16-PM pole rotor exhibited a mean cogging torque of 6 Nm while the design with eight PM pole rotor was 3.42 Nm. Peak-to-peak net cogging torque steady-state values of 13.59 Nm and 9.46 Nm were observed for the 16-PM pole rotor and eight PM pole rotor, respectively. Hence, with a simple design modification

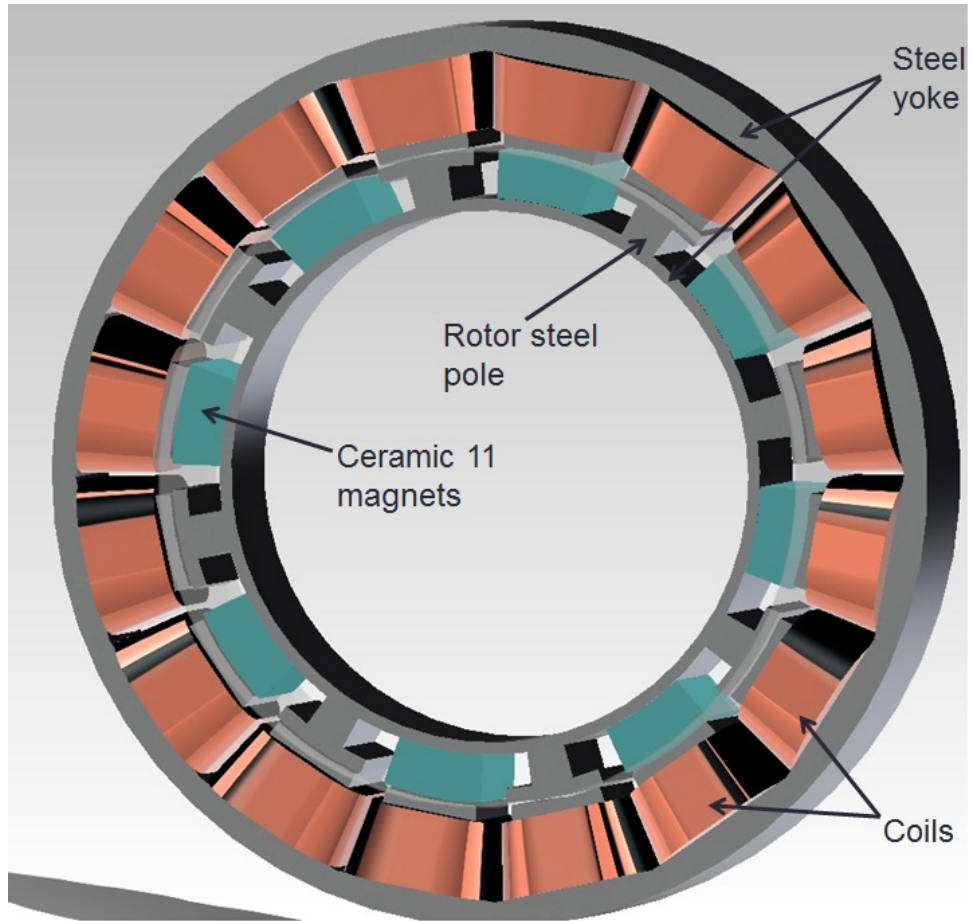


FIGURE 5.8. A 16 EM-pole stator with eight PM and eight salient steel poles on the rotor

of the reduction in the number of surface PMs, the cogging torque loss was improved.

## 5.5 Prototyping Considerations

The prototyping of the PM brake synchronizer was discarded as the costs of fabrication of the device exceeded the funds available. The design topology was challenging to fabricate, requiring high labour costs. In pursuit of fabricating a low-cost design, other alternatives were sought. The knowledge and skills developed here were used to create a novel low-cost alternative, which is reported in Chapter 6.

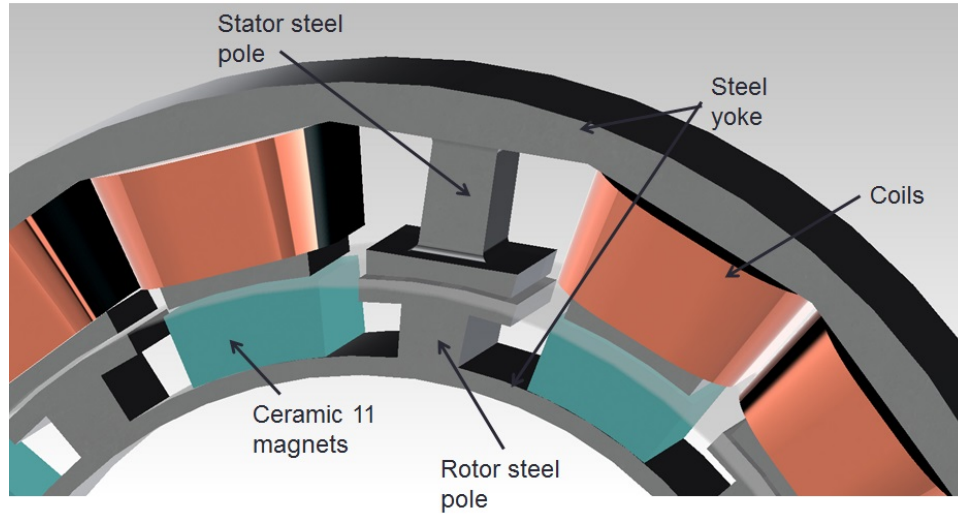


FIGURE 5.9. A zoom-in on a section of the rotor surface

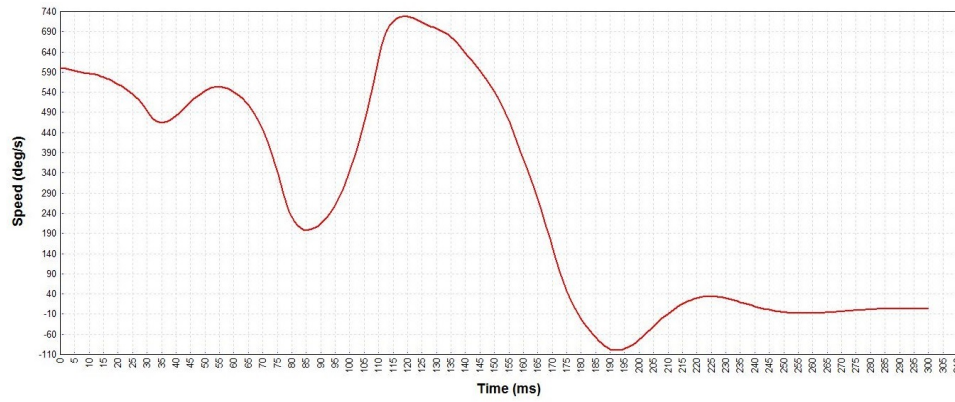


FIGURE 5.10. Rotor speed plot of the eight PM pole rotor

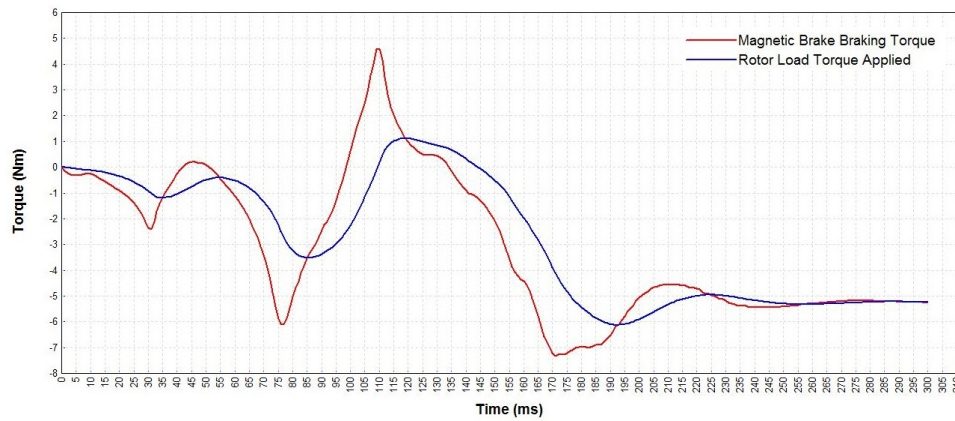


FIGURE 5.11. Rotor torque plot of the eight-PM pole rotor

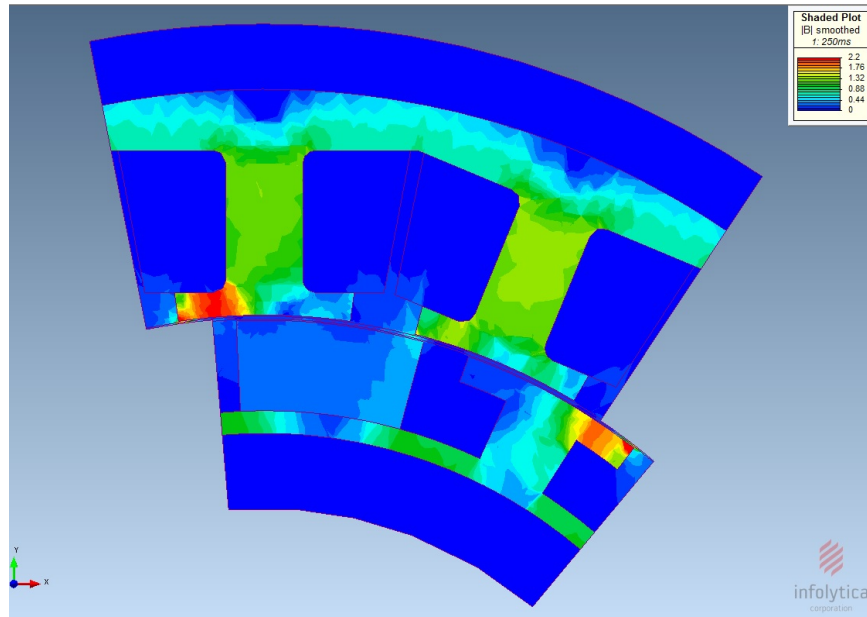


FIGURE 5.12. Magnetic flux density plot of the eight-PM pole rotor at 250 ms

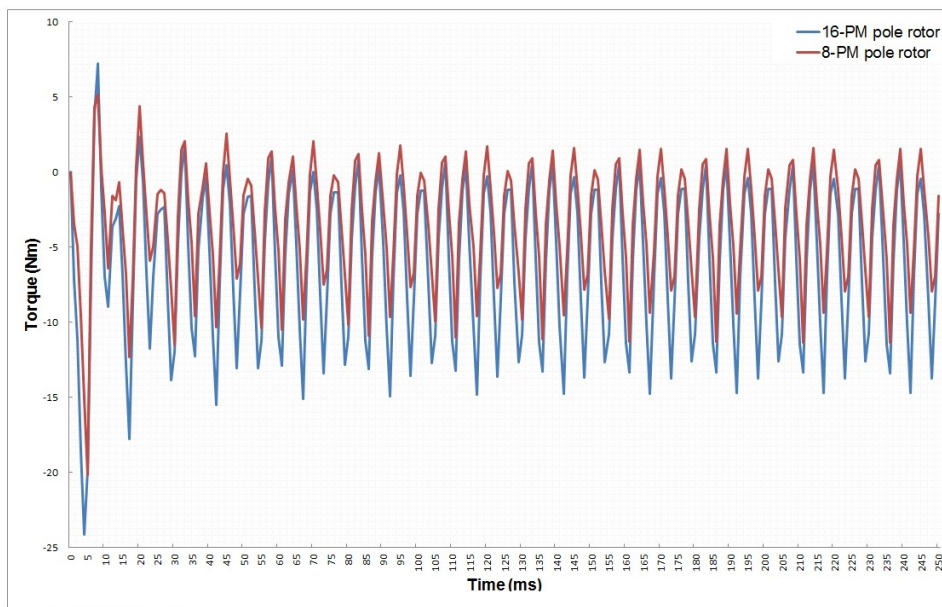


FIGURE 5.13. Drag torque of the open PM-based brake operation of the two designs

Dynamics simulation tests conducted using the 3D transient with motion solver in MagNet demonstrate the feasibility of the PM-based brake concept; these tests provide detailed-enough performance information that the fabrication of a prototype

is obviated. With advances in FEM software, quick, efficient designs can be readily validated, as illustrated by this study.

## 5.6 Design and Discussion of a Potential Dog Clutch System

A brief discussion on the design of a dog clutch system to be used in conjunction with the EM brake synchronizer is outlined. A synchronizer sleeve is a mechanical coupler that can be slid into position to couple the rotations of the transmission elements through the use of prismatic joints, known as dog teeth. This mechanism will obviate the need for external power input during the operation of a clutch. Energy will only be required for initial actuation at engagement and disengagement. A translational system is required to take the ring between disengaged and engaged positions, as shown in Figs 5.14(a) and (b). The compact translation system would

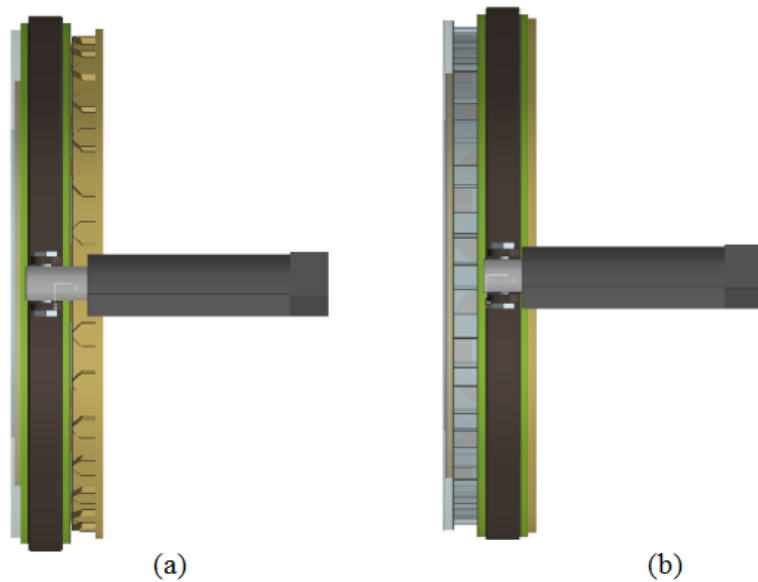


FIGURE 5.14. Dog clutch synchronizer: (a) disengaged; (b) engaged

consist of a small DC or stepper motor, a spur gear pinion, an input and output external dog tooth ring, a partially geared roller-carrier ring, and a sliding sleeve. Displayed in Fig. 5.15 is the translational mechanism showing the arrangement of the

spur gear pinion, geared roller-carrier ring and grooved sleeve. The grooved sleeve

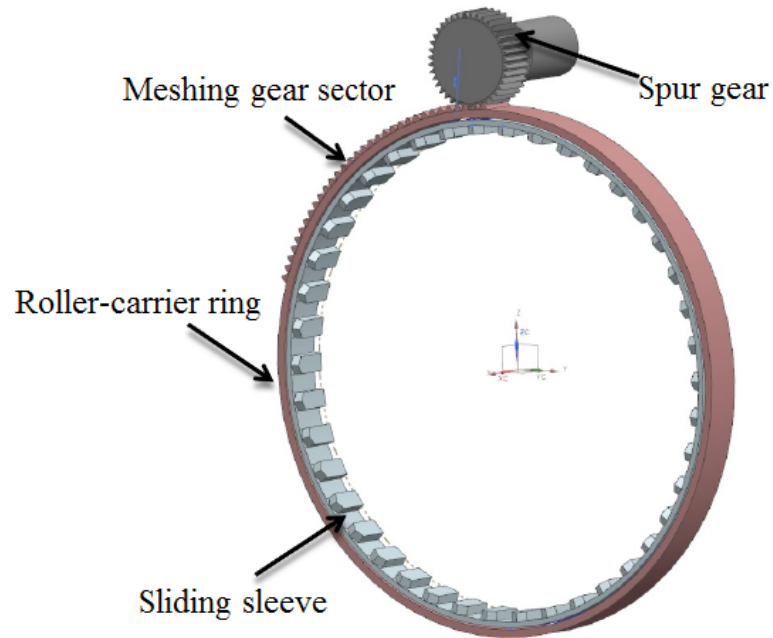


FIGURE 5.15. Compact translational mechanism

would carry a cam-profile, such that when mated with the roller-carrier ring, the pair would convert rotational motion into translation. The motor, spur gear pinion and dog teeth rings are standard components, i.e., they are readily available off-the-shelf. However, the trajectory for roller-cam pair is a custom job which is discussed here.

The type of trajectory appropriate for the sleeve actuation is one commonly found in robotic “pick and place” operations. This is a smooth trajectory between the initial and final positions, that preferably starts and ends with zero velocity, acceleration and jerk. To this end, the 4-5-6-7 interpolating polynomial is proposed (Angeles, 2007), namely,

$$s(\sigma) = -20\sigma^7 + 70\sigma^6 - 84\sigma^5 + 35\sigma^4, \quad 0 \leq \sigma \leq 1 \quad (5.2a)$$

whose first three derivatives w.r.t.  $\sigma$  are given by

$$s'(\sigma) = -140\sigma^6 + 420\sigma^5 - 420\sigma^4 + 140\sigma^3 \quad (5.2b)$$

$$s''(\sigma) = -840\sigma^5 + 2100\sigma^4 - 1680\sigma^3 + 420\sigma^2 \quad (5.2c)$$

$$s'''(\sigma) = -4200\sigma^4 + 8400\sigma^3 - 5040\sigma^2 + 840\sigma \quad (5.2d)$$

A plot of the displacement profile  $s$  is shown in Fig. 5.16. This profile would be

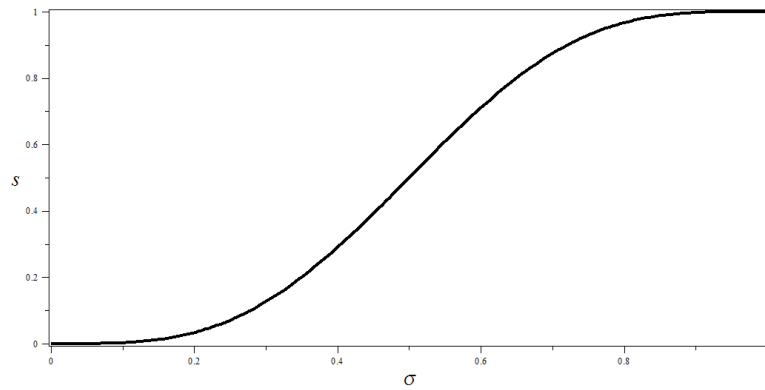


FIGURE 5.16. Interpolating 4-5-6-7 polynomial

machined as a groove on the sliding sleeve, as illustrated in Figs. 5.17, to produce a drum cam (Rothbart and Klipp, 2004). Rollers pinned to the inner diameter of the roller-carrier ring would follow the grooved cam profile on the outer diameter of the sliding grooved sleeve. The latter is splined to the dog teeth above the stator, which is fixed, thus allowing for a smooth translation in the axial direction. By axially constraining the sleeve, the grooved curve acts like a variable pitch thread that modulates an axial response to any given rotational input at  $90^\circ$ , thereby converting the motor rotations into smooth axial motion without complex motor control. Two sets of diametrically opposed grooves with a slight offset to one another is the best means to reduce backlash. Each roller pair would only be in contact with one side of

the groove. Moreover, multiple grooves would better distribute the load. This design needs further development, which is left for future work.

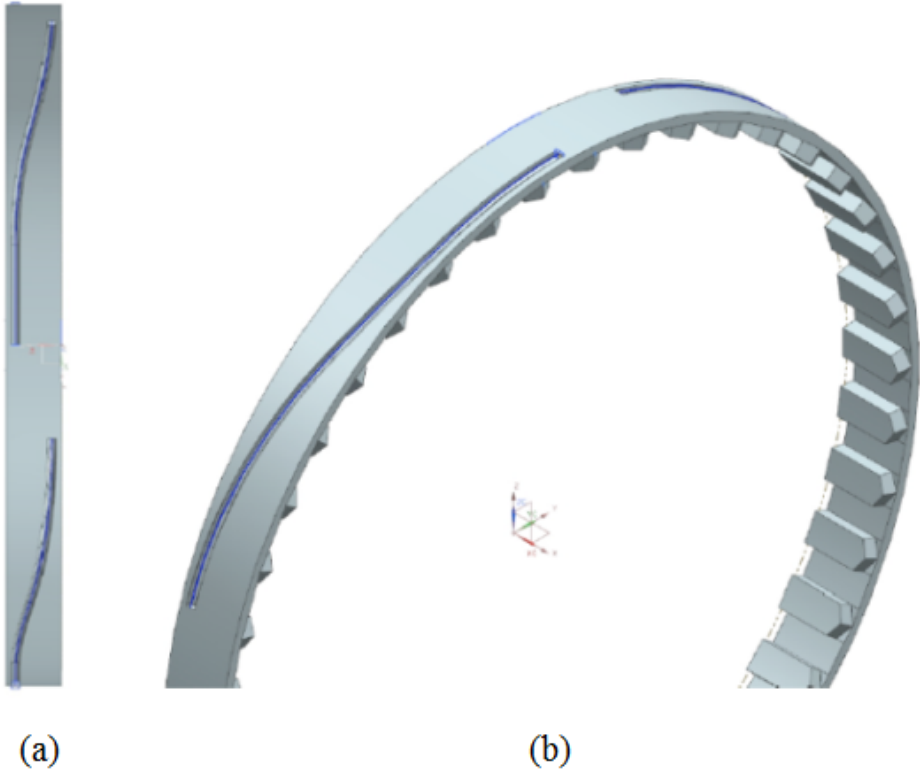


FIGURE 5.17. Sliding grooved ring: (a) top view; (b) 3D view

## CHAPTER 6

---

# Design and Analysis of the Electromagnetic Synchronizer

In this chapter, a novel EM synchronizer is developed to function as a contactless brake synchronizer for use in HEV and EV transmissions. The electromagnetic design is called a synchronizer because it will function in conjunction with the dog clutch of Section 5.6 to facilitate clutch lockup independent of external power. The EM synchronizer consists of four components: a salient rotor; a claw-type stator; a single toroidal wound coil; and a DC power source. Simulation in Infolytica's MagNet showed feasible results within a desirable torque capacity and time duration. A physical prototype was fabricated for proof-of-concept tests. The prototype was made using solid steel in order to keep the fabrication costs to a minimum.

### 6.1 Brake-clutch Synchronizer Design

An in-depth examination of the EM synchronizer is outlined with its design considerations and modelling of the system.

**6.1.1 Design Principle and Operation.** The brake-clutch synchronizer works on the basis of magnetic reluctance. Torque is produced as a result of the

variable reluctance in the air gap between rotor and stator. When the stator winding is energized, producing a single magnetic field, a reluctance torque is produced by the tendency of the rotor to move to its minimum reluctance position. Machines that operate under this phenomenon include switched reluctance motors (SRM) (Lawrenson et al., 1980).

The EM design was envisioned to be constructed with the lowest complexity of all electrical machines to carry the promise of low cost. The design consists of a single-piece stator, made of steel, a single coil winding and a single-piece steel rotor. The coil winding is embedded within the stator. The rotor contains no conductors or permanent magnets. In order to produce reluctance torque the stator and rotor should bear salient features (Miller, 2002). By designing claw-shaped structures on the stator and matching poles on the rotor, synchronizing elements can be created.

The basic operating principle of the EM synchronizer is simple; as current is passed through the stator winding, a magnetic field is produced within the stator. This same field is induced within the rotor steel. Braking torque is generated by the tendency of the rotor poles to align with the excited stator claws. The direction of torque generated is a function of the rotor position but independent of the direction of current flow through the coil winding. Synchronization is brought about at the specific stator claw-rotor pole alignment.

**6.1.2 Design Specifications and Layout.** The envelope of design possibilities is limited by physical constraints, as defined at the outset. In the application of the synchronizer system, the electric motor connected to the rotor is capable of bringing the rotor slip to range between  $\pm 100$  rpm. This range is attributed to feedback error and exogenous disturbances. The load torque for the test condition varies with the rotor speed: starting at 100 rpm, zero load is applied, which linearly increases to

60 Nm at zero rpm. This load-rpm relation is given in eq.(5.1), where the EM synchronizer is required to be able to synchronize the rotor with the active load-torque applied. With exception of a 13.8 V, 138 W DC power supply and  $\tau_{\max} = 60$  Nm, the specifications for additional rotor inertia, volume budget and performance are similar to those of Table 5.1.

It is mandatory to reduce magnetic saturation within the steel components as much as possible. The design should exhibit a low saturation and accommodate as many coil turns as possible. It must also be manufacturable both as a prototype and as a production part. Shown in Fig. 6.1 is a sketch of a cross-section of the EM synchronizer. Calculations are carried out to have approximately equal cross sectional areas (and thus similar flux density) in sections 1 (below), 2 (bottom right), 3 (top right) and 4 (above the coil). The yoke on the inner diameter of the stator was made thicker than the outer diameter to ensure even flux density throughout the stator yoke. Similar calculations were done on the rotor components. Angled stator claws and rotor poles make better use of steel at the top and the bottom of the cross section, which can be readily manufactured on a milling machine. Moreover, with the angled stator claws, the toroidal coil can be conveniently inserted within the stator cavity. The angled stator-rotor interface leads to an angled air-gap, which provides a sensible design as the air gap reluctance can be controlled; by displacing the stator axially, the air gap clearance can be varied; it can be maintained at 0.5 mm or even lower. Compared to flat air-gaps, the angled air-gap provides a larger air-gap surface area with a smaller clearance aiding in flux leakage reduction and a gain in torque capacity. A trapezoidal shape of the coil allows for a snug fit within the stator and provides for additional wire turns. The top-right and bottom-right corners of the stator are chamfered for mass reduction, as those sections carry low flux density.



coil by Faraday's law (Krishnan, 2001):

$$V = iR + \frac{d\phi}{dt} \quad (6.1)$$

where  $V$  is the terminal voltage,  $i$  the coil current,  $R$  the coil resistance,  $\phi$  the flux linked by the winding, and  $t$  is time. Given the salient construction of both the rotor and the stator, the flux linked in the coil varies as a function of rotor position  $\theta$  and current  $i$ . Thus, eq.(6.1) can be expanded as

$$V = iR + \frac{\partial\phi}{\partial i} \frac{di}{dt} + \frac{\partial\phi}{\partial\theta} \frac{d\theta}{dt} \quad (6.2)$$

to give the transfer of electrical energy to the magnetic field. The instantaneous inductance  $L(\theta, i)$  is defined as  $\partial\phi/\partial i$ , while the instantaneous back EMF is given by  $\partial\phi/\partial\theta$ .

To obtain instantaneous power in the EM synchronizer, eq.(6.1) is multiplied by  $i$  to yield

$$P_e = P_l + i \frac{d\phi}{dt} \quad (6.3)$$

where  $P_e$  represents the instantaneous electrical input power and  $P_l$  is the Ohmic losses in the coil winding. Assuming that energy is conserved, then the second term in the right-hand side of eq.(6.3) represents the sum of the mechanical power output and any power stored in the magnetic field. Thus,

$$i \frac{d\phi}{dt} = \tau \frac{d\theta}{dt} + \frac{dW_s}{dt} \quad (6.4)$$

with  $\tau$  as the torque and  $W_s$  as the magnetic field energy. Using the concept of magnetic field co-energy (Krishnamurthy et al., 2006), the magnetic field energy can be given by

$$W_s = i\phi - W_c, \quad W_c = \frac{1}{2}Li^2 \quad (6.5)$$

where  $W_c$  is the magnetic field co-energy. It is assumed here that the EM synchronizer remains magnetically unsaturated during operation. Moreover, the coil inductance varies only as a function of the rotor angle. Differentiating both sides of eq.(6.5) with respect to time and substituting them into eq.(6.4), yields

$$\tau \frac{d\theta}{dt} = L(\theta) \frac{di}{dt} + \frac{i^2}{2} \frac{dL(\theta)}{dt} - \phi \frac{di}{dt} \quad (6.6)$$

At steady state operation, i.e., when current is constant in the winding, braking torque is produced when  $dL/d\theta < 0$ . The overall electro-magneto-mechanical brake model for a rigid stator and a rigid rotor can be formulated as

$$J\dot{\omega} = \tau_L - \tau_b \quad (6.7)$$

with  $J$  as the rotor moment of inertia,  $\tau_L$  and  $\omega$  were defined in eq.(5.1), and  $\tau_b$  as the braking torque. The latter is generated, primarily, by the reluctance of the rotor poles against the stator steel claws. Assuming a quasi-static magnetic field, a model for the reluctance torque is

$$\tau_b(\theta) = \frac{1}{\mu_0} \oint r B_r B_t z d\lambda \quad (6.8)$$

where the line integral is over the magnetic circuit,  $\mu_0$ ,  $\lambda$ ,  $r$ ,  $B_r$ ,  $B_t$  and  $z$  are the air permeability, contour length, radial distance, radial flux density, tangential flux density, and axial depth, respectively. The periodic reluctance torque, dependent on the rotor position, is calculated using the Maxwell stress method and time-stepping approach in MagNet.

### 6.3 Finite Element Analysis

In order to obtain feasible solutions of eq.(6.8) by taking into account the effects of magnetic saturation, the MagNet finite element software package is employed. Shown

in Fig. 6.2 is one stator claw, a section of the toroidal coil and one rotor pole section of the EM synchronizer, modelled in MagNet. Features that do not play a major role in terms of electromagnetic modelling were ignored. The nonlinear problem is solved in MagNet using the Newton–Raphson method (with a 1% convergence tolerance), the linearized system of equations is solved using the Conjugate Gradient (CG) iterative method (with a CG tolerance: 0.01%), and the torque calculation is carried out using the Maxwell stress tensor (Lowther and Silvester, 1986). The transient-with-motion solver is used with a simulation time-step of 1 ms in the simulation stepping algorithm. For 3D simulation tests of a device with a periodic architecture such as this, the modelling of one single claw-pole section is required, which reduces the computation time by  $1/4n$ , where  $n$  is the number of periodic claw-pole sections. A sensitivity analysis, based on refining the mesh and solver settings, was carried out to ensure that the FEA results were stable and the torque calculations as accurate as possible. The rotor pole and its surrounding air sections were defined as the motion component of the system. The meshing in the air-gap at the motion interface was split into four equally thick sections to ensure small mesh elements. The second-order polynomial interpolation for these elements showed results with good accuracy and reasonable computation time.

The dimensioning of the MagNet model was done as discussed in Subsection 6.1.2. The sectional winding was modelled as a stranded coil with current traversing along circumferentially. A coil packing factor of 60% was used that accommodates 250 turns of No. 14 gauge double-layer insulated wire. A 13.8 V DC source was connected in series to the coil. Solid ANSI 1010 cold-rolled steel was assigned to the stator and rotor material. All parameters, including the rotor moment of inertia, associated with the periodicity of the device, were adjusted accordingly. However, simulation tests were needed to determine an optimum claw-pole number. To this end, simulations

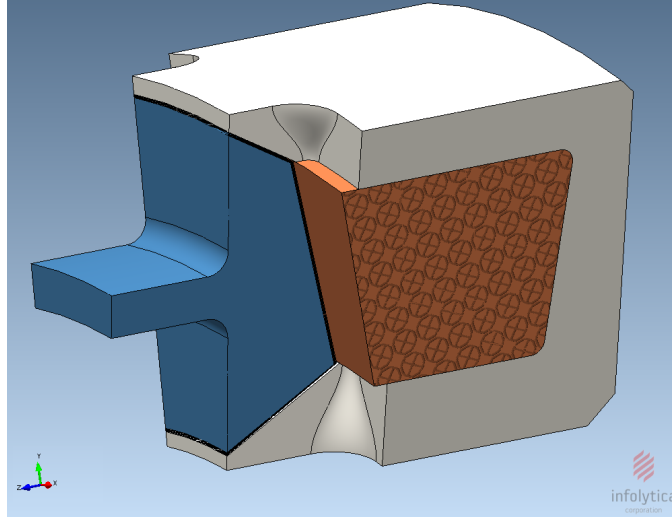


FIGURE 6.2. MagNet model of one stator claw and one rotor pole

were conducted using 6, 12, 15, 16, 18, 20, 24, and 30 claw-pole combinations, while keeping all other parameters at their original values. Each claw and rotor pole were modelled with the same angular width of  $2\pi/2n$ . The rotor in each simulation test was rotated about its axis to the position where  $dL/d\theta$  is maximum, as derived in eq.(6.6). The latter yields the maximum reluctance torque, which, for this geometry is at a rotor angle of  $2\pi/4n$ . Using the 3D transient solver, each combination was tested without motion to observe the peak torque values. Shown in Table 6.1 is a summary of each claw-pole combination solved in MagNet. From the results, the 16 claw-pole combination was observed to be the one with the highest torque.

TABLE 6.1. Summary of maximum torque of each claw-pole set

No. of claw-poles	Peak torque (Nm)
6	30.20
12	34.32
15	38.10
16	39.42
18	38.64
20	37.60
24	34.20
30	27.12

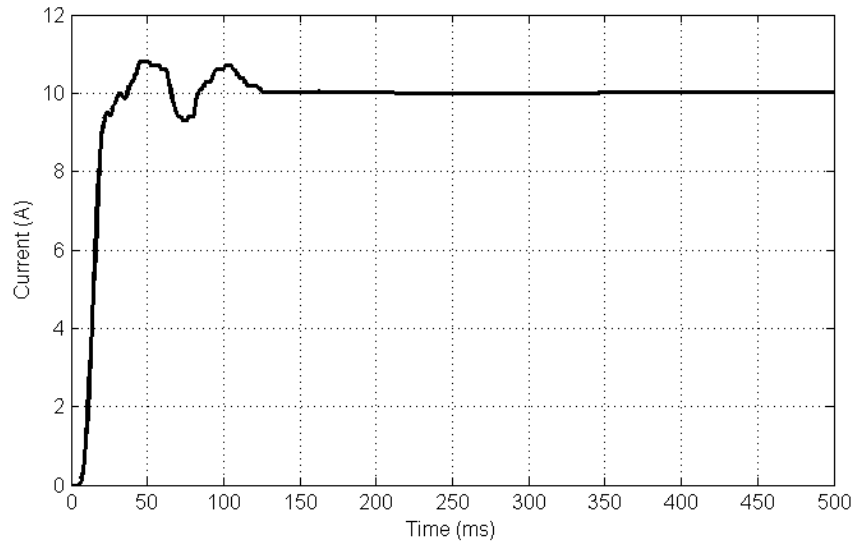


FIGURE 6.3. Current in the coil winding

Next, one sixteenth of the 16 claw-pole set was simulated dynamically. With the rotor initially spinning at 100 rpm, the speed-controlled load torque  $\tau_L$  was applied, starting at zero load for 100 rpm and linearly increasing to  $\tau_{\max}$  at zero rpm of rotor slip, as defined in eq.(5.1). The coil was excited with a DC voltage of 13.8 V, which was modelled as a ramp input starting with zero volts at 10 ms and constant at 13.8 V from 20 ms, while the simulation test lasted 500 ms. The results, adjusted to represent the entire 16 claw-pole geometry of the simulation test are shown in Figs. 6.3–6.5. The rotor comes to a halt at the 110 ms mark while utilizing a steady state current of 10 A. Therefore, the EM system takes only 90 ms from the moment power at 13.8 V is supplied. The magnetic braking torque  $\tau_b$  balances the load  $\tau_L$  to hold the rotor at its maximum reluctance position. Shown in Fig. 6.6 is a flux density plot of 1/16 of the entire geometry. The arrows display the direction of the magnetic field. The saturation in the rotor pole and stator claw was observed to be time-varying. Without exceeding the design volume budget, stator claw and rotor-pole saturation were unavoidable.

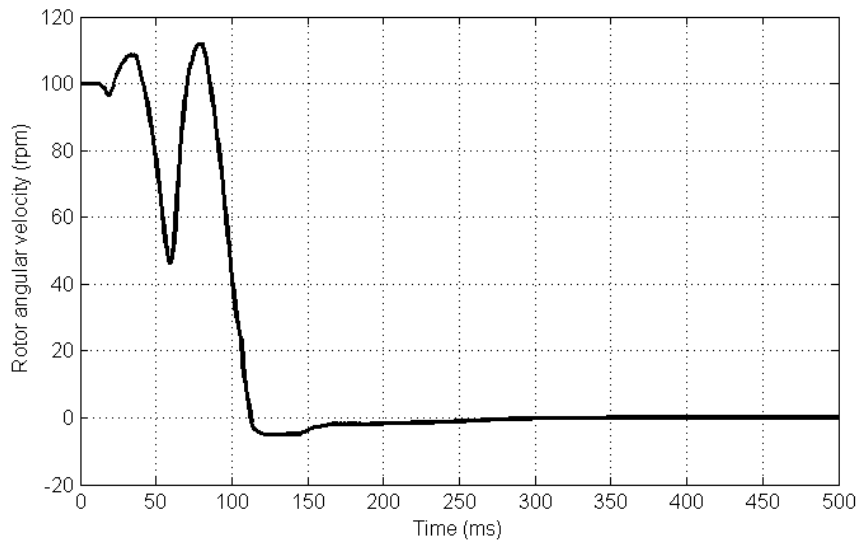


FIGURE 6.4. Rotor speed

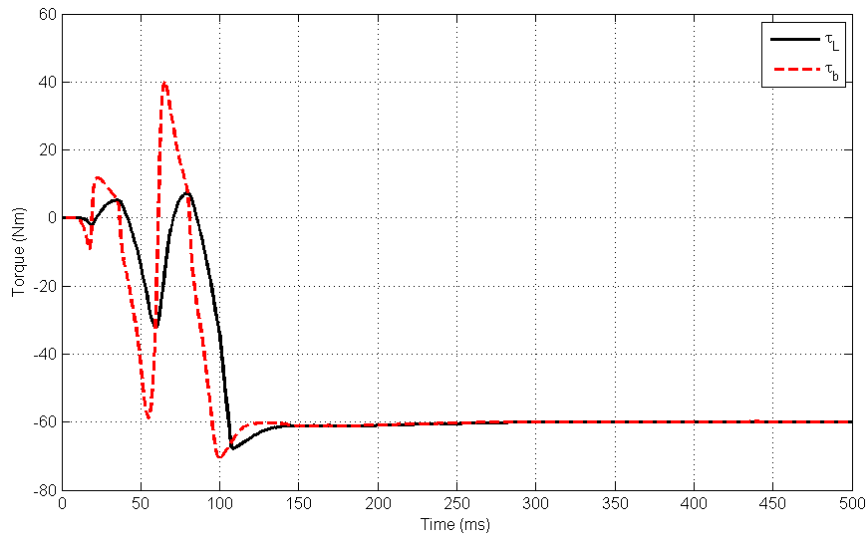


FIGURE 6.5. Rotor torque

*Powdered Metal Design.* Further investigation of the design for mass-production was carried out. The choice of powdered metals for mass-production, to replace the solid stator and rotor steel, is obvious. Powdered metals offer unique designs, very low manufacturing cost, good dimensional stability and complete recyclability. They can be pressed within 5% of the density of solid steel. Powdered material is compacted

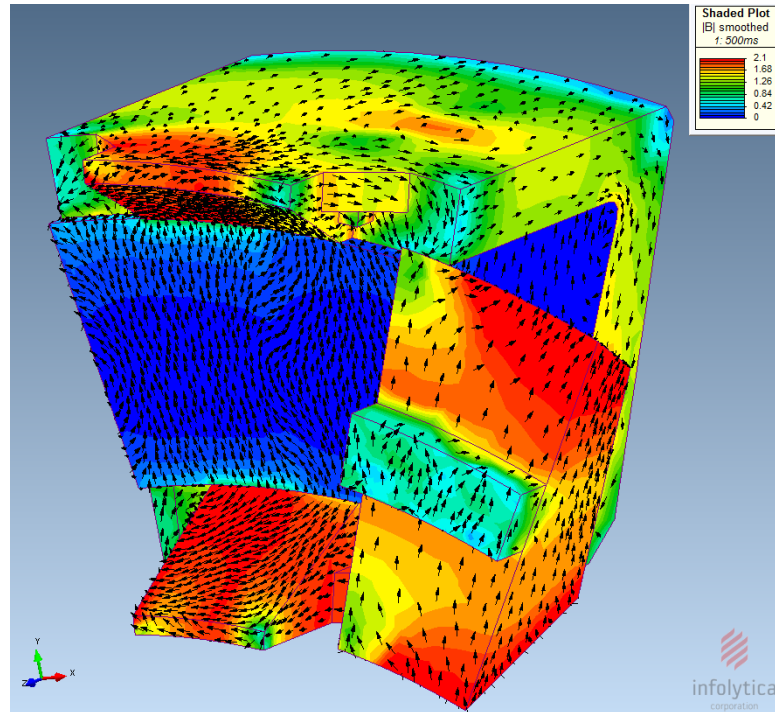


FIGURE 6.6. Flux density plot of one-sixteenth of the geometry

and then thermally treated to relieve stresses and replenish high strength (Persson et al., 2003). Normally, iron particles are covered with an insulation layer, to prevent core losses and minimize eddy-currents. However, the EM brake design would use the powdered material without the insulation layer, as the generation of eddy currents will aid in energy dissipation. In order to simulate the 16-claw-pole model, the magnetic properties of an appropriate soft magnetic powdered iron was sought. One such material found for the application was FY-4500, a powder with 99.55% iron and 0.45% phosphorus, available from Burgess-Norton. Material density, electrical resistivity, core losses, and magnetic permeability (B-H data) were obtained from the company<sup>1</sup>. The material B-H properties of both 1010 steel and FY-4500, as modelled in MagNet, are shown in Fig. 6.7. Solid 1010 steel was replaced with FY-4500 for

<sup>1</sup>[www.burgessnorton.com/powder.html](http://www.burgessnorton.com/powder.html)

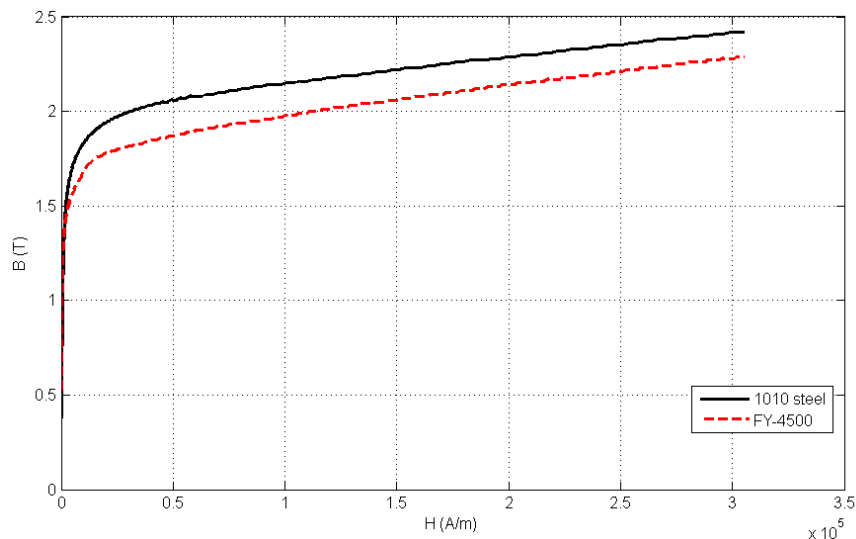


FIGURE 6.7. A MagNet extrapolation of the initial B-H curves of 1010 steel and FY-4500

the stator and rotor material. Using the properties of FY-4500, simulations were conducted to evaluate the feasibility of the design for mass-production.

All parameter and simulation test conditions were kept the same as the one for solid steel. Shown in Fig. 6.8 is the rotor speed plot. The rotor comes to a stop within 213 ms for the same current and input voltage as 1010 steel. In comparison with solid 1010 steel, FY-4500 material takes about a 100 ms longer to complete the braking action. Although the design exhibits acceptable results, it needs further investigation for mass production.

## 6.4 Experimental Testing

The EM synchronizer was fabricated and installed on a testbed to conduct proof-of-concept tests. The testbed consists of the EM stator, the EM rotor, the toroidal coil assembly, a 13.8 V DC power supply, thrust bearings, a motor and a gearbox. Shown in Figs. 6.10 and 6.11 is the testbed and a CAD model of the testbed cross-section for the EM synchronizer with all its supports, connections, bearings, keys and mounting arrangement. The rotor and stator were machined out of ANSI 1018

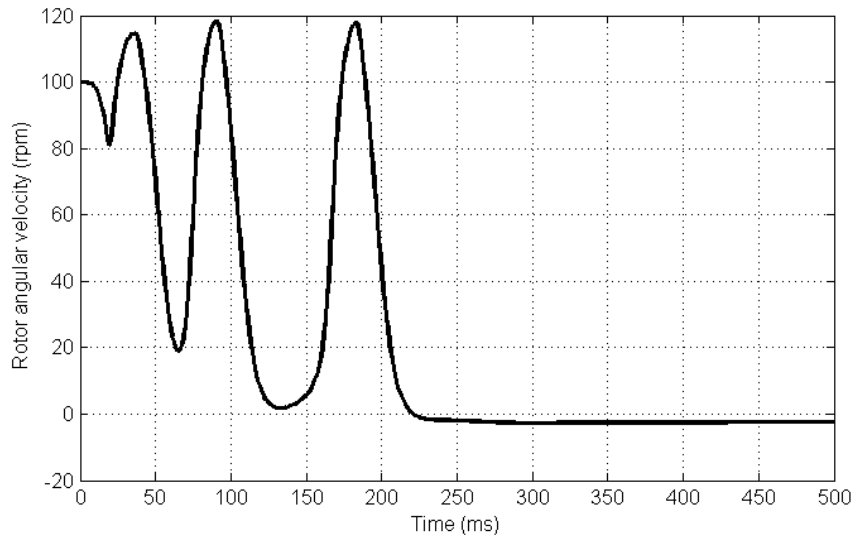


FIGURE 6.8. Rotor speed using FY-4500

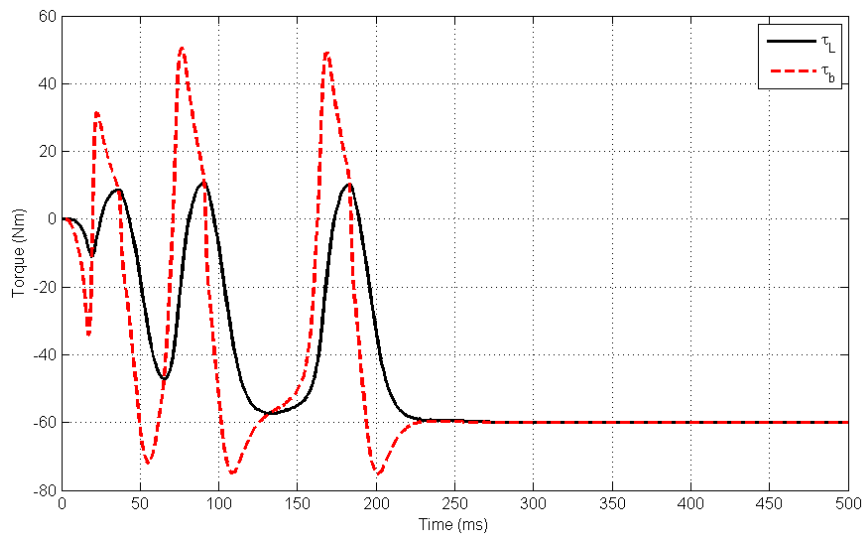


FIGURE 6.9. Rotor load using FY-4500

hot-rolled steel on a CNC machine. Note that ANSI 1018 hot-rolled steel was used instead of ANSI 1010 cold-rolled steel, because 1018 steel is a more stable product for CNC machining, as reported by the local machine shop's Mr. Sam Minter. The rotor was designed such that its inertia takes into account an addition of  $0.05 \text{ kg}\cdot\text{m}^2$ . A FEA of the rotor was conducted to examine the stresses within the rotor at stall

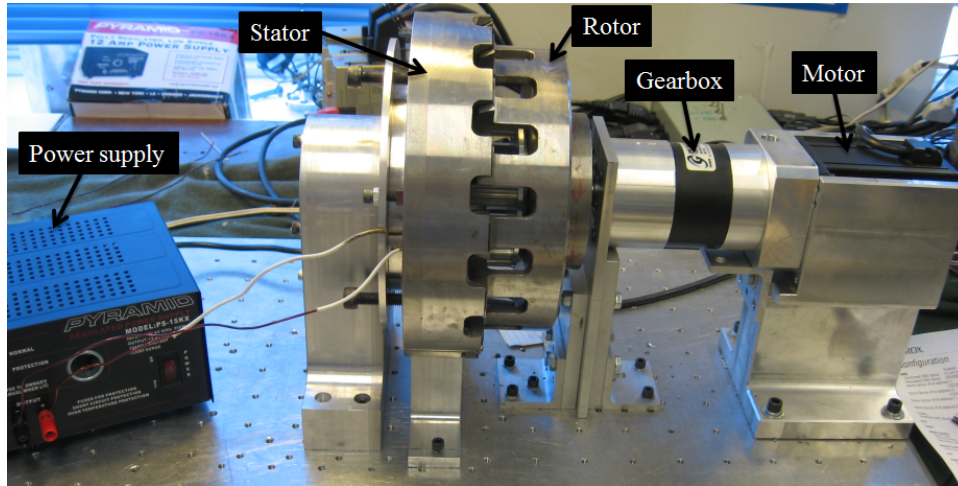


FIGURE 6.10. The testbed for the EM synchronizer

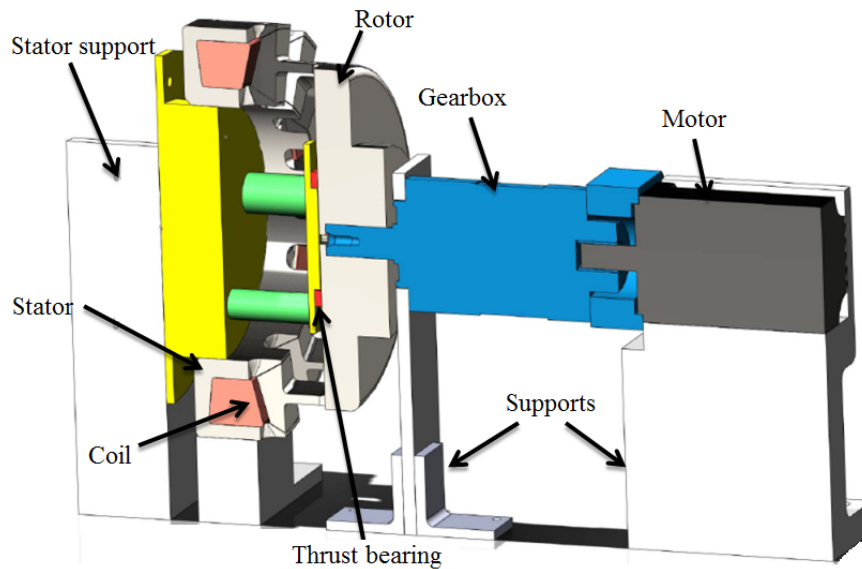


FIGURE 6.11. Cross-sectional view of the testbed

loads. To this end, the rotor was fixed and pinned at its internal keyway with a load of 70 Nm applied at its external boundary. Shown in Figs 6.12, 6.13 and 6.14 are the loading conditions, von-Mises stress and displacement fields of the FEA results. The yield strength of AISI 1018 is 275 MPa, which provides a safety factor of 1.54 for the stresses. The machined rotor is shown in Fig. 6.15.

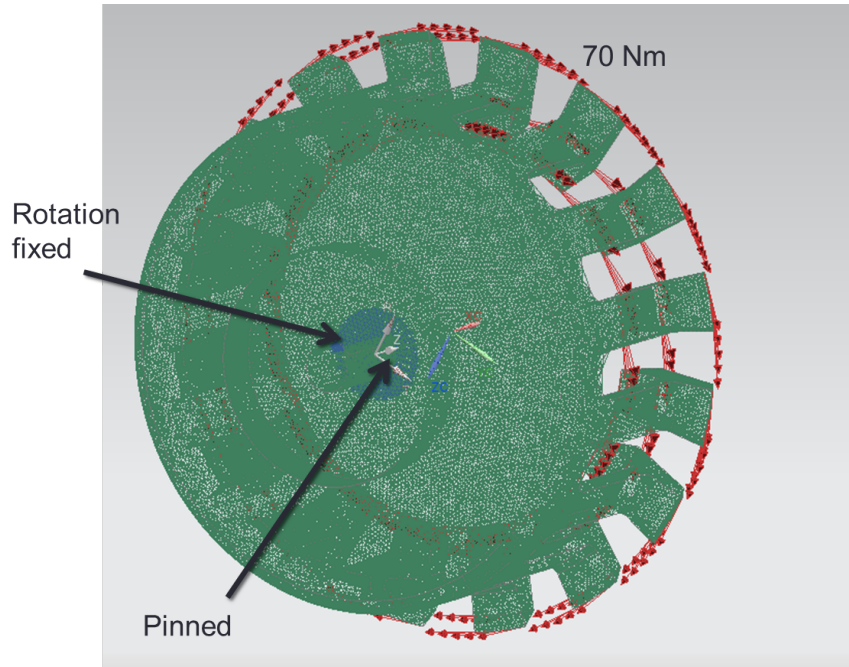


FIGURE 6.12. Static loading conditions for rotor FEA

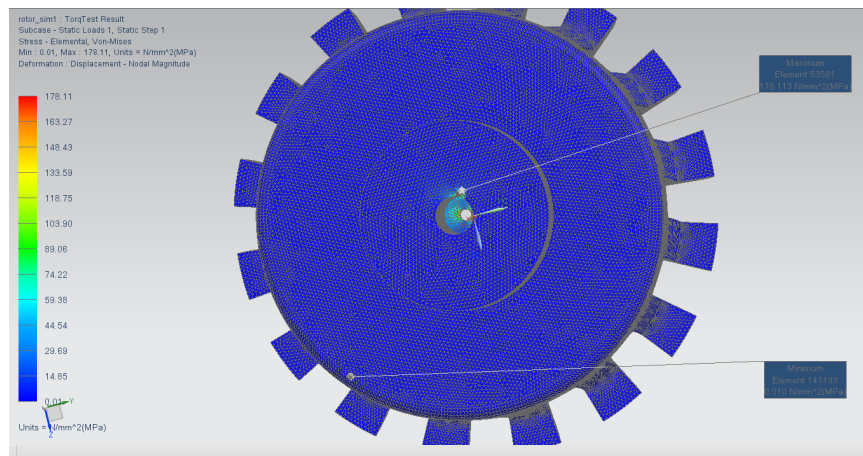


FIGURE 6.13. von Mises stress distribution in the rotor

Shown in Fig. 6.16 is the fabricated stator piece. The coil winding was created using special bobbin which outlined the stator cavity. RenShape 460 material was used to create a two-piece bobbin, as shown in Fig. 6.17. The stranded coil wire was held together with a heat-treated epoxy glue. The stator is fixed onto the baseplate with a support. The motor is coupled to the gearbox via a flexible coupling. The

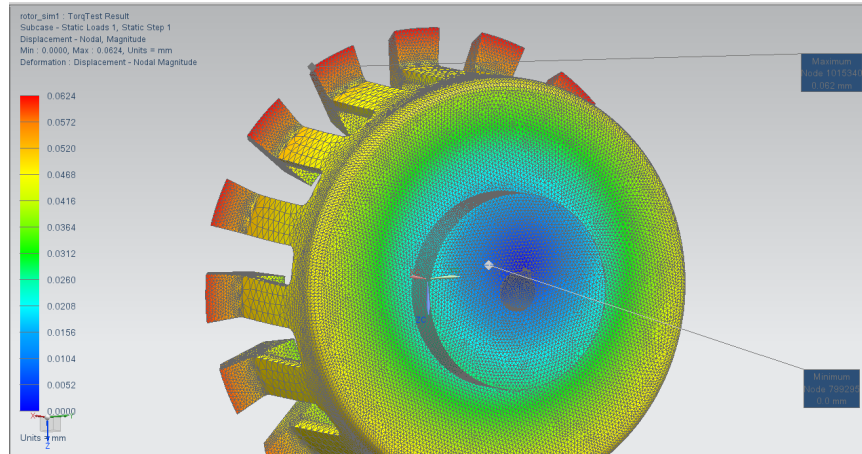


FIGURE 6.14. Elastic deformation displacement plot of the rotor FEA



FIGURE 6.15. Machined rotor

rotor is keyed and pinned directly onto the gearbox output shaft. The gearbox consists of a two-stage planetary gear train with an overall ratio of 1 : 20 and an output efficiency of 92%; which is taken into account while conducting the experiments. The motor-gear assembly is used to drive the rotor and to provide the resistive load torque. Data acquisition and processing of the experiments relied on MATLAB/Simulink with Quanser's QuaRC embedded software. Numerical data are recorded from the motor

amplifier at a sampling frequency of 1 kHz and for a duration of 5 s. The motor amplifier is equipped with a digital signal processor capable of capturing the motor angular velocity from the position encoder of the motor. The motor angular velocity signal had been previously validated (Chopra, Zargarbashi and Angeles, 2013). Moreover, the motor amplifier was tuned to control the motor current and, correspondingly, its resistive load torque in the form of eq.(5.1). The 13.8 V power supply is connected directly across the coil terminals. The power supply is manually switched on, at an instant past the 2.5 s mark, while rotor load and velocity data are recorded.



FIGURE 6.16. Machined stator

The experiment commences with the rotor spinning at a steady velocity of 100 rpm. As the 13.8 V power supply is switched on, the field generated by the coil magnetizes the rotor, which brakes to a complete stop. Plotted in Figs. 6.18 and 6.19 are the data recorded for the rotor velocity and the rotor load. The fast response of the EM system is emulated as braking action takes only 100 ms, typical of electromagnetic systems. Furthermore, the EM synchronizer is capable of resisting  $\tau_{\max}$ , the 60 Nm of peak rotor load torque. The rotor pole is held at the maximum reluctance position of  $5.625^\circ$  with respect to the stator claw.

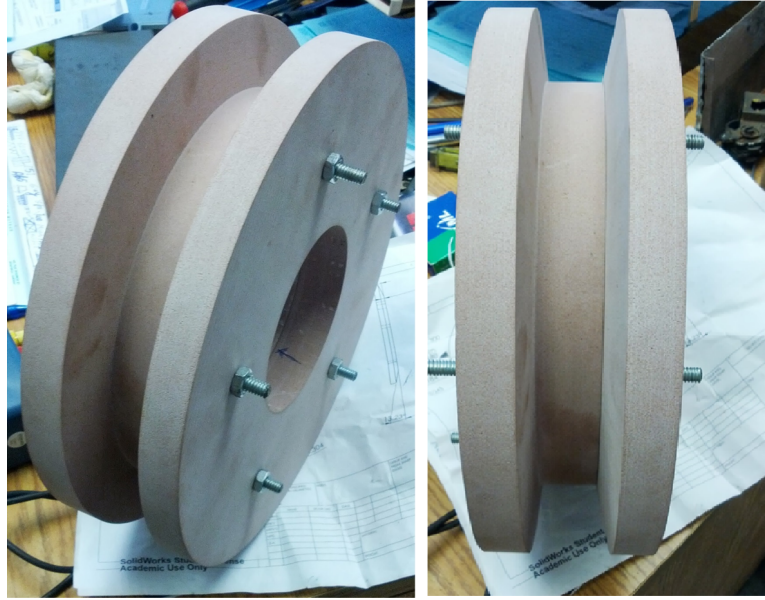


FIGURE 6.17. Reshape coil bobbin

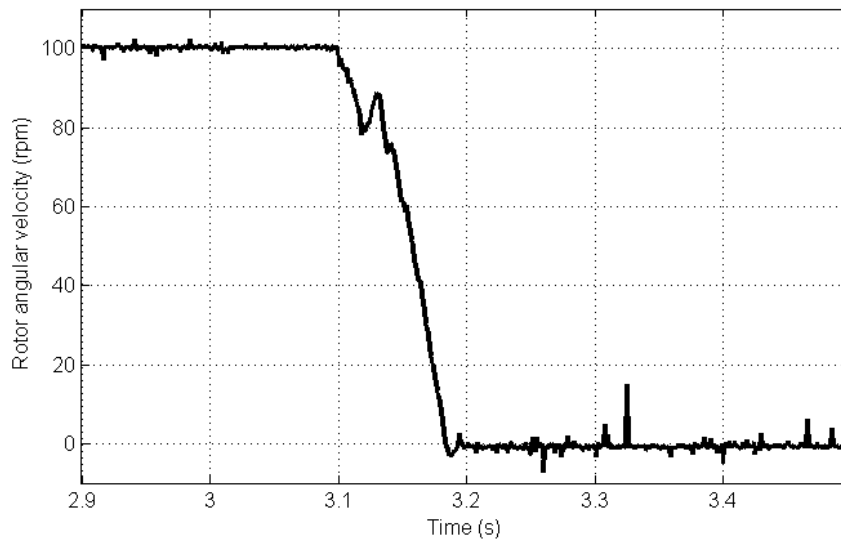


FIGURE 6.18. Rotor speed recorded

Listed in table 6.2 is an overall summary of the final EM synchronizer performance. Some differences are observed between experiments and simulation tests. The response in the experiments was 10 ms faster than the simulation, as bearing frictional losses were not taken into account in the simulation. The application of

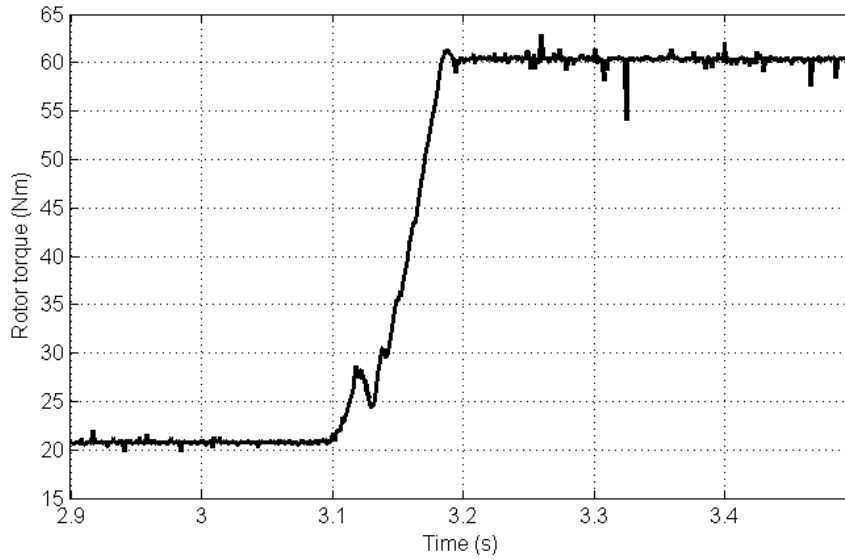


FIGURE 6.19. Rotor load torque

the 13.8 V input in the experiment was done arbitrarily, whereas, in simulation, it occurred close to the onset of the test. Consequently, the response depends on the rotor pole position during operation. Other noteworthy differences lie in the materials used; ANSI 1010 cold-rolled steel for simulation and ANSI 1018 hot-rolled steel for the physical model. The B-H data for ANSI 1010 cold-rolled steel was obtained from manufacturer catalogues which was available in MagNet. Testing of magnetic properties of 1018 steel was not carried out but is observed to not vary substantially given its low carbon content (Rumiche, Indacochea and Wang, 2008).

Clutching-action duration	0.1 s
No. of stator claws	16
No. of rotor claws	16
Wire gauge	14 AWG
Coil packing factor	60%
No. of turns	250
Total resistance	1.379 Ohms
Moment of inertia of rotor	0.06448 kgm <sup>2</sup>
Initial rotor speed	100 rpm
Peak load applied on rotor at 0 rpm	60 Nm

TABLE 6.2. Final prototype performance

## CHAPTER 7

---

# Conclusions and Recommendations for Future Research

### 7.1 Conclusions

In this thesis, design techniques for automotive clutching mechanisms for use in hybrid transmissions were laid out. The techniques, based on systematic engineering design, were used to produce novel clutch devices which serve as feasible alternatives to current technology. A thorough investigation was undertaken to understand the working principles and drawbacks of wet clutches. Pertinent technical specifications and goals were established. A rich set of design variants was produced; following an initial screening, a short list of four concepts was evaluated. Two top design concepts were identified and developed to advance the state of the art.

An electromechanical clutch actuator was designed, analyzed and evaluated. The layout of the design, based on a high-performance screw joint with a built-in locking mechanism, was designed and tested. The screw joint was implemented with two sub-variants, namely, a lead screw and a ball screw with a ratchet and pawl lock. An important component, namely the apply-plate, was designed with Lamé curves to replace commonly used circular fillets. Finite-element analysis of the apply-plate

showed that the safety factor was improved by about 20%, with respect to the circular-fillet version.

The testbed for the electromechanical clutch actuator was set up for experiments. An iconic model of the testbed led to the mathematical model, based on which, the testbed was simulated. Experiments were conducted and results thereof were compared with those obtained by simulation. Subsequently, friction parameters of the model were estimated. Friction is observed to greatly reduce the lead screw performance. The lead screw system requires high motor torques to overcome frictional losses to provide high clutching forces. However, friction is also important to preserve the self-locking ability of the lead screw. Compressive force testing of the clutch actuator shows its capability in providing high clamping forces for clutches of 500 Nm capacity. The ball-screw variant showed promising results, while requiring lower motor input torque. Frictional losses were reduced; an independently actuated pawl-and-ratchet lock maintained the clamping force without an external power. In both variants, simplicity of the design and their locking ability render them a promising solution for clutch actuators, where maintaining clutch lock-up without input power leads to energy savings, a quintessential feature required in next-generation HEV transmissions.

The novel design of an electromagnetic brake synchronizer was then introduced. The design features a single-phase compound-wound salient stator and a permanent magnet-based salient rotor. Dynamics simulation tests conducted using the 3D transient with motion solver in MagNet demonstrated the feasibility of the design concept; these tests provide detailed-enough performance information that the fabrication of a prototype is obviated. On evaluating the performance of the design, an innovative modification was made to aid in the reduction of PM mass, which consequently lowered cogging torque and potential fabrication costs. With advances in finite element

magnetic software, quick, efficient designs can be readily validated, as illustrated in this thesis.

Moreover, an alternate electromagnetic brake clutch synchronizer without any permanent magnets was designed, analyzed and physically tested. The layout of the innovative system was described with a brief electromagnetic model. A complete electromagnetic finite-element analysis with motion dynamics was carried out to assess the design feasibility; the results thereof were used to obtain the right claw-pole combination. A testbed was set-up for proof-of-concept tests. Experiments were conducted, its results showing agreement with those obtained by simulation. The electromagnetic synchronizer performed within the design specification. It functions to synchronize its rotor with an active torque applied. Requiring only a 13.8 V DC supply, this design boasts of low current usage with a high power density, thereby making it readily applicable in most automotive transmissions. Once the system is locked via a dog clutch system, all input power is turned off. The contactless medium provides a robust rugged system with advantages of no wear. No contact also results in low spin losses in the open clutch state.

Both clutching mechanisms match the power density of current clutches, achieve quick engage/disengage action, showcase simple controls, fit within a volumetric budget, minimize spin losses and reduce energy expenditure. Moreover, both mechanisms were electrically actuated.

## 7.2 Recommendations for Future Research

The work reported here has made apparent the need for further research and development on a number of complementary topics, as outlined below.

- The techniques discussed in Chapter 2 can be extended further to incorporate the multi-disciplinary nature of automotive design. The meshing of

electrical, mechanical, magnetic, pneumatic, and hydraulic systems, to list a few, requires designers to be knowledgeable in multiple disciplines. Further development of the multidisciplinary design process should help increase the automotive designer's productivity.

- Although compressive tests of the ball- and lead-screw actuators were done; their testing on a clutch dynamometer testbed will be highly beneficial. The testing under vehicle loads is needed to observe whether the variants preserve their locking ability with the effects of vibration.
- Bench-marking tests on energy efficiency of hydraulically actuated clutches versus the electromechanical clutch actuator are needed to validate the energy saving claims of the electromechanical actuator. This can be done in two ways: installing the EMC actuator in vehicles to conduct fuel efficiency tests; and producing two testbeds where both clutch actuation systems are tested by measuring power input and output.
- In the electromagnetic synchronizer's design, the stator mass can be subject to optimization to make it more lightweight. Powdered metal use for mass production will also serve as an important future contribution to the work reported here.
- The FEA analysis conducted for the rotor of the EDC variant was for its use within the proof-of-concept testbed. However, a clutch used within a HEV powertrain would experience considerable dynamic impact loads which can be significantly higher than the static loads. A dynamic and fatigue analysis of the rotor would be required for further development.
- Further development of the dog clutch system is required. Important design work was outlined in this thesis. The incorporation, detail design and fabrication of the dog clutch mechanism to be used with the electromagnetic

## 7.2 RECOMMENDATIONS FOR FUTURE RESEARCH

synchronizer will be beneficial in developing an advanced product for HEV transmission use.



# BIBLIOGRAPHY

---

- Angeles, J., 2007 *Fundamentals of Robotic Mechanical Systems*, Third Edition, Springer, New York, USA.
- Anwar, S., and Stevenson, R. C., 2011, "Torque characteristics analysis for optimal design of a copper-layered eddy current brake system," *Int. Journal of Automotive Technology*, Vol. 12, No. 4, pp. 497-502.
- Anwar, M. N., Gleason, S. E., and Grewe, T. M. , 2010, "Design considerations for high-voltage DC bus architecture and wire mechanization for hybrid and electric vehicle applications," *IEEE in Energy Conversion Congress and Exposition (ECCE)*, pp. 877-884.
- Arakawa, Y., Yauchibara, R., and Murakami, Y. , 2003, "Development of a Multi-purpose ATF Meeting DEXRON III, MERCON and JASO M315 Specifications," *SAE Technical Paper*, No. 2003-01-1984.
- Armstrong-Hélouvy, B., 1991, "Control of Machines with Friction," Kluwer Academic Publishers, Massachusetts, USA.
- Bianchi, N., and Bolognani, S., 2002, "Design techniques for reducing the cogging torque in surface-mounted PM motors," *IEEE Transactions on Industry Applications*, Vol. 38, pp. 1259-1265.
- Benford, H. L., and Leising, M. B., 1981, "The lever analogy: a new tool in transmission analysis," *SAE Technical Paper*, No. 810102.

## BIBLIOGRAPHY

- Bertoluzzo, M., and Buja, G., 2011, "Development of Electric Propulsion Systems for Light Electric Vehicles," *IEEE Trans. Ind. Info.*, Vol. 7, No. 3, pp. 428-435.
- Bezzazi, M., Khamlichi, A., Jabbouri, A., Reis, P., and Davim, J.P., 2006, "Experimental characterization of frictional behaviour of clutch facings using Pin-on-disk machine," *Materials & Design*, Vol. 28, No. 7, pp. 2148-2153.
- Bloxham, D.A., and Wright, M.T., 1972, "Eddy-current coupling as an industrial variable-speed drive," *PROC. IEE*, Vol. 119, No. 8, pp. 1149-1154.
- Canova, A., Freschi, F., Gruosso, G., and Vusini, B., 2005, "Genetic optimisation of radial eddy current couplings," *COMPEL - The Int. J. Computation and Mathematics in Electrical and Electronic Engineering*, Vol. 24, No. 3, pp. 767-783.
- Chan, C.C., Bouscayrol, A., and Chen, K., 2010, "Electric, Hybrid, and Fuel-Cell Vehicles: Architectures and Modelling," *IEEE Trans. Veh. Technol.*, Vol. 59, No. 2, pp. 589-598.
- Chopra, V., Zargarbashi, S.H.H., and Angeles, J., 2013, "Parameter Identification of the Testbed of a Novel Gearless Pitch-Roll Wrist," *Mechanical Systems and Signal Processing*, Vol. 41, No. 1-2, pp. 71-85.
- Chopra, V., Smith, A.L., Ma, X.Q., and Angeles, J., 2012, "GM Collaborative Report: Design of Innovative Clutching Mechanisms," Technical Report TR-CIM-12-09, GM report No. CL-12/42/PSL, Department of Mechanical Engineering and Centre for Intelligent Machines, McGill University, Montreal.
- Chopra, V., Smith, A.L., and Angeles, J., 2013, "Electromechanical Clutch Actuator: Design, Analysis and Experiments," *SAE Technical Paper*, No. 2013-01-2496.
- Chen, L., Zhu, F., Zhang, M., Huo, Y., Yin, C., and Peng, H., 2011, "Design and analysis of an electrical variable transmission for a series-parallel hybrid electric vehicle," *IEEE Trans. Veh. Technol.*, Vol. 60, No. 5, pp. 2354-2363.

- Daun, S., Zhou, L., and Wang, J., 2012, "Flux Weakening Mechanism of Interior Permanent Magnet Synchronous Machines With Segmented Permanent Magnets," *IEEE Trans. Appl. Superconductivity*, Vol. 24, No. 3, pp. 1-7.
- Dieter, G. E., 2000, *Engineering Design*, Third Edition, McGraw-Hill.
- Dixon, J.R., and Poli, C., 1995, *Engineering Design and Design for Manufacturing*, Field Stone Publishers, Conway, MA.
- Dym, C. L. and Little, P., 2000, *Engineering Design - a project-based introduction*, Wiley.
- Eberleh, B., and Hartkopf, T., 2006, "A high speed induction machine with two-speed transmission as drive for electric vehicles," *International Symposium on Power Electronics, Electrical Drives, Automation and Motion*, Vol. 23, No. 26, pp. 249-254.
- Eguchi, M., and Yamamoto, T., 2005, "Shear characteristics of a boundary film for a paper-based wet friction material: friction and real contact area measurement," *Tribology International*, Vol. 38, pp. 327-335.
- Estima, J.O. and Marques-Cardoso, A.J., 2012, "Efficiency Analysis of Drive Train Topologies Applied to Electric/Hybrid Vehicles," *IEEE Trans. Veh. Technol.*, Vol. 61, No. 3, pp. 1021-1031.
- Fan, J.-J., and Wu, J.-H., 2013, "Reduction of cogging torque in permanent magnet synchronous motor using the taguchi method," *Applied Mechanics and Materials*, Vol. 278-280, pp. 143-148.
- Fatima, N., Marklund, P., and Larsson, R., 2013, "Influence of clutch output shaft inertia and stiffness on the performance of the wet clutch," *Tribology Transactions*, Vol. 56, No. 2, pp. 310-319.
- Froslic, L.E., Milek, T., and Smith, R.W., 1973, "Automatic Transmission Friction Elements," *Des Pract, Passenger Car Autom Transm, SAE Transm. Workshop*

## BIBLIOGRAPHY

- Meet*, Second Edition, pp. 106-124.
- Fish, R.L., 1991, "Using the SAE # 2 Machine to Evaluate Wet Clutch Drag Losses," *SAE International Congress & Exposition*, Detroit, U.S.A., February.
- Furlani, E.P., 2001, *Permanent Magnet and Electromechanical Devices*, Academic Press, London.
- Gao, H., Barber, G. C., and Chu, H., 2002, "Friction characteristics of a paper-based friction material," *International Journal of Automotive Technology*, Vol. 3, No. 4, pp. 171-176.
- Gao, H., and Barber, G. C., 2002, "Engagement of a Rough, Lubricated and Grooved Disk Clutch with a Porous Deformable Paper-Based Friction Material," *Tribology Transactions*, Vol. 45, No. 4, pp. 464-470.
- General Motors, 2007, *Hydra-matic 6T70 Technician's Guide*, Powertrain Group of General Motors Corporation.
- Gardiner, M., 1965, "The superellipse: a curve that lies between the ellipse and the rectangle," *Sci. Am.*, Vol. 21, pp. 222-234.
- Gosselin, C., and Angeles, J., 1989, "Optimization of planar and spherical function generators as minimum-defect linkages," *Mechanism and Machine Theory*, Vol. 24, No. 4, pp. 293-307.
- Gutierrez-Castaneda, E. J., and Salinas-Rodriguez, A., 2011, "Effect of annealing prior to cold rolling on magnetic and mechanical properties of low carbon non-oriented electrical steels," *Journal of Magnetism and Magnetic Materials*, Vol. 323, No. 20, pp. 2524-2530.
- Hanitsch, R., 1991, "Design and performance of electromagnetic machines based on Nd-Fe-B magnets," *Journal of magnetism and magnetic materials*, Vol. 101, No. 1, pp. 271-275.

- Hata, H., Kojima, M., Watanabe, H., Mizutani, T., Kamiya, M., and Yanagida, E., 2005, "Development of a new hybrid transmission for FWD sports utility vehicles" *JSAE Annual Congress In Proceedings*, Vol. 8, No. 5, pp. 1-6.
- Huang, F., Mo, Y., and Lv, J., 2010, "Study on heat fading of phenolic resin friction material for micro-automobile clutch," *International Conference on Measuring Technology and Mechatronics Automation, ICMTMA*, Article No. 5459128, pp. 596-599.
- Hauser, J.R., and Clausing, D., 1988, "The House of Quality," *Harvard Business Review*, pp. 63-73, May-June.
- Hauser, H., Grssinger, R., Keplinger, F., and Schnhart, M., 2008, "Effect of structural changes on hysteresis properties of steel," *Journal of Magnetism and Magnetic Materials*, Vol. 320, No. 20, pp. 983-987.
- Hendrickson, J., Holmes, A. and Freiman, D., 2009, "General Motors Front Wheel Drive Two-Mode Hybrid Transmission," *SAE Technical Paper*, No. 2009-01-0508.
- Holdstock, T., Sornioti, A., Everitt, M., Fracchia, M., Bologna, S., and Bertolotto, S., 2012, "Energy consumption analysis of a novel four-speed dual motor drivetrain for electric vehicles," *IEEE Veh. Power and Propulsion Conf.*, pp. 295-300.
- Hoseinnezhad, R., Bab-Hadiashar, A., and Rocco, T., 2008, "Real-time clamp force measurement in electromechanical brake calipers," *IEEE Transactions on Vehicular Technology*, Vol. 57, No. 2, pp. 770-777.
- Hwang, C. C., Wu, M. H., and Cheng, S. P., 2006, "Influence of pole and slot combinations on cogging torque in fractional slot PM motors," *Journal of Magnetism and Magnetic Materials*, Vol. 304, No. 1, pp. 430-432.
- Huang, F., Mo, Y., and Lv, J., 2010, "Study on heat fading of phenolic resin friction material for micro-automobile clutch ," *International Conference on Measuring Technology and Mechatronics Automation, ICMTMA*, Article No. 5459128, pp.

## BIBLIOGRAPHY

596-599.

Husain, I., and Ehsani, M., 1996, "Torque ripple minimization in switched reluctance motor drives by PWM current control," *IEEE Trans. Power Electronics*, Vol. 11, No. 1, pp. 83-88.

Ingram, M., Spikes, H., Noles, J., and Watts, R., 2010, "Contact properties of a wet clutch friction material," *Tribology International*, Vol. 43, No. 4, pp. 815-821.

Jo, C., Hwang, S., and Kim, H., 2010, "Clamping-force control for electromechanical brake," *IEEE Transactions on Vehicular Technology*, Vol. 59, No. 7, pp. 3205-3212.

Juvinall, R.C., and Marshek, K. M., 2000, "Fundamentals of Machine Component Design," John Wiley & Sons Inc., New York, N.Y..

Karden, E., Ploumen, S., Fricke, B., Miller, T., and Snyder, K., 2007, "Energy storage devices for future hybrid electric vehicles," *Journal of Power Sources*, Vol. 168, No. 1, pp. 2-11.

Khan, W.A., 2007, *The conceptual design of robotic architectures using complexity criteria*, Doctorate of Engineering Thesis, Department of Mechanical Engineering, McGill University, Montreal, August.

Kim, J., and Choi, S. B., 2011, "Design and modelling of a clutch actuator system with self-energizing mechanism," *IEEE/ASME Transactions on Mechatronics*, Vol. 16, No. 5, pp. 953-966.

Kim, J., Oh, J., and Choi, S. B., 2012, "Nonlinear estimation method of a self-energizing clutch actuator load," *IEEE First International Conference on Innovative Engineering Systems (ICIES)*, pp. 231-236, Alexandria, Dec. 7-9.

Kim, J., Park, S., Seok, C., Song, H., Sung, D., Lim, C., Kim, J. and Kim, H., 2003, "Simulation of the shift force for a manual transmission," *Proc. Inst. Mechanical Engineers - Part D: J. Automobile Engineering*, Vol. 217, pp.573-581.

- Kitabayashi, H., Li, C.Y., and Hiraki, H., 2003, "Analysis of the various factors affecting drag torque in multiple-plate wet clutches," *SAE Transactions ISSN 0096-736X*, Vol. 112, No. 4, pp. 1840-1845.
- Klingenberg, D.J., 2001, "Magnetorheology: Applications and Challenges," *AICHE Journal*, Vol. 47, No. 2, pp. 246249.
- Kluger, M.A., Fussner, D.R., and Roethler, B., 1996, "A performance comparison of various automatic transmission pumping systems," *SAE Technical Paper*, No. 960424.
- Kluger, M.A., and Long, D.M., 1999, "An Overview of Current Automatic, Manual and Continuously Variable Transmission Efficiencies and Their Projected Future Improvements," *SAE Technical Paper*, No. 1999-01-1259.
- Krishnamurthy, M., Edrington, C. S., Emadi, A., Asadi, P., Ehsani, M. and Fahimi, B. 2006, "Making the case for applications of switched reluctance motor technology in automotive products," , *IEEE Trans. on Power Elect.* Vol. 21, No. 3, pp. 659-675.
- Krishnan, R., 2001, *Switched Reluctance Motor Drives: Modelling, Simulation, Analysis, Design, and Applications*, First Edition, Crc Press Llc, Boca Raton, USA.
- Kugimiya, T., Yoshimura, N., Kuribayashi, T., Mitsui, J., Ueda, F., Ando, Y., Takanori, T., and Ohira, H., 1997, "Next Generation High Performance ATF for Slip-Controlled Automatic Transmissions," *SAE Technical Paper*, No. 972927.
- Lam, R.C., Chavdar, B., and Newcomb, T., 2006, "New Generation Friction Materials and Technologies," *SAE Technical Paper*, No. 2006-01-0150.
- Larsson, R., 2009, "Modelling the effect of surface roughness on lubrication in all regimes," *Tribology International*, Vol. 42, pp. 512-516.
- Lawrenson, P. J., Stephenson, J. M., Fulton, N. N., Blenkinsop, P. T., and Corda, J., 1980, "Variable-speed switched reluctance motors," *IEE Proceedings Electric Power Applications*, Vol. 127, No. 4, pp. 253-265.

## BIBLIOGRAPHY

- Lee, K., and Park, K., 1999, "Optimal robust control of a contactless brake system using an eddy current," *Mechatronics*, Elsevier, Vol. 9, No. 6, pp. 615-631.
- Lee, H. D., Sul, S. K., Cho, H. S., and Lee, J. M., 2000, "Advanced gear-shifting and clutching strategy for a parallel-hybrid vehicle," *IEEE Industry Applications*, Vol. 6, No. 6, pp. 26-32.
- Lewis, C., and Bollwahn, B., 2007, "General Motors Hydra-Matic & Ford New FWD Six-Speed Automatic Transmission Family," *SAE Technical Paper*, No. 2007-01-1095.
- Lhomme, W., Trigui, R., Delarue, P., Jeanneret, B., Bouscayrol, A., and Badin, F., 2008, "Switched causal modeling of transmission with clutch in hybrid electric vehicles," *IEEE Trans. Veh. Technol.*, Vol. 57, No. 4, pp. 2081-2088.
- Line, C., Manzie, C., and Good, M., 2004, "Control of an Electromechanical Brake for Automotive Brake-By-Wire Systems with an Adapted Motion Control Architecture," *SAE Technical Paper*, No. 2004-01-2050.
- Liu, C. Y., Jiang, K. J., and Zhang, Y., 2011 "Design and use of an eddy current retarder in an automobile," *International Journal of Automotive Technology*, Vol. 12, No.4, pp. 611-616.
- Liu, Z., and Angeles, J., 1992, "The properties of Constant-Branch Four-bar Linkages and Their Applications," *Trans. of the ASME. Journal of Mechanical Design*, Vol. 114, pp. 574-579.
- Lowther, D. A., and Silvester, P. P., 1986, "Computer aided design in magnetics," Springer-Verlag New York, Inc.
- Lovas, L., Play, D., Marialigeti, J., and Rigal, J.F., 2006, "Mechanical behaviour simulation for synchromesh mechanism improvements," *Proceedings of the Institution of Mechanical Engineers, Part D: Journal of Automobile Engineering*, Vol. 220, No. 7, pp. 919-945.

- Mapelli, F.L., Tarsitano, D., and Mauri, M., 2010, "Plug-In Hybrid Electric Vehicle: Modelling, Prototype Realization, and Inverter Losses Reduction Analysis," *IEEE Trans. on Ind. Elec.*, Vol. 57, No. 2, pp. 598-607.
- Marklund, P., and Larsson, R., 2007, "Permeability of Sinter Bronze Friction Material For Wet Clutches," *Tribology & Lubrication Technology*, Vol. 51, No. 3, pp. 303-309.
- Meirovitch, L., 1967, *Analytical Methods in Vibrations*, The Mcmillan Company, New York, USA.
- Miller, T. J. E., 2002, "Optimal design of switched reluctance motors," *IEEE Trans Ind. Elect.*, Vol. 49, No. 1, pp. 15-27.
- Moon, S. E., Kim, M. S., Yeo, H., and Kim, H. S., 2004, "Design and implementation of clutch-by-wire system for automated manual transmissions," *International Journal of Vehicle Design*, Vol. 36, No. 1, pp. 83-100.
- Mott, R. L., 2004, *Machine Elements in Mechanical Design*, Fourth Edition, Pearson Education Inc., Upper Saddle River, N.J.
- NASA Tech Briefs, 2001, "Rugged Iris Mechanism," *Technical Support Package*, GSC-14550-1, Goddard Space Flight Center, Greenbelt, Maryland 20771.
- Neelakantan, V. A., Washington, G. N., and Bucknor, N. K., 2008, "Model predictive control of a two stage actuation system using piezoelectric actuators for controllable industrial and automotive brakes and clutches," *Journal of Intelligent Material Systems and Structures*, Vol. 19, No. 7, pp. 845-857.
- Orthwein, W. C., 1991, "Plotting cone clutch/brake design ," *Machine Design* , Vol. 63, No. 2, pp. 42, 44-45.
- Osborne, A., 1963, *Applied Imagination: Principles and procedures of creative problem solving*, Third Edition, Charles Scriber & Sons, New York, NY.
- Pahl, G., Beitz, W., Feldhusen, J. and Grote, K.H., 2007, *Engineering Design: A Systematic Approach*, Third Edition, Wallace, K.M. and Blessing, L. (translators

## BIBLIOGRAPHY

- and editors), Springer-Verlag London Ltd., London.
- Palej, R., Piotrowski, S., and Stojek, M., 1993, "Mechanical Properties of an Active Pneumatic Spring," *Journal of Sound and Vibration*, Vol. 168, No. 2, pp. 299-306.
- Parmley, R. o., 2000, *Illustrated Source book of Mechanical Components*, First Edition, McGraw-Hill Co., New York, USA.
- Pendrill, A., Magnus, K., and Henrik, R., 2012, "Stopping a roller coaster train," *Physics Education*, Vol. 47, No. 6 pp. 728.
- Persson, M., Jansson, P., Jack, A.G., and Mecrow, B.C., 1995, "Soft magnetic composite materials-use for electrical machines," *Seventh International Conference on Electrical Machines and Drives*, No. 412, pp. 242-246.
- Rabinow, J., 1948, "The Magnetic Fluid Clutch," *AJEE TRANSACTIONS*, Vol. 67, No. 2, pp. 1308-1315.
- Rao, A. S., 1993, "Alnico permanent magnets an overview," *IEEE Proceedings EEIC/ICWA Exposition*, Chicago, IL.
- ReVelle, J., Moran, J., and Cox, C., 1998, *The QFD Handbook*, Wiley, New York.
- Rivire, J. C., and Myhra, S., 2009, *Handbook of Surface and Interface Analysis*, Second Edition, CRC Press, New York, USA.
- Rothbart, H. A., and Klipp, D. L., 2004, *Cam design handbook*, Vol. 394, McGraw-Hill, New York, USA.
- Rumiche, F., Indacochea, J. E., and Wang, M. L. , 2008, "Assessment of the effect of microstructure on the magnetic behaviour of structural carbon steels using an electromagnetic sensor," *Journal of Materials Engineering and Performance*, Vol. 17, No. 4, pp. 586-593.
- Ryoo, H., Kim, J., Kang, D., Rim, G., Kim, Y., and Won, C., 2000, "Design and analysis of an eddy current brake for a high-speed railway train with constant torque control," *IEEE Industry Applications Conference*, Vol. 1, pp. 277-281.

- Sfarni, S., Bellenger, E., Fortin, J., and Malley, M., 2011, "Numerical and experimental study of automotive riveted clutch discs with contact pressure analysis for the prediction of facing wear," *Finite Elements in Analysis and Design*, Vol. 47. No. 2, pp. 129-141.
- Shannon, C, 1948, "A mathematical theory of communication," *The Bell Systems Technical Journal*, Vol. 27, No. 1, pp. 379-423, 623-656.
- Shirahama, S., 1994, "Adsorption of Additives on Wet Friction Pairs and Their Frictional Characteristics," *Japanese Journal of Tribology*, Vol. 39, No. 12, pp. 1479-1486.
- Smith, A.L., and Kenndy, L.C., 2007, "Magnetorheological Fluid Fan Drive for Trucks," *Journal of Intelligent Material Systems and Structures*, Vol. 18, No. 1, pp. 1131-1136.
- Stokes, A., 1992, *Manual Gearbox Design*, First Edition, Elsevier, ButterworthHeinemann, Oxford, UK.
- Syed, F.U., Kuang, M.L., Czubay, J., and Ying, H., 2006, "Derivation and experimental validation of a power-split hybrid electric vehicle model," *IEEE Trans. Veh. Technol.*, Vol. 55, No. 6, pp. 1731-1747.
- Thompson, M. T., 2009, "Practical Issues in the Use of NdFeB Permanent Magnets in Maglev, Motors, Bearings, and Eddy Current Brakes," *Proceedings of the IEEE*, Vol. 97, No. 11, pp. 1758-1767.
- Thornley, J. K., Preston, M. E., and King, T. G., 1991, "A fast electro-mechanical clutch element using a piezoelectric multilayer actuator," *IEE Colloquium In Robot Actuators*, Vol. 1, No. 2, pp. 1-4.
- Ting, L.L., 1975, "Engagement behaviour of lubricated porous annular disks. Part 1: Squeeze film phase - surface roughness and elastic deformation effects," *Wear*, Vol. 34, No. 2, pp. 159-172.

## BIBLIOGRAPHY

- Treder, M., and Woernle, C., 2004, "Simulation and experimental validation of the dynamic behavior of an electromechanically actuated multiple-disk clutch," *Proceedings Applied Mathematics and Mechanics*, Vol. 4, No. 1, 171-172.
- Tretsiak, D.V., Kliuzovich, S.V., Augsburg, K., Sendler, J., and Ivanov, V.G., 2008, "Research in hydraulic brake components and operational factors influencing the hysteresis losses ," *Proceedings of the Institution of Mechanical Engineers, Part D: Journal of Automobile Engineering*, Vol. 222, No. 9, pp. 1633-1645.
- Wishart, J., Zhou, Y. L., and Dong, Z., 2008, "Review of multi-regime hybrid vehicle powertrain architecture," *International Journal of Electric and Hybrid Vehicles*, Vol. 1, No. 3, pp. 248-275.
- Wu, G., Zhang X., and Dong, Z., 2013, "Impacts of Two-Speed Gearbox on Electric Vehicle's Fuel Economy and Performance," *SAE Technical Paper*, No. 2013-01-0349.
- Vidal, N., Aguirre-Zamalloa, G., Barandiaran, J.M., Garcia-Arribas, A., and J. Gutierrez, 2006, "FEM analysis of an eddy current water flow meter," *J. of Magnetism and Magnetic Materials*, Vol. 304, No. 2, pp. 838-840,.
- Xu, W., and King, T., 1998, "Flexure hinges for piezoactuator displacement amplifiers: flexibility, accuracy, and stress considerations," *Precision Engineering*, Vol. 19, No. 1, pp. 4-10.
- Yang, Y., and Lam, R.C., 1998, "Theoretical and experimental studies on the interface phenomena during the engagement of automatic transmission clutch," *Tribology Letters*, Vol. 5, No. 1, pp. 57-67.
- Yao, J., Chen, L., Yin, C., and Shu, J., 2010, "Modeling of a Wedge Clutch in an Automatic Transmission," *SAE Technical Paper*, No. 2010-01-0186.
- Yuan, Y., Lui, E.A., Zhang, S., and Li, R., 2007, "An improved hydrodynamic model for open wet transmission clutches," *Journal of Fluid Engineering*, Vol. 129, No. 1,

pp. 333-337.

Zagrodzki, P., 1990, "Analysis of thermomechanical phenomena in multidisc clutches and brakes," *Wear*, Vol. 140, No. 2, pp. 291-308.

Zagrodzki, P., and Truncone, S. A., 2003, "Generation of hot spots in a wet multidisk clutch during short-term engagement," *Wear*, Vol. 254, No. 1, pp. 474-491.

Zhang, D., Chen, J., Hsieh, T., Rancourt J. and Schmidt, M. R., 2001, "Dynamic modelling and simulation of twomode electric variable transmission," *Proc. Instn Mech. Engrs, Part D, Journal of Automobile Engineering*, Vol. 215, No. 1, pp. 1217-1223.



# APPENDIX A

---

## Spatial Clutch Linkage Analysis

An interesting and unique class of four-bar linkages capable of switching branches is called *cross-branch bimodal* (Gosselin and Angeles, 1989). These special linkages can be designed as a clutching mechanism wherein the linkage can attain a constant branch, i.e., a layout whereby the output link remains stationary (Liu and Angeles, 1992). This property was understood by Gosselin and Angeles (1989) as an architecture singularity of closed kinematic chains. However, it can be exploited to produce a clutch effect; by switching between constant-branch (disengaged mode) to nonconstant-branch (engaged mode). With a small change in its dimensions, the linkage can switch out of its constant to its non-constant mode, thereby allowing motion to be transmitted via the double-crank linkage. Constant-branch four-bar linkages exist in planar, spherical and spatial linkages. Here, a RSSR linkage is analyzed, where R denotes a revolute joint and S denotes a spherical joint.

An input vector array  $\mathbf{u}$ , a function of the input angle  $\psi$ , an output vector array  $\mathbf{v}$ , a function of the output angle  $\phi$ , and the  $3 \times 3$  linkage-parameter matrix  $\mathbf{A}$  are introduced below. The input-output equation for bimodal linkages can be expressed as (Liu and Angeles, 1992)

$$\mathbf{u}^T(\psi)\mathbf{A}\mathbf{v}(\phi) = 0 \tag{A.1}$$

APPENDIX A. SPATIAL CLUTCH LINKAGE ANALYSIS

where

$$\mathbf{u} \equiv \begin{bmatrix} \cos \psi \\ \sin \psi \\ 1 \end{bmatrix}, \quad \mathbf{v} \equiv \begin{bmatrix} \cos \phi \\ \sin \phi \\ 1 \end{bmatrix}, \quad \mathbf{A} = \begin{bmatrix} A_{11} & A_{12} & A_{13} \\ A_{21} & A_{22} & A_{23} \\ A_{31} & A_{32} & A_{33} \end{bmatrix}$$

The entries of  $\mathbf{A}$  are

$$A_{11} = -\cos \alpha_4, \quad A_{12} = 0, \quad A_{13} = -\frac{s_4 \sin \alpha_4}{a_3}, \quad A_{21} = 0, \quad A_{22} = -1, \quad A_{23} = -\frac{a_4}{a_3},$$

$$A_{31} = \frac{s_1 \sin \alpha_4}{a_1}, \quad A_{32} = \frac{a_4}{a_1}, \quad A_{33} = \frac{a_1^2 - a_2^2 + a_3^2 + a_4^2 + s_1^2 + s_4^2 - 2s_1 s_4 \cos \alpha_4}{2a_1 a_3}$$

with the linkage shown in Fig. A.1.

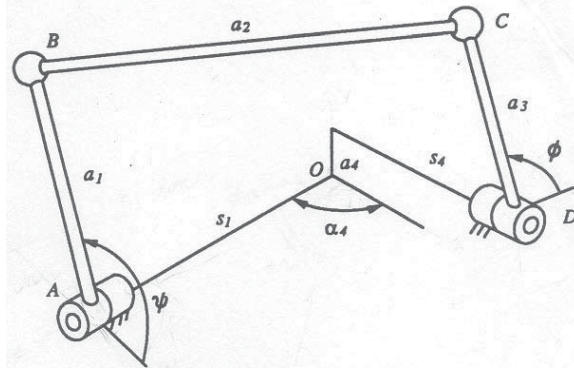


FIGURE A.1. RSSR linkage representation (Liu and Angeles, 1992)

Liu and Angeles (1992) described the basic criterion and general properties for the unique constant-branch feature. In the constant-branch mode, the output link remains stationary for all positions of the input link. This implies that the four-bar linkage has an input crank. At a certain value,  $\phi_0$ , of the output angle the condition of interest is

$$\mathbf{A}\mathbf{v}(\phi_0) = \mathbf{0} \tag{A.2}$$

where  $\mathbf{0}$  is the 3-dimensional zero vector, thus guaranteeing the verification of eq.(A.1) for any value of  $\psi$ . Using the parameters for the RSSR linkage from Fig. A.1, eq.(A.2)

yields

$$A_{11} \cos \phi_0 + A_{13} = 0 \quad (\text{A.3a})$$

$$A_{22} \sin \phi_0 + A_{23} = 0 \quad (\text{A.3b})$$

Hence

$$A_{13}^2 A_{22}^2 + A_{11}^2 A_{23}^2 - A_{11}^2 A_{22}^2 = 0 \quad (\text{A.4})$$

From eq.(A.2)  $\mathbf{A}$ , must be singular, as  $\mathbf{v} \neq \mathbf{0}$ , and hence,

$$\det(\mathbf{A}) = 0 \quad (\text{A.5})$$

or

$$A_{11} A_{22} A_{33} - A_{11} A_{23} A_{32} - A_{13} A_{22} A_{31} = 0 \quad (\text{A.6})$$

The implication of a stationary output link is that its velocity and acceleration vanish simultaneously at the same input value, i.e.,

$$\phi'(\psi_0) = 0, \quad \phi''(\psi_0) = 0 \quad (\text{A.7})$$

The geometric parameters can be readily derived from eqs.(A.4 and A.6). A constant-branch spatial RSSR linkage must verify

$$s_4^2 \tan^2 \alpha_4 + a_4^2 = a_3^2 \quad (\text{A.8a})$$

$$a_1^2 + \left( s_1 - \frac{s_4}{\cos \alpha_4} \right)^2 = a_2^2 \quad (\text{A.8b})$$

The transmission quality of four-bar linkages is defined as the rms value of the sine of the transmission angle (Gosselin and Angeles, 1989). In the special case of a constant-branch spatial RSSR linkage, the transmission quality, is  $(1/2)(a_1/a_2)^2$ , with  $a_2 \geq a_1$ . Therefore, the maximum transmission quality that can be attained is 0.5.

In order for a four-bar linkage to function as a clutch mechanism, it must go beyond the layouts of engagement or disengagement. It must be capable of producing a smooth transition between the two layouts. Moreover, this response needs to be fast and utilize the least amount of energy possible. The RSSR configuration can be realized by replacing the spherical joints by a universal (U) and a revolute joint. Thus, a RURUR spatial linkage is obtained, which is simpler to fabricate.

A CAD model was constructed as shown in Fig. A.2. The linkage dimensions are

$$a_1 = 2.00, \quad a_2 = 2.50, \quad a_3 = 1.00, \quad a_4 = 0.80, \quad s_1 = 2.841640786,$$

$$s_4 = 1.20, \quad \alpha_4 = 26.565051171^\circ, \quad \phi_0 = 233.130102426$$

These dimensions were obtained by solving the linkage eqs.(A.1–A.8). A purely kinematic solution was generated with an animation for visualization. Kinematic simulation was carried out in Unigraphics NX 7.5 and MSC ADAMS—software packages with numerical analysis. The simulation tests revealed the dependency of the linkage on its dimensional precision. When dimensions were specified to the ninth decimal place, the linkage was capable of maintaining the constant-branch mode. However, any numerical change in the last decimal place would result in the undesired switching of branches.

Moreover, the transition between constant and nonconstant-branch needed to be smooth, i.e., the plots of the two branches must blend smoothly. This blending is vital in order to avoid mechanical shock, which in turn may have dire consequences in an automotive application. The input-output curve of the synthesized linkage is plotted in Fig. A.3. Notice that the plot contains a cross point where the output can



FIGURE A.2. RURUR clutch linkage

switch from one mode to the other. As  $C^2$ -continuity<sup>1</sup> is not possible for a four-bar linkage<sup>2</sup>, this switch can be blended only with  $C^1$ -continuity.

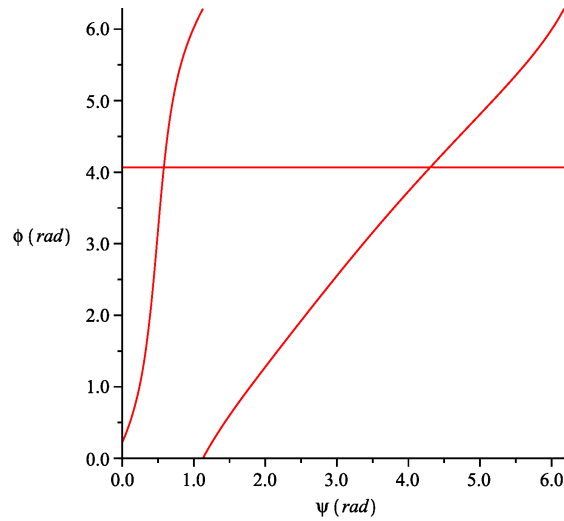


FIGURE A.3. The input-output curve of the clutch linkage

<sup>1</sup> $C$  represent analytical continuity.  $C^2$ -continuity is to have continuous derivatives up to the second order.

<sup>2</sup>The nature of the input-output equations prevents both output velocity and acceleration to vanish simultaneously

## APPENDIX A. SPATIAL CLUTCH LINKAGE ANALYSIS

From this analysis some conclusions were drawn. First, under numerical simulation, the linkage would switch branches with any perturbation in the dimension set-up. Second, given the linkage transmission quality of 0.5, two linkages, one the mirror image of the other, would be required. Lastly, a smooth transition between branches increases the complexity of clutch implementation. With the brief analysis reported here, an in-depth investigation is recommended to design a feasible clutch linkage.

## APPENDIX B

---

### Eddy-current Clutch Analysis

Here a brief analysis is conducted to understand the eddy-current application for a potential low-speed clutch variant. An eddy-current braking effect can be observed when a metallic conductor disk rotates around its axis in the presence of a stationary source of magnetic field (permanent magnet or electromagnet). Given the rotation of the conductor disk, it experiences a time-varying magnetic flux density, which by virtue of Lenz’s law results in an electric field. This field,  $\mathbf{e}$ , is given by the Maxwell-Faraday equation as

$$\nabla \times \mathbf{e} = -\frac{\partial \mathbf{b}}{\partial t} \quad (\text{B.1})$$

with  $\mathbf{b}$  denoting the magnetic flux density (Furlani, 2001). The electric field induces circulating currents, referred to as “eddy-currents,” on the conductor-disk surface. Using Ohm’s law, the current density  $\mathbf{j}$  and the electric field obey the relation

$$\mathbf{j} = \sigma \mathbf{e} \quad (\text{B.2})$$

where  $\sigma$  is the conductivity of the disk. Then, the secondary magnetic field generated by the eddy currents opposes the original change in magnetic flux density. This phenomenon results in a force that opposes the motion as the source of the magnetic

field is stationary. The braking force  $\mathbf{f}_b$  is given by Lorentz's force law as

$$\mathbf{f}_b = \mathbf{j} \times \mathbf{b} \quad (\text{B.3})$$

The eddy-current system performance depends on several factors, such as field-source dimensions, magnetic flux density, air-gap size, number of poles, conductor thickness, conductor rotor material and stator material (Canova et al., 2005).

The eddy-current brake principle can be illustrated by means of 2D simulation in MagNet. Initially, a 2D cross-section of a cylindrical capsule with the dimensions of a typical brake-clutch is constructed, as shown in Fig. B.1. Since the device features a pie section of  $72^\circ$  with boundary conditions denoting the even periodicity, i.e., an even-periodic pattern, only the pie section is constructed in MagNet. Stranded insulated copper wire is used to wrap the steel cores, forming the electromagnets. A copper rotor is placed between the air gap of the inner and the outer stators, as shown in the same figure. Here, the electromagnets are kept stationary, while the copper rotor is subject to an initial angular velocity of 100 rpm (600 deg/s).

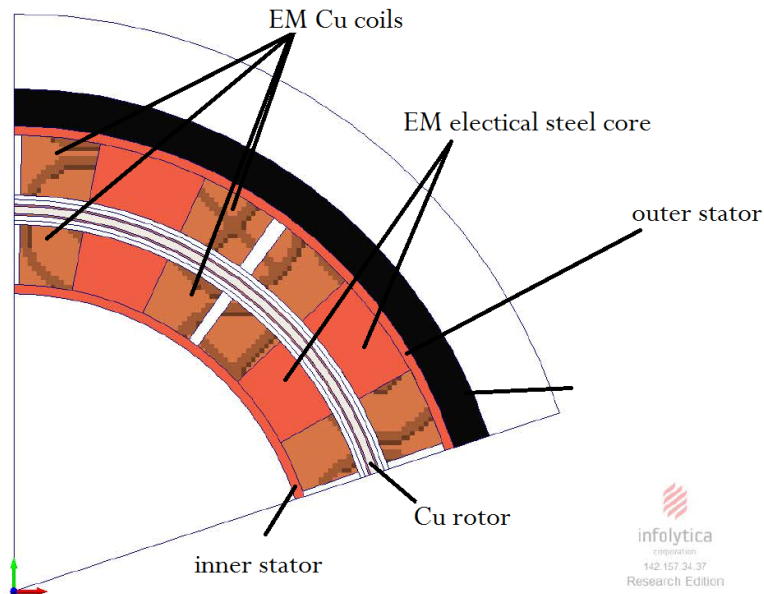


FIGURE B.1. A  $72^\circ$  pie section of a four-electromagnetic-pole configuration

A 42 V DC source is connected to the stranded coil windings. A varying load torque applied on the rotor is specified as a function of the slip-speed. This load increases with a decrease in the rotor speed, wherein maximum load is applied at zero speed. The 2D transient with motion simulation is run for 200 ms. A current of 20 A was observed in the coil windings which produced a radially polarizing field, as shown in the contour plot of Fig. B.2.

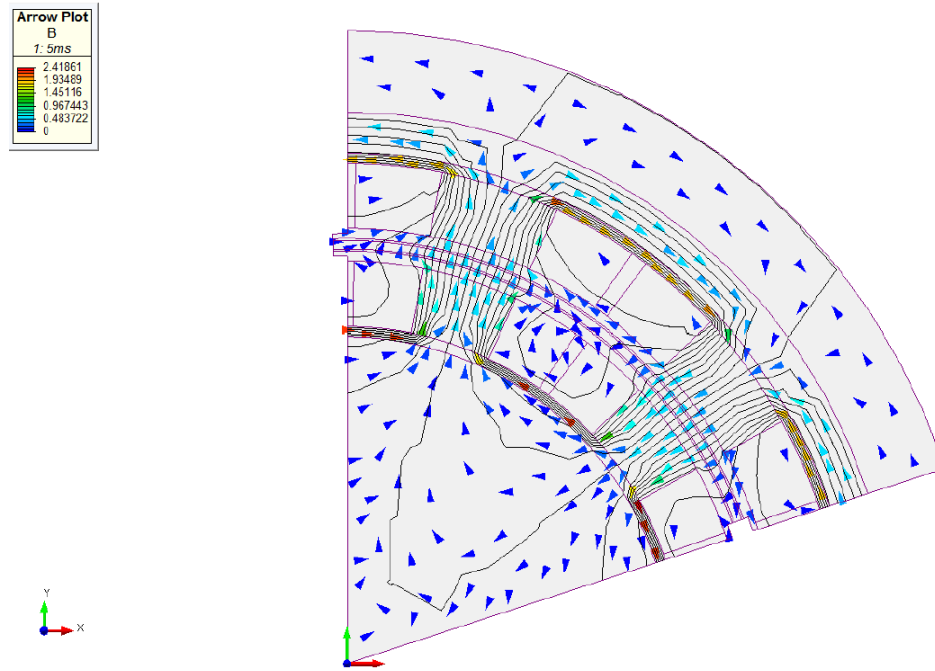


FIGURE B.2. Magnetic-flux contour and arrow plot

A rotor speed plot of the MagNet simulation is displayed in Fig. B.3. Past the 20 ms mark, the voltage source was activated. The electromagnetic torque generated in the system was observed to fluctuates as the speed decreased. The rotor initial speed of 600 deg/s is lowered but the system fails to reduce rotor slip further. Thus, this preliminary analysis shows that a DC eddy-current system is ineffective in the application of an active load-torque low-speed brake-clutch.

APPENDIX B. EDDY-CURRENT CLUTCH ANALYSIS

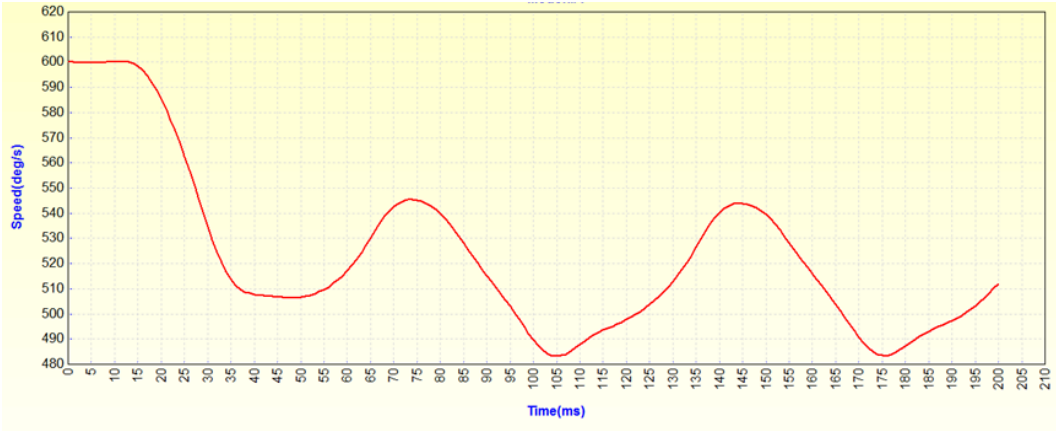


FIGURE B.3. Rotor speed response

## Document Log:

Manuscript Version 0

Typeset by  $\mathcal{A}\mathcal{M}\mathcal{S}$ - $\mathcal{L}\mathcal{A}\mathcal{T}\mathcal{E}\mathcal{X}$  — 24 March 2014

VIKRAM CHOPRA

CENTRE FOR INTELLIGENT MACHINES, MCGILL UNIVERSITY, 3480 UNIVERSITY ST., MONTREAL (QUÉBEC), H3A 2A7, CANADA

*E-mail address:* [vikram@cim.mcgill.ca](mailto:vikram@cim.mcgill.ca)

Typeset by  $\mathcal{A}\mathcal{M}\mathcal{S}$ - $\mathcal{L}\mathcal{A}\mathcal{T}\mathcal{E}\mathcal{X}$